ANL-6359
Metals, Ceramics,
and Materials
(TID-4500, 16th Ed.)
AEC Research and
Development Report

ARGONNE NATIONAL LABORATORY
9700 South Cass Avenue
Argonne, Illinois

# PAPERS AND DISCUSSION FROM THE X-RAY PREFERRED ORIENTATION MEETING HELD AT ARGONNE NATIONAL LABORATORY DECEMBER 15 AND 16, 1960

edited by Melvin H. Mueller

May 1961

Operated by The University of Chicago
under
Contract W-31-109-eng-38

## DISCLAIMER

TABLE OF CONTENTS

# PAPERS AND DISCUSSION FROM THE X-RAY PREFERRED ORIENTATION MEETING HELD AT ARGONNE NATIONAL LABORATORY

December 15 and 16, 1960

Melvin H. Mueller, Editor

## ABSTRACT

Papers and discussion presented at the X-ray Preferred Orientation Meeting at Argonne National Laboratory on December 15 and 16, 1960 have been compiled. Papers were presented on several topics on the physical metallurgy of uranium, such as preferred orientation in recrystallized material, diffraction intensities and uranium atom position as a function of temperatures, as well as papers on methods for and results of growth index calculations and predictions. Agreement was obtained within the committee on certain techniques and definitions, such as calculated intensities for alpha uranium, $G_2$ based on 20 planes, and $G_3$ based on 18 planes. The committee also recognizes that further work needs to be done in instrumental techniques including automization as well as further correlation of results with irradiation.

## INTRODUCTION AND BRIEF RESUME OF MEETING

One of the main objectives of the preferred orientation meeting held at Argonne was to define the areas of current agreement within this group and to define some of the areas for future investigation This report has therefore been assembled in order to summarize the present status. This is in keeping with the previously established policy in which the summary of the 1959 meeting of this group held at National Lead Company of Ohio was published as NLCO-804.

The Preferred Orientation Committee met at Argonne National Laboratory December 15 and 16, 1960, with the following people in attendance:

Edward F. Sturcken
Savannah River Plant

Robert B. Russell
Nuclear Metals, Inc.

Dale A. Vaughan
Battelle Memorial Institute

Leonard Robins
Bridgeport Brass Company

J. P. LeGeros
Savannah River Plant

W. Gary Jolley
HAPO Fuels Preparation Dept.

Henry C. Kloepper, Jr.
Mallinckrodt Chemical Works

James W. Starbuck
Mallinckrodt Chemical Works

R. N. Thudium
National Lead Co. of Ohio

P. R. Morris
National Lead Co. of Ohio

V. I. Montenyohl
Savannah River Plant

Lowell T. Lloyd
Argonne National Laboratory

Melvin H. Mueller, Chairman
Argonne National Laboratory

The eleven papers presented are included in this report. Although all of the discussion on each paper is not presented, much of the discussion terminated in recommendations of the committee which concerned common grounds of agreements or areas of investigation to be undertaken.

The following recommendations were adopted: that

1. The standard calculated random intensities for alpha uranium shall be those given in NLCO-804, Table III, page 57, column marked I**.

2. The $G_2$ value shall be as defined in NLCO-804 using the 20 plane set as specified in column 1 of Table II, page 22.

3. The $G_3$ shall be as defined in NLCO-804 using the 18 plane set as specified in column 2 of Table II, page 22.

4. The $G_3$ value be tentatively adopted as standard for between-site communication and that the $G_2$ value also be reported if means of calculation are available, and that all investigators be encouraged to also collect intensity data for the (040), (240), and (241) planes in addition.

5. If the $G_3$ or $G_2$ values in the future be calculated on a different set of planes, the new $G_3$ or $G_2$ value be designated by an additional digit in the subscript, for example $G_{2,0}$, $G_{2,1}$, etc.

6. The committee more thoroughly investigate the problem of sampling. The need for this was especially evident from three papers presented at the meeting, which clearly indicated a difference of texture as a result of cooling rates. This difference showed up between inside and outside surfaces of bars. The subcommittee appointed is LeGeros, Morris, and Thudium.

7 The committee continue to investigate the preparation and use of a standard sample for intersite comparison of X-ray intensity and instrumental conditions. Subcommittee appointed consisted of Vaughan, LeGeros, and Kloepper.

8 The committee follow the work of Sturcken and LeGeros for the correlation of growth and texture as being carried out in their in-pile experiments.

9 The committee investigate the matter of statistics as applied to texture work. Subcommittee appointed included LeGeros, Starbuck, Kloepper, and Russell

10 The committee accepts the offer of Russell to investigate point weighting, and together with Jolley to review the $I_{max}$ versus $I_{area}$ technique

11 Since a number of laboratories are concerned with automatizing the diffraction equipment, the committee have an active group concerned with this phase in order to share information, appointed on the subcommittee Morris, Sturcken, Mueller, and Starbuck.

12 The committee accepts the offer of Sturcken to investigate the determination of grain size by Xrays as discussed by Warren in NYO-4836, and that Sturcken also investigate the application of Alexander's paper, given at the Pittsburgh Conference 1960, on measurement of X-ray intensity to the texture determination techniques.

13 That the next meeting of the P. O. Committee be held at Hanford some time in June, 1961, but not the first week.

# PREDICTION OF DIMENSIONAL CHANGES IN URANIUM FUEL ELEMENTS DURING IRRADIATION - THE ELASTIC SOLUTION INTERIM REPORT*

Peter R. Morris and Richard N. Thudium
National Lead Company of Ohio

## ABSTRACT

Equations have been derived for the prediction of dimensional changes and stresses in thick-walled, hollow, cylindrical uranium fuel element cores during thermal neutron irradiation. The equations provide a means for combining discrete preferred orientation data obtained from a finite series of X-ray diffraction measurements. A comparison of calculated stresses with the creep strength of uranium should determine whether a plastic solution is necessary.

## INTRODUCTION

The strain tensor has been applied to preferred orientation data by E. F. Sturcken[1] to predict dimensional changes in uranium fuel elements during irradiation. Sturcken's original method has been modified by Morris[2] and by Sturcken.[3] In its present form, the method finds direct application in the prediction of dimensional changes in plates and thin-walled tubes. The application of the method to thick-walled cylindrical fuel elements presents additional complications.

In the case of a thick-walled cylinder, the predicted growth and degree of self-constraint will generally be functions of both direction and radial position. An example of variation in predicted dimensional change during irradiation with radial position is illustrated in Fig. 1, a plot of experimentally determined values of growth index $G_3$ in the longitudinal direction for a hollow cylindrical uranium fuel core rapidly quenched from the beta phase. In obtaining the data for Fig. 1, a 0.090-inch-wide X-ray beam was employed to irradiate successive increments of the sample surface from the inside radius to the outside radius.

---

*Much of this report has previously appeared in NLCO-816 (Nov. 15, 1960).

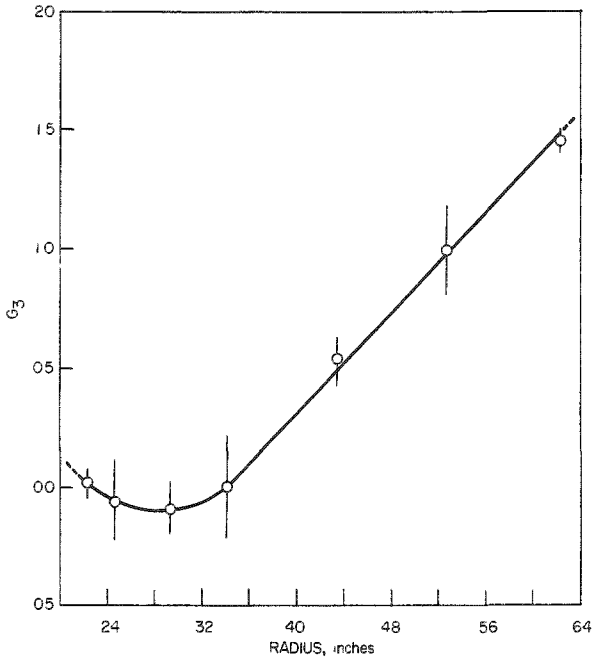


Fig. 1

Growth Index $G_3$ in the Longitudinal Direction as a Function of Radial Position.

A method for combining preferred orientation data to predict dimensional changes of the whole is desired. These data will generally be obtained for three mutually perpendicular directions. The selection of coordinates and sampling scheme are dictated by the particular symmetry being studied. For the present case, the use of cylindrical coordinates is indicated.

In the derivation which follows we have assumed:

1. The cores adjust elastically to stresses occasioned by anisotropic dimensional changes within individual crystallites.
2. There exists a cylindrical symmetry of dimensional changes, stress, and strain.
3. Elastic isotropy and homogeneity (elastic constants uniform throughout and independent of direction) are assumed.
4. A state of plane strain exists (end effects may be neglected).

There is admittedly some question concerning the rigorous application of these assumptions to a physical problem. The only defense we offer for adopting these assumptions is that by so doing we are able to obtain an approximate solution of an otherwise formidable problem. Equations obtained for stresses may be employed to test the validity of the first assumption, and are, in fact, prerequisite to the plastic solution, if such a solution is indicated.

## STRESS-STRAIN RELATIONSHIPS IN CYLINDRICAL COORDINATES

If a circular cylinder conforming to the above assumptions is subjected to a plane strain which is symmetrical about the axis of the cylinder, the state of strain at any point is completely specified by the values of $\epsilon_r$, $\epsilon_\theta$, and $\epsilon_z$, the radial, tangential, and longitudinal strain components at the point. Similarly, the state of stress at any point is completely specified by the values of $\sigma_r$, $\sigma_\theta$, and $\sigma_z$, the radial, tangential, and longitudinal stress components at the point.

We shall denote by $g_r$, $g_\theta$, and $g_z$ the radial, tangential, and longitudinal components of strain due to neutron irradiation. Estimates of $g_r$, $g_\theta$, and $g_z$ may be obtained from the appropriate values of $G_2$ or $G_3$[4] and anticipated burnup.

Except for the anisotropic nature of the strains, the present problem is quite similar to the problem of thermal stresses.[5] The stress-strain relations are

$$\epsilon_r - g_r = \frac{1}{E}\left[\sigma_r - \nu\,(\sigma_\theta + \sigma_z)\right] \tag{1}$$

$$\epsilon_\theta - g_\theta = \frac{1}{E}\left[\sigma_\theta - \nu\,(\sigma_r + \sigma_z)\right] \tag{2}$$

$$\epsilon_z - g_z = \frac{1}{E}\left[\sigma_z - \nu\,(\sigma_r + \sigma_\theta)\right] \tag{3}$$

where E is Young's modulus, $\nu$ is Poisson's ratio, and the other symbols are as noted above. Equations 1, 2, and 3 may be solved for the stresses $\sigma_r$, $\sigma_\theta$, and $\sigma_z$ to yield

$$\sigma_r = \frac{E[(1-\nu)(\epsilon_r - g_r) + \nu(\epsilon_\theta - g_\theta + \epsilon_z - g_z)]}{(1+\nu)(1-2\nu)} \tag{4}$$

$$\sigma_\theta = \frac{E[(1-\nu)(\epsilon_\theta - g_\theta) + \nu(\epsilon_r - g_r + \epsilon_z - g_z)]}{(1+\nu)(1-2\nu)} \tag{5}$$

$$\sigma_z = \frac{E[(1-\nu)(\epsilon_z - g_z) + \nu(\epsilon_r - g_r + \epsilon_\theta - g_\theta)]}{(1+\nu)(1-2\nu)} \quad . \tag{6}$$

The stresses $\sigma_r$ and $\sigma_\theta$ satisfy the equation of equilibrium:[6]

$$\frac{d\sigma_r}{dr} + \frac{\sigma_r - \sigma_\theta}{r} = 0 \quad . \tag{7}$$

Substituting $\sigma_r$ and $\sigma_\theta$ from Equations 4 and 5 in Equation 7, and combining terms give

$$r\left[(1-\nu)\frac{d\epsilon_r}{dr}+\nu\frac{d\epsilon_\theta}{dr}\right]+(1-2\nu)(\epsilon_r-\epsilon_\theta)=r\left[(1-\nu)\frac{dg_r}{dr}+\nu\left(\frac{dg_\theta}{dr}+\frac{dg_z}{dr}\right)\right]$$

$$+(1-2\nu)(g_r-g_\theta) \quad . \tag{8}$$

In obtaining Equation 8, we have placed $d\epsilon_z/dr = 0$ in compliance with the assumption that a state of plane strain exists.

If we denote radial displacement by u, the strains $\epsilon_r$ and $\epsilon_\theta$ and their derivatives with respect to r are given by

$$\epsilon_r=\frac{du}{dr} \tag{9}$$

$$\frac{d\epsilon_r}{dr}=\frac{d^2u}{dr^2} \quad . \tag{10}$$

$$\epsilon_\theta=\frac{u}{r} \tag{11}$$

$$\frac{d\epsilon_\theta}{dr}=\frac{1}{r}\frac{du}{dr}-\frac{u}{r^2} \quad . \tag{12}$$

Substitution of $\epsilon_r$, $\epsilon_\theta$, and their derivatives from Equations 9 through 12 in Equation 8 gives

$$(1-\nu)\left(\frac{d^2u}{dr^2}+\frac{1}{r}\frac{du}{dr}-\frac{u}{r^2}\right)=(1-\nu)\frac{dg_r}{dr}+\nu\left(\frac{dg_\theta}{dr}+\frac{dg_z}{dr}\right)$$

$$+\frac{1}{r}(1-2\nu)(g_r-g_\theta) \quad . \tag{13}$$

Equation 13 may be rewritten as

$$\frac{d}{dr}\left[\frac{1}{r}\frac{d(ur)}{dr}\right]=\frac{dg_r}{dr}+\frac{\nu}{(1-\nu)}\left(\frac{dg_\theta}{dr}+\frac{dg_z}{dr}\right)+\frac{1}{r}\frac{(1-2\nu)}{(1-\nu)}(g_r-g_\theta) \quad . \tag{14}$$

Equation 14 is a second-order differential equation of the first degree. Solution of Equation 14 for u is accomplished by integrating twice with respect to r to yield

$$u=\frac{1}{R}\int_{a'}^{R}\mathcal{R}g_r\,d\mathcal{R}+\frac{\nu}{(1-\nu)}\frac{1}{R}\int_{a'}^{R}\mathcal{R}\,(g_\theta+g_z)\,d\mathcal{R}$$

$$+\frac{(1-2\nu)}{(1-\nu)}\frac{1}{R}\int_{a'}^{R}\left[\mathcal{R}\int_{a}^{\mathcal{R}}\frac{1}{r}(g_r-g_\theta)dr\right]d\mathcal{R}+C_1R+\frac{C_2}{R} \quad . \tag{15}$$

In each of the above integrations, the lower limit is arbitrary. The selection of lower limits in each case determines the values of $C_1$ and $C_2$. We shall denote the radius corresponding to the inner surface by a, and set this as the lower limit for both integrations.

An expression for $C_2$ in terms of $C_1$ and $\epsilon_z$ may be obtained by evaluating Equation 4 at r = a, and equating to the normal stress $\sigma_{ra}$ at the boundary.

To do this, we first differentiate Equation 15 with respect to r, obtaining

$$\frac{du}{dr} = g_r - \frac{1}{R^2}\int_a^R \mathcal{R}\, g_r\, d\mathcal{R} + \frac{\nu}{(1-\nu)}(g_\theta + g_z) - \frac{\nu}{(1-\nu)}\frac{1}{R^2}\int_a^R \mathcal{R}\,(g_\theta + g_z)\, d\mathcal{R}$$

$$+ \frac{(1-2\nu)}{(1-\nu)}\int_a^R \frac{1}{\mathcal{R}}(g_r - g_\theta)\, d\mathcal{R} - \frac{(1-2\nu)}{(1-\nu)}\frac{1}{R^2}\int_a^R \left[\mathcal{R}\int_a^{\mathcal{R}} \frac{1}{r}(g_r - g_\theta)\, dr\right] d\mathcal{R}$$

$$+ C_1 - \frac{C_2}{R^2} \quad . \tag{16}$$

Evaluating Equations 15 and 16 at r = a, we have

$$u_a = C_1 a + \frac{C_2}{a} \tag{17}$$

$$\left(\frac{du}{dr}\right)_a = g_{ra} + \frac{\nu}{(1-\nu)}(g_{\theta a} + g_{za}) + C_1 - \frac{C_2}{a^2} \quad . \tag{18}$$

We shall denote the values of the strains $\epsilon_r$ and $\epsilon_\theta$ at r = a, by $\epsilon_{ra}$ and $\epsilon_{\theta a}$, respectively. These are obtained by substituting $u_a$ and $(du/dr)_a$ from Equations 17 and 18 in Equations 9 and 11 to yield

$$\epsilon_{ra} = g_{ra} + \frac{\nu}{(1-\nu)}(g_{\theta a} + g_{za}) + C_1 - \frac{C_2}{a^2} \tag{19}$$

$$\epsilon_{\theta a} = C_1 + \frac{C_2}{a^2} \quad . \tag{20}$$

Substituting the values of $\epsilon_r$ and $\epsilon_\theta$ from Equations 19 and 20 in Equation 4, and equating to the stress $\sigma_{ra}$ at the boundary give

$$C_2 = a^2\left[\frac{C_1 + \nu\epsilon_z}{1-2\nu} - \frac{\sigma_{ra}(1+\nu)}{E}\right] \quad . \tag{21}$$

To obtain an expression for $C_1$ in terms of $g_r$, $g_\theta$, $g_z$, and $\epsilon_z$, we proceed in similar vein to evaluate Equation 4 at r = b, the radius corresponding to the outer surface, and equate to the normal stress $\sigma_{rb}$ at the boundary.

The radial and tangential strains, $\epsilon_{rb}$ and $\epsilon_{\theta b}$, at the outer surface are obtained by evaluation of Equations 15 and 16 for u and du/dr at r = b and substitution of these values and the value for $C_2$ from Equation 21 in Equations 9 and 11 to yield

$$\epsilon_{\theta b} = \frac{u_b}{b} = \frac{1}{b^2}\int_a^b \mathcal{R}\, g_r\, d\mathcal{R} + \frac{\nu}{(1-\nu)}\frac{1}{b^2}\int_a^b \mathcal{R}\,(g_\theta + g_z)\, d\mathcal{R}$$

$$+ \frac{(1-2\nu)}{(1-\nu)}\frac{1}{b^2}\int_a^b \left[\mathcal{R}\int_a^{\mathcal{R}} \frac{1}{r}(g_r - g_\theta)\, dr\right] d\mathcal{R}$$

$$+ \frac{C_1[b^2(1-2\nu)+a^2]+\nu a^2\epsilon_z}{(1-2\nu)\, b^2} - \frac{(1+\nu)\, a^2\sigma_{ra}}{b^2\, E} \qquad (22)$$

$$\epsilon_{rb} = \left(\frac{du}{dr}\right)_b = g_{rb} - \frac{1}{b^2}\int_a^b \mathcal{R}\, g_r\, d\mathcal{R} + \frac{\nu}{(1-\nu)}(g_{\theta b} + g_{zb})$$

$$- \frac{\nu}{(1-\nu)}\frac{1}{b^2}\int_a^b \mathcal{R}\,(g_\theta + g_z)\, d\mathcal{R} + \frac{(1-2\nu)}{(1-\nu)}\int_a^b \frac{1}{\mathcal{R}}(g_r - g_\theta)\, d\mathcal{R}$$

$$- \frac{(1-2\nu)}{(1-\nu)}\frac{1}{b^2}\int_a^b \left[\mathcal{R}\int_a^{\mathcal{R}} \frac{1}{r}(g_r - g_\theta)\, dr\right] d\mathcal{R}$$

$$+ \frac{C_1[b^2(1-2\nu) - a^2] - a^2\nu\epsilon_z}{b^2\,(1-2\nu)} + \frac{(1+\nu)\, a^2\sigma_{ra}}{b^2\, E} \quad . \qquad (23)$$

Substituting $\epsilon_{rb}$ and $\epsilon_{\theta b}$ from Equations 22 and 23 in Equation 4 and equating to the normal stress $\sigma_{rb}$ at the outer surface give

$$C_1 = -\nu\epsilon_z + \left\{\frac{1-2\nu}{b^2-a^2}\right\}\left\{\frac{(1+\nu)(b^2\sigma_{rb}-a^2\sigma_{ra})}{E} + \int_a^b \mathcal{R}\, g_r\, d\mathcal{R}\right.$$

$$+ \frac{\nu}{(1-\nu)}\int_a^b \mathcal{R}\,(g_\theta + g_z)\, d\mathcal{R} - b^2\int_a^b \frac{1}{\mathcal{R}}(g_r - g_\theta)\, d\mathcal{R}$$

$$\left. + \frac{(1-2\nu)}{(1-\nu)}\int_a^b \left[\mathcal{R}\int_a^{\mathcal{R}} \frac{1}{r}(g_r - g_\theta)\, dr\right] d\mathcal{R}\right\} \quad . \tag{24}$$

Substitution of $C_1$ from Equation 24 in Equation 21 yields

$$C_2 = \left\{\frac{a^2}{b^2-a^2}\right\}\left\{\frac{b^2(1+\nu)(\sigma_{rb}-\sigma_{ra})}{E} + \int_a^b \mathcal{R}\, g_r\, d\mathcal{R}\right.$$

$$+ \frac{\nu}{(1-\nu)}\int_a^b \mathcal{R}\,(g_\theta + g_z)\, d\mathcal{R} - b^2\int_a^b \frac{1}{\mathcal{R}}(g_r - g_\theta)\, d\mathcal{R}$$

$$\left. + \frac{(1-2\nu)}{(1-\nu)}\int_a^b \left[\mathcal{R}\int_a^{\mathcal{R}} \frac{1}{r}(g_r - g_\theta)\, dr\right] d\mathcal{R}\right\} \quad . \tag{25}$$

We may now obtain expressions for the stresses $\sigma_r$, $\sigma_\theta$, and $\sigma_z$ by substituting $C_1$ and $C_2$ from Equations 24 and 25 in Equations 15 and 16 to obtain u and $du/dr = \epsilon_r$. The expressions for $\epsilon_r$ and $\epsilon_\theta = u/r$ are substituted in Equations 4, 5, and 6, giving

$$\sigma_r = \frac{(a^2b^2-a^2R^2)\sigma_{ra} + (R^2b^2-a^2b^2)\sigma_{rb}}{(b^2-a^2)R^2} + \left(\frac{E}{1+\nu}\right)\left(-\frac{1}{R^2}\int_a^R \mathcal{R}\, g_r\, d\mathcal{R}\right.$$

$$- \frac{\nu}{(1-\nu)R^2}\int_a^R \mathcal{R}\,(g_\theta + g_z)\, d\mathcal{R} - \frac{(1-2\nu)}{(1-\nu)R^2}\int_a^R \left[\mathcal{R}\int_a^{\mathcal{R}} \frac{1}{r}(g_r - g_\theta)\, dr\right] d\mathcal{R}$$

$$- \int_a^R \frac{1}{\mathcal{R}}(g_r - g_\theta)\, d\mathcal{R} + \left\{\frac{R^2-a^2}{(b^2-a^2)R^2}\right\}\left\{\int_a^b \mathcal{R}\, g_r\, d\mathcal{R} + \frac{\nu}{(1-\nu)}\int_a^b \mathcal{R}\,(g_\theta + g_z)\, d\mathcal{R}\right.$$

$$\left.\left. - b^2\int_a^b \frac{1}{\mathcal{R}}(g_r - g_\theta)\, d\mathcal{R} + \frac{(1-2\nu)}{(1-\nu)}\int_a^b \left[\mathcal{R}\int_a^{\mathcal{R}} \frac{1}{r}(g_r - g_\theta)\, dr\right] d\mathcal{R}\right\}\right) \tag{26}$$

$$\sigma_\theta = \frac{b^2(a^2+R^2)\sigma_{rb} - a^2(b^2+R^2)\sigma_{ra}}{(b^2-a^2)\,R^2} + \left(\frac{E}{1+\nu}\right)\left(\frac{1}{R^2}\int_a^R \mathcal{R}\, g_r\, d\mathcal{R}\right.$$

$$+ \frac{\nu}{(1-\nu)R^2}\int_a^R \mathcal{R}\,(g_\theta + g_z)\, d\mathcal{R} + \frac{(1-2\nu)}{(1-\nu)R^2}\int_a^R \left[\mathcal{R}\int_a^{\mathcal{R}} \frac{1}{r}(g_r - g_\theta)\, dr\right] d\mathcal{R}$$

$$+ \frac{\nu}{(1-\nu)}\int_a^R \frac{1}{\mathcal{R}}(g_r - g_\theta)\, d\mathcal{R} - \frac{g_\theta + \nu g_z}{1-\nu} + \left\{\frac{a^2+R^2}{(b^2-a^2)R^2}\right\}\left\{\int_a^b \mathcal{R}\, g_r\, d\mathcal{R} + \frac{\nu}{(1-\nu)}\right.$$

$$\left.\left.\int_a^b \mathcal{R}\,(g_\theta + g_z)\, d\mathcal{R} - b^2\int_a^b \frac{1}{\mathcal{R}}(g_r - g_\theta)\, d\mathcal{R} + \frac{(1-2\nu)}{(1-\nu)}\int_a^b \left[\mathcal{R}\int_a^{\mathcal{R}} \frac{1}{r}(g_r - g_\theta)\, dr\right] d\mathcal{R}\right\}\right) \tag{27}$$

$$\sigma_z = \frac{2\nu(b^2\sigma_{rb} - a^2\sigma_{ra})}{(b^2-a^2)} + E\left(\epsilon_z + \left\{\frac{1}{1-\nu^2}\right\}\left\{\nu\int_a^R \frac{1}{\mathcal{R}}(g_r - g_\theta)\, d\mathcal{R} - g_z - \nu g_\theta\right\}\right.$$

$$+\left\{\frac{2\nu}{b^2-a^2}\right\}\left\{\frac{\nu}{(1-\nu^2)}\int_a^b \mathcal{R}\,(g_\theta + g_z)\, d\mathcal{R} + \frac{(1-2\nu)}{(1-\nu^2)}\int_a^b \left[\mathcal{R}\int_a^{\mathcal{R}} \frac{1}{r}(g_r - g_\theta)\, dr\right] d\mathcal{R}\right.$$

$$\left.\left. + \frac{1}{(1+\nu)}\int_a^b \mathcal{R}\, g_r\, d\mathcal{R} - \frac{b^2}{(1+\nu)}\int_a^b \frac{1}{\mathcal{R}}(g_r - g_\theta)\, d\mathcal{R}\right\}\right) \quad . \tag{28}$$

To find $\sigma_z$, we apply Saint-Venant's principle, assuming that the net force represented by the integral of the longitudinal stress $\sigma_z$ over the cross section is in equilibrium with the net force represented by the product of the normal stress $\sigma_z$ at the boundary and the cross-sectional area:

$$2\pi\int_a^b \mathcal{R}\,\sigma_z\, d\mathcal{R} = \pi\,(b^2-a^2)\,\sigma_{z'} \quad . \tag{29}$$

Substituting $\epsilon_z$ from Equation 28 in Equation 29 and solving for $\sigma_z$ yields

$$\epsilon_z = \frac{\sigma_{z\ell}}{E} + \left(\frac{1}{b^2-a^2}\right)\left(-\frac{2\nu(b^2\sigma_{rb} - a^2\sigma_{ra})}{E} - \left\{\frac{2}{1-\nu}\right\}\left\{\nu\int_a^b \mathcal{R}\, g_r\, d\mathcal{R}\right.\right.$$

$$+ \frac{\nu^2}{1-\nu}\int_a^b \mathcal{R}\,(g_\theta + g_z)\, d\mathcal{R} + 2\nu\int_a^b \left[\mathcal{R}\int_a^{\mathcal{R}} \frac{1}{r}(g_r - g_\theta)\, dr\right] d\mathcal{R}$$

$$\left.\left. - \frac{1}{1-\nu}\int_a^b \mathcal{R}\,(g_z + \nu g_\theta)\, d\mathcal{R} - \nu b^2\int_a^b \frac{1}{\mathcal{R}}(g_r - g_\theta)\, d\mathcal{R}\right\}\right) \tag{30}$$

Substitution of the longitudinal strain $\epsilon_z$ from Equation 30 in Equations 24 and 28 gives

$$C_1 = -\frac{\nu\sigma_{z\ell}}{E} + \left(\frac{1}{b^2-a^2}\right)\left(\frac{(1-\nu)(b^2\sigma_{rb}-a^2\sigma_{ra})}{E} + \left\{\frac{1}{1+\nu}\right\}\left\{(1-\nu)\int_a^b \mathcal{R} g_r \, d\mathcal{R}\right.\right.$$

$$+ \nu\int_a^b \mathcal{R}\,(g_\theta + g_z)\, d\mathcal{R} - \frac{2\nu}{(1-\nu)}\int_a^b \mathcal{R}\,(g_z + \nu g_\theta)\, d\mathcal{R}$$

$$- b^2(1-\nu)\int_a^b \frac{1}{\mathcal{R}}(g_r - g_\theta)\, d\mathcal{R} + \frac{(1-3\nu+4\nu^2)}{(1-\nu)}$$

$$\left.\left.\int_a^b \left[\mathcal{R}\int_a^{\mathcal{R}} \frac{1}{r}(g_r - g_\theta)\, dr\right] d\mathcal{R}\right\}\right) \qquad (31)$$

and

$$\sigma_z = \sigma_{z\ell} + \left(\frac{E}{1-\nu^2}\right)\left(-(g_z + \nu g_\theta) + \nu\int_a^R \frac{1}{\mathcal{R}}(g_r - g_\theta)\, d\mathcal{R}\right.$$

$$\left.+\left\{\frac{2}{b^2-a^2}\right\}\left\{\int_a^b \mathcal{R}\,(g_z + \nu g_\theta)\, d\mathcal{R} - \nu\int_a^b \left[\mathcal{R}\int_a^{\mathcal{R}} \frac{1}{r}(g_r - g_\theta)\, dr\right] d\mathcal{R}\right\}\right) \quad . (32)$$

We may now proceed to evaluate Equation 15 for displacements $u_a$, of the inner surface, and $u_b$, of the outer surface, by replacing $C_2$ and $C_1$ in Equation 15 by the expressions given for these quantities in Equations 25 and 31, yielding

$$u_a = a\left[-\frac{\nu\sigma_{z\ell}}{E} + \left(\frac{1}{b^2-a^2}\right)\left(\frac{2b^2\sigma_{rb} - [a^2(1-\nu)+b^2(1+\nu)]\sigma_{ra}}{E}\right.\right.$$

$$+\left\{\frac{2}{1+\nu}\right\}\left\{\int_a^b \mathcal{R}\, g_r\, d\mathcal{R} + \nu\int_a^b \mathcal{R}\, g_\theta\, d\mathcal{R} - b^2\int_a^b \frac{1}{\mathcal{R}}(g_r - g_\theta)\, d\mathcal{R}\right.$$

$$\left.\left.\left.+ (1-\nu)\int_a^b \left[\mathcal{R}\int_a^{\mathcal{R}} \frac{1}{r}(g_r - g_\theta)\, dr\right] d\mathcal{R}\right\}\right)\right] \qquad (33)$$

and

$$u_b = b\left[-\frac{\nu\sigma_{z\ell}}{E}+\left(\frac{1}{b^2-a^2}\right)\left(\frac{[b^2(1-\nu)+a^2(1+\nu)]\sigma_{rb}-2a^2\sigma_{ra}}{E}\right.\right.$$

$$+\left\{\frac{1}{1+\nu}\right\}\left\{2\int_a^b \mathcal{R}\ g_r\,d\mathcal{R}+2\nu\int_a^b \mathcal{R}\ g_\theta\,d\mathcal{R}-\left[b^2(1-\nu)+a^2(1+\nu)\right]\right.$$

$$\left.\left.\left.\int_a^b \frac{1}{\mathcal{R}}(g_r-g_\theta)\,d\mathcal{R}+2(1-\nu)\int_a^b\left[\mathcal{R}\int_a^{\mathcal{R}}\frac{1}{r}(g_r-g_\theta)\,dr\right]\,d\mathcal{R}\right\}\right)\right] \quad . (34)$$

## SUMMARY AND CONCLUSIONS

Equations have been derived for the prediction of dimensional changes and stresses in thick-walled, hollow, cylindrical uranium fuel cores during thermal neutron irradiation.

In the derivation, we have assumed that:

1. The cores adjust elastically to stresses occasioned by anisotropic dimensional changes within individual crystallites.
2. There is cylindrical symmetry of dimensional changes, stress, and strain.
3. There is elastic isotropy and homogeneity (elastic constants uniform throughout and independent of direction).
4. A state of plane strain exists (end effects may be neglected).

The radial displacements of the inside surface, $u_a$, of the outside surface, $u_b$, and the longitudinal displacement $u_z$ are given by

$$u_a = a\left[-\frac{\nu\sigma_{z\ell}}{E}+\left(\frac{1}{b^2-a^2}\right)\left(\frac{2b^2\sigma_{rb}-[a^2(1-\nu)+b^2(1+\nu)]\sigma_{ra}}{E}\right.\right.$$

$$+\left\{\frac{2}{1+\nu}\right\}\left\{\int_a^b \mathcal{R}\ g_r\,d\mathcal{R}+\nu\int_a^b \mathcal{R}\ g_\theta\,d\mathcal{R}-b^2\int_a^b \frac{1}{\mathcal{R}}(g_r-g_\theta)\,d\mathcal{R}\right.$$

$$\left.\left.\left.+(1-\nu)\int_a^b\left[\mathcal{R}\int_a^{\mathcal{R}}\frac{1}{r}(g_r-g_\theta)\,dr\right]\,d\mathcal{R}\right\}\right)\right] \quad (35)$$

$$u_b = b\left[-\frac{\nu\sigma_{z\ell}}{E}+\left(\frac{1}{b^2-a^2}\right)\left(\frac{[b^2(1-\nu)+a^2(1+\nu)]\sigma_{rb}-2a^2\sigma_{ra}}{E}\right.\right.$$

$$+\left\{\frac{1}{1+\nu}\right\}\left\{2\int_a^b \mathcal{R}\ g_r\,d\mathcal{R}+2\nu\int_a^b \mathcal{R}\ g_\theta\,d\mathcal{R}-[b^2(1-\nu)+a^2(1+\nu)]\right.$$

$$\left.\left.\left.\int_a^b \frac{1}{\mathcal{R}}(g_r-g_\theta)\,d\mathcal{R}+2(1-\nu)\int_a^b\left[\mathcal{R}\int_a^{\mathcal{R}}\frac{1}{r}(g_r-g_\theta)\,dr\right]d\mathcal{R}\right\}\right)\right] \quad (36)$$

$$u_z = L\epsilon_z = L\left[\frac{\sigma_{z\ell}}{E}+\left(\frac{1}{b^2-a^2}\right)\left(-\frac{2\nu(b^2\sigma_{rb}-a^2\sigma_{ra})}{E}\right.\right.$$

$$-\left\{\frac{2}{1+\nu}\right\}\left\{\nu\int_a^b \mathcal{R}\ g_r\,d\mathcal{R}+\frac{\nu^2}{(1-\nu)}\int_a^b \mathcal{R}\ (g_\theta+g_z)\,d\mathcal{R}\right.$$

$$+2\nu\int_a^b\left[\mathcal{R}\int_a^{\mathcal{R}}\frac{1}{r}(g_r-g_\theta)\,dr\right]d\mathcal{R}-\frac{1}{(1-\nu)}\int_a^b \mathcal{R}\ (g_z+\nu g_\theta)\,d\mathcal{R}$$

$$\left.\left.\left.-\nu b^2\int_a^b \frac{1}{\mathcal{R}}(g_r-g_\theta)\,d\mathcal{R}\right\}\right)\right] \quad (37)$$

The radial stress $\sigma_r$, the tangential stress $\sigma_\theta$, and the longitudinal stress $\sigma_z$, are given by

$$\sigma_r = \frac{(a^2b^2-a^2R^2)\sigma_{ra}+(R^2b^2-a^2b^2)\sigma_{rb}}{(b^2-a^2)R^2}+\left(\frac{E}{1+\nu}\right)\left(-\frac{1}{R^2}\int_a^R \mathcal{R}\ g_r\,d\mathcal{R}\right.$$

$$-\frac{\nu}{(1-\nu)R^2}\int_a^R \mathcal{R}\ (g_\theta+g_z)\,d\mathcal{R}-\frac{1-2\nu}{(1-\nu)R^2}\int_a^R\left[\mathcal{R}\int_a^{\mathcal{R}}\frac{1}{r}(g_r-g_\theta)\,dr\right]d\mathcal{R}$$

$$+\int_a^R \frac{1}{\mathcal{R}}(g_r-g_\theta)\,d\mathcal{R}+\left\{\frac{R^2-a^2}{(b^2-a^2)R^2}\right\}\left\{\int_a^b \mathcal{R}\ g_r\,d\mathcal{R}+\frac{\nu}{(1-\nu)}\int_a^b \mathcal{R}\ (g_\theta+g_z)\,d\mathcal{R}\right.$$

$$\left.\left.-b^2\int_a^b \frac{1}{\mathcal{R}}(g_r-g_\theta)\,d\mathcal{R}+\frac{(1-2\nu)}{(1-\nu)}\int_a^b\left[\mathcal{R}\int_a^{\mathcal{R}}\frac{1}{r}(g_r-g_\theta)\,dr\right]d\mathcal{R}\right\}\right) \quad (38)$$

$$\sigma_\theta = \frac{b^2(a^2+R^2)\sigma_{rb} - a^2(b^2+R^2)\sigma_{ra}}{(b^2-a^2)R^2} + \left(\frac{E}{1+\nu}\right)\left(\frac{1}{R^2}\int_a^R \mathcal{R}\, g_r\, d\mathcal{R}\right.$$

$$+ \frac{\nu}{(1-\nu)R^2}\int_a^R \mathcal{R}\,(g_\theta + g_z)\, d\mathcal{R} + \frac{1-2\nu}{(1-\nu)R^2}\int_a^R \left[\mathcal{R}\int_a^{\mathcal{R}} \frac{1}{r}(g_r - g_\theta)\, dr\right] d\mathcal{R}$$

$$+ \frac{\nu}{(1-\nu)}\int_a^R \frac{1}{\mathcal{R}}(g_r - g_\theta)\, d\mathcal{R} - \frac{g_\theta + \nu g_z}{1-\nu}$$

$$+\left\{\frac{a^2+R^2}{(b^2-a^2)R^2}\right\}\left\{\int_a^b \mathcal{R}\, g_r\, d\mathcal{R} + \frac{\nu}{(1-\nu)}\int_a^b \mathcal{R}\,(g_\theta + g_z)\, d\mathcal{R}\right.$$

$$\left.\left. - b^2\int_a^b \frac{1}{\mathcal{R}}(g_r - g_\theta)\, d\mathcal{R} + \frac{(1-2\nu)}{(1-\nu)}\int_a^b \left[\mathcal{R}\int_a^{\mathcal{R}} \frac{1}{r}(g_r - g_\theta)\, dr\right] d\mathcal{R}\right\}\right) \tag{39}$$

$$\sigma_z = \sigma_{z\ell} + \left(\frac{E}{1-\nu^2}\right)\left(-g_z - \nu g_\theta + \nu\int_a^R \frac{1}{\mathcal{R}}(g_r - g_\theta)\, d\mathcal{R}\right.$$

$$\left.+\left\{\frac{2}{b^2-a^2}\right\}\left\{\int_a^b \mathcal{R}\,(g_z + \nu g_\theta)\, d\mathcal{R} - \nu\int_a^b \left[\mathcal{R}\int_a^{\mathcal{R}} \frac{1}{r}(g_r - g_\theta)\, dr\right] d\mathcal{R}\right\}\right) \tag{40}$$

## LIST OF SYMBOLS EMPLOYED

| | |
|---|---|
| E | Young's Modulus |
| $\nu$ | Poisson's Ratio |
| r, $\mathcal{R}$ | Radial coordinate in cylindrical coordinate system. |
| R | Specified value of radial coordinate. |
| $\theta$ | Angular coordinate in cylindrical coordinate system. |
| z | Linear coordinate in cylindrical coordinate system. |
| a | Value of radial coordinate at inner surface. |
| b | Value of radial coordinate at outer surface. |
| L | Length of fuel element core. |

$\sigma_{ra}$ Normal stress applied to inner surface of fuel element core - positive for applied tension, negative for applied compression.

$\sigma_{rb}$ Normal stress applied to outer surface of fuel element core - positive for applied tension, negative for applied compression.

$\sigma_{z\ell}$ Normal stress applied to ends of fuel element core - positive for applied tension, negative for applied compression.

$g_r$ Estimate of local radial strain arising from thermal neutron irradiation if constraints are neglected.

$g_\theta$ Estimate of local tangential strain arising from thermal neutron irradiation if constraints are neglected

$g_z$ Estimate of local longitudinal strain arising from thermal neutron irradiation if constraints are neglected

Approximate values for $g_r$, $g_\theta$, and $g_z$ may be obtained by multiplying the appropriate value of $G_2$ or $G_3$[4] by a proportionality constant relating these values to dimensional changes for unit burnup, and by total burnup.

If the stress at any point calculated from Equations 38, 39 and 40 exceeds the creep strength of the metal at that point, a plastic solution is indicated.

## SUGGESTIONS FOR FURTHER STUDY

The above analysis fails to include stresses arising from thermal gradients in the cross section of the fuel element core.

An elastic solution for thermal stresses in a solid cylindrical fuel element core has been reported by Cadwell and Merckx.[7] A plastic solution for thermal stresses in solid cylindrical reactor fuel elements has been reported by Merckx.[8] An extensive review of the subject of thermal stresses in solid and hollow cylindrical fuel element cores, including the time dependence of strain, is given by Merckx.[9] Residual stresses arising from fabrication processes have been studied by Joseph.[10]

A more rigorous solution should incorporate stresses arising from thermal gradients and fabrication processes, and include the variation in elastic constants with position and direction.

Experimental data will be collected and predicted stresses calculated from Equations 38, 39 and 40 in an effort to ascertain whether a plastic solution is required.

# REFERENCES


1. Sturcken, E. F., An X-ray Method for Predicting the Stability of Natural Uranium at Low Burn-up, DP-251 (Nov. 1957) (Classified).

2. Sturcken, E. F., "A Generalized Growth Index Formalism," Papers Presented at the X-Ray Preferred Orientation Meeting Held at National Lead Company of Ohio, November 9 and 10, 1959, edited by P. R. Morris, NLCO-804 (July 15, 1960), p. 20.

3. Ibid., p. 17.

4. Ibid., p. 17, p. 20.

5. Timoshenko, S., and Goodier, J. N., Theory of Elasticity, 2nd ed., McGraw-Hill, New York, (1951), p. 408.

6. Ibid., p. 56, p. 406.

7. Cadwell, J. J., and Merckx, K. R., Elastic Solution for the Thermal Stresses in a Finite Solid Cylinder Fuel Element, HW-45965 (Oct. 12, 1956).

8. Merckx, K. R., Thermal Stresses in Cylindrical Reactor Fuel Elements, HW-42665 (Sept. 15, 1956).

9. Merckx, K. R., "Thermal Stresses in Fuel Elements," Chapter 700, Fuel Element Design Handbook, HW-51000 (Sept. 1, 1958) (Classified)

10. Joseph, J. W., Jr., Unpublished work.

# STATUS OF THE GROWTH INDEX FORMALISM*

Edward F. Sturcken
Savannah River Laboratories,
E. I. duPont de Nemours and Company

## SUMMARY

Since NLCO-804 was published, work has continued on various aspects of the irradiation growth parameter $G_2$ and the quantitative preferred orientation parameter J.[1] The $P(u,\phi)$ matrix for $G_2$ was computed and has gone through various stages of error correction, it is now correct by independent verification from MCW for the 20-plane case, and by NLO for the 18-plane case An IBM-650 program was written by Dr. J. C. English of SRL for computing $G_2$ and J from raw X-ray intensity data.

The ability of J to describe the same shape at different orientations in space was tested J was found to be invariant for six spatial orientations of the same ellipsoid, was shown to be related through a simple constant to statistical variance, $\sigma^2$, and was also demonstrated to be a physical analogue to the neutron physicist's "Roughness Factor " J was applied with success to Mueller et al.'s[2] preferred orientation (PO) studies of varying reduction in hot- and cold-rolled uranium rods.

A set of two-dimensional Fourier expansion functions, $P(\gamma,\phi)$, were tried in place of $P(u,\phi)$ to see if they were superior. The present set of expansion functions, $P(u,\phi)$, are composed of the product of $e^{im\phi}$ and the Associated Legendre polynomials, $\textcircled{H}_{\ell m}(u)$. It was found that the Fourier functions required more complex calculations for $G_2$ and J and, hence, were undesirable.

An irradiation experiment was prepared, in which PO is the only variable, to study PO as expressed by the strain tensor concept, i.e., $G_2$ or $G_3$, versus irradiation growth. The encapsulation technique and the PO X-ray measurements for the irradiation test specimens are described.

## INTRODUCTION

### The $P(u,\phi)$ Matrix**

An IBM-650 program has been written by Dr J. C. English of SRL for computing $\overline{G_2}$, $\overline{J}$, $\overline{B_{00}}$, $\overline{A_{\ell m}}$, and $\overline{P(u,\phi)}$ for 20 or 14 planes from raw

*The information contained in this article was developed during the course of work under contract AT(07-2)-1 with the U.S Atomic Energy Commission.

**Use notation given in Reference (1)

intensity data. The program also computes the 95% confidence interval of the mean, $\sigma t/\sqrt{N}$, for $G_2$, J, and $B_{00}$. The matrix [A] may be computed for any number of planes from input data composed only of the Miller indices and the lattice parameters (we used those of M. H. Mueller). The [A] matrix for the 20-plane case is compared in Table I with that computed by MCW employing a different routine and computer, but the same input data. The differences are insignificant insofar as their use for computing $G_2$ and J are concerned. The [A] matrix for the 18-plane case has been compared with that calculated by Thudium of NLO and found to be in essential agreement.

Table I

SRL AND MCW MATRICES (20-PLANE CASE)*

| | | | | | | | | | |
|---|---|---|---|---|---|---|---|---|---|
| 15.957 | 0.51086 | 2.8425 | 1.5208 | -0.05569 | 3.1782 | -1.0579 | 0.03942 | 1.6720 | -0.96082 |
| 15.957 | -0.51085 | 2.8322 | 1.5208 | -0.05549 | 3.1668 | -1.0579 | 0.03927 | -1.6660 | -0.95739 |
| 0.45693 | 15.146 | -1.6518 | -0.40187 | 1.4208 | -2.8770 | 3.5205 | -0.08042 | 1.9193 | 1.7991 |
| -0.45692 | 15.146 | -1.6458 | 0.40185 | 1.4157 | -2.8666 | 3.5206 | -0.08013 | 1.9124 | 1.7926 |
| 1.4625 | -0.95027 | 9.9390 | 0.23784 | -1.7337 | 0.80895 | 0.03878 | 1.9766 | 1.4619 | 2.1058 |
| 1.4625 | -0.95024 | 9.9032 | 0.23785 | -1.7275 | 0.80602 | -0.03879 | 1.9695 | 1.4566 | 2.0983 |
| 1.3518 | -0.39938 | 0.41088 | 16.955 | -1.7398 | 2.3892 | 2.0081 | 0.36524 | 0.33933 | 1.9374 |
| 1.3518 | -0.39936 | 0.40942 | 16.955 | -1.7335 | 2.3806 | 2.0081 | 0.36394 | -0.33811 | -1.9304 |
| -0.03308 | 0.94384 | -2.0019 | -1.1629 | 11.339 | 0.85975 | -0.08679 | -0.37484 | 3.1176 | -2.0537 |
| -0.03308 | 0.94385 | -1.9947 | -1.1628 | 11.298 | 0.85663 | -0.08680 | -0.37351 | 3.1061 | -2.0464 |
| 1.4274 | -1.4446 | 0.70611 | 1.2072 | 0.64991 | 8.1666 | -0.60220 | -0.24466 | 1.7712 | 2.9889 |
| 1.4274 | -1.4446 | 0.70355 | 1.2072 | 0.64755 | 8.1372 | -0.60223 | -0.24378 | -1.7649 | 2.9732 |
| -0.93895 | 3.4933 | -0.06689 | 2.0050 | -0.12965 | 1.1900 | 22.756 | -2.3657 | 0.56442 | 0.98274 |
| -0.93895 | 3.4934 | -0.06667 | 2.0050 | -0.12920 | -1.1857 | 22.756 | -2.3572 | 0.56239 | 0.97921 |
| 0.02405 | 0.05487 | 2.3443 | 0.25074 | -0.38500 | -0.33243 | 1.6266 | 13.414 | 1.1168 | 1.2684 |
| 0.02405 | -0.05486 | 2.3359 | 0.25075 | -0.38363 | -0.33124 | -1.6266 | 13.365 | 1.1147 | 1.2638 |
| -0.93145 | 1.1954 | 1.5827 | -0.21266 | 2.9231 | -2.1969 | 0.35427 | 1.0213 | 9.1471 | 0.15720 |
| -0.93145 | 1.1954 | 1.5770 | -0.21266 | 2.9126 | -2.1891 | 0.35427 | 1.0176 | 9.1143 | 0.15661 |
| 0.39531 | 0.82761 | 1.6838 | -0.89675 | -1.4221 | 2.7334 | 0.45557 | 0.85514 | 0.11610 | 11.652 |
| -0.39532 | 0.82756 | 1.6778 | 0.89674 | -1.4170 | 2.7236 | 0.45561 | 0.85209 | 0.11566 | 11.610 |

*For matrix terminology see Ref. 1. Each MCW element is listed under the SRL element.

## DISCUSSION

### Test of Goodness of Fit for $P(u,\phi)$

$P(u,\phi)$ was fitted to 20 points (hk$\ell$ poles) on the surface of an ellipsoid (see Fig. 1). The points calculated from the resulting $P(u,\phi)$ distribution function are compared with those calculated from the equation for the ellipsoid in Table II. Note that the agreement is exceptionally good.

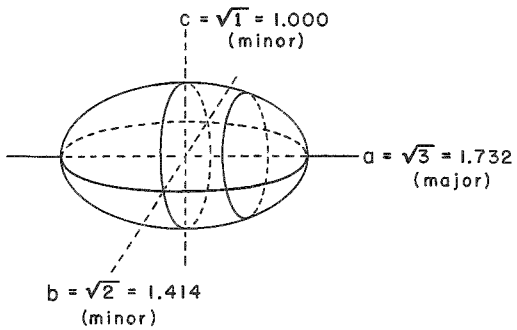


Fig. 1. Ellipsoid

$P(u,\phi)$ was also fitted to experimental data for beta-treated uranium rod and alpha-rolled uranium plate. The rod data came from a single specimen, and the plate data represent an average of eight specimens.

Table II

GOODNESS OF FIT TEST FOR ELLIPSOID

| hkℓ | P(u,φ) | |
|---|---|---|
| | Theoretical* | Experimental** |
| 020 | 1.732 | 1.730 |
| 110 | 1.461 | 1.461 |
| 021 | 1.404 | 1.402 |
| 002 | 1.000 | 0.998 |
| 111 | 1.312 | 1.312 |
| 022 | 1.176 | 1.173 |
| 112 | 1.159 | 1.158 |
| 130 | 1.608 | 1.607 |
| 131 | 1.498 | 1.500 |
| 023 | 1.091 | 1.094 |
| 200 | 1.414 | 1.414 |
| 041 | 1.607 | 1.610 |
| 113 | 1.088 | 1.088 |
| 132 | 1.324 | 1.324 |
| 133 | 1.206 | 1.205 |
| 114 | 1.054 | 1.055 |
| 150 | 1.672 | 1.671 |
| 223 | 1.222 | 1.222 |
| 152 | 1.472 | 1.474 |
| 312 | 1.337 | 1.337 |

*See ellipsoid in Fig. 1, whose equation in spherical coordinates is given in Table IV.

**Calculated P(u,φ) values from least-squares coefficients.

The experimentally measured points are compared with those calculated from P(u,φ) in Table III. Note that the goodness of fit is much poorer for the beta-treated rod data. This is as it should be, since the rod data contain large statistical fluctuations which P(u,φ) should not follow.

Table III

LEAST-SQUARES FIT OF $P(u,\phi)$ TO HOT-ROLLED PLATE AND BETA-TREATED ROD

| $hk\ell$ | Alpha-rolled Plate* | | Beta-treated Rod** | |
|---|---|---|---|---|
| | Experimental | $P(u,\phi)$ | Experimental | $P(u,\phi)$ |
| 020 | 4.08 | 3.68 | 0.53 | 0.60 |
| 110 | 1.28 | 1 26 | 0.74 | 0.72 |
| 021 | 0.34 | 0 14 | 0.58 | 0.82 |
| 002 | 0.01 | 0.00 | 0.27 | 0.32 |
| 111 | 0.23 | 0 30 | 0.71 | 0.77 |
| 022 | 0.11 | 0.00 | 0.75 | 0.70 |
| 112 | 0 04 | 0.00 | 1.07 | 0.81 |
| 130 | 2.64 | 2.31 | 0.40 | 0.39 |
| 131 | 0.99 | 1.20 | 0.49 | 0.39 |
| 023 | 0.02 | 0.33 | 0 54 | 0 54 |
| 200 | 0.47 | 0 45 | 0.60 | 0.70 |
| 041 | 1.77 | 2.11 | 1.00 | 0.71 |
| 113 | 0.03 | 0.07 | 0.53 | 0.73 |
| 132 | 0.19 | 0.05 | 0.52 | 0.43 |
| 133 | 0 04 | 0 00 | 0.49 | 0.50 |
| 114 | 0.04 | 0.08 | 0.81 | 0.63 |
| 150 | 2.92 | 2.90 | 0.26 | 0.41 |
| 223 | 0.06 | 0.03 | 0.46 | 0.80 |
| 152 | 0.63 | 0.77 | 0.54 | 0.52 |
| 312 | 0.23 | 0.18 | 1.14 | 0.92 |
| | J = 3.02 | | J = 1.09 | |

*Experimental data for 8-specimen average; grain size approximately 20 microns.

**Experimental data for a single specimen, grain size approximately 250 microns.

## Invariance of J with Respect to Rotation

The ability of J to describe the same shape at different orientations in space has been tested. For mathematical simplicity, the shape chosen was the ellipsoid in Fig. 1. The ellipsoid was rotated about its axes to six positions while the directions defining the points ($hk\ell$ poles) on the surface of the ellipsoid to be fitted to $P(u,\phi)$ remained fixed. In this manner these 20 spatial directions were given six different sets of "intensities," each set

being fitted by a $P(u,\phi)$ function. Values of J were computed for each $P(u,\phi)$ function and are given in Table IV. Note that J remains unchanged as it should, since the volume and shape of the surface were not changed.

Table IV

TEST OF INVARIANCE OF J

The ellipsoid $\frac{x^2}{a^2} + \frac{y^2}{b^2} + \frac{z^2}{c^2} = 1$ in spherical coordinates is

$$r^2 \left\{ \frac{\sin^2\gamma \cos^2\phi}{a^2} + \frac{\sin^2\gamma \sin^2\phi}{b^2} + \frac{\cos^2\gamma}{c^2} \right\} = 1 \quad .$$

The ellipsoid is given one and two-fold rotations by permutating the axes a, b, and c. J was calculated for the following orientations:

| Ellipsoid Axes | | | | Ellipsoid Axes | | | |
|---|---|---|---|---|---|---|---|
| $a^2$ | $b^2$ | $c^2$ | J | $a^2$ | $b^2$ | $c^2$ | J |
| 3 | 2 | 1 | 1.0210 | 3 | 1 | 2 | 1.0211 |
| 2 | 3 | 1 | 1.0211 | 2 | 1 | 3 | 1.0211 |
| 1 | 2 | 3 | 1.0210 | 1 | 3 | 2 | 1.0210 |

Relation of "J" to Statistical Variance, $\sigma^2$ - by J. W. Croach

J has been defined as

$$J = \frac{\pi}{2} \int_0^1 \int_0^{\pi/2} P^2(u,\phi)\, du\, d\phi = \frac{\pi}{2} \sum_{\ell} \sum_{m} A^2_{\ell m} \quad , \tag{1}$$

where $A_{\ell m}$ are the normalized coefficients of the least-squares fit. For $P(u,\phi)$ = constant only $A_{00}$, which is independent of u and $\phi$, is required to describe $P(u,\phi)$, so (1) reduces to

$$J = \frac{\pi}{2} A^2_{00} = 1 \quad .$$

By definition, the statistical variance of $P(u,\phi)$ is given as

$$\sigma^2 = \frac{2}{\pi} \int_0^1 \int_0^{\pi/2} (P - \bar{P})^2\, du\, d\phi \quad , \tag{2}$$

where $P(u,\phi)$ is abbreviated to P.

Expanding equation (2)

$$\sigma^2 = \frac{2}{\pi}\int_0^1 \int_0^{\pi/2} \left\{ P^2 - 2P\bar{P} + \bar{P}^2 \right\} \, du d\phi$$

$$= \frac{2}{\pi}\int_0^1 \int_0^{\pi/2} P^2 \, du d\phi - \frac{2}{\pi} 2\bar{P} \int_0^1 \int_0^{\pi/2} P \, du d\phi + \frac{2}{\pi} \bar{P}^2 \int_0^1 \int_0^{\pi/2} du d\phi$$

$$= \left(\frac{2}{\pi}\right)\left(\frac{2}{\pi}\right) J - \left(\frac{2}{\pi}\right)(2)(\bar{P})(1) + \left(\frac{2}{\pi}\right)(\bar{P}^2)\left(\frac{\pi}{2}\right) \quad . \tag{3}$$

But $\bar{P} = \frac{2}{\pi}$, so

$$\sigma^2 = \left(\frac{2}{\pi}\right)^2 J - 2\left(\frac{2}{\pi}\right)^2 + \left(\frac{2}{\pi}\right)^2 = \left(\frac{2}{\pi}\right)^2 (J - 1) \quad .$$

Thus

$$\sigma^2 = \frac{4}{\pi^2} (J - 1)$$

and

$$J = 1 + \frac{\sigma^2}{(\bar{P})^2} \quad .$$

Interpretation of J as a "Roughness Factor" - by J. W. Croach

Consider the ratio of the average value of $P^2(u,\phi)$ to the square of the average value of $P(u,\phi)$, i.e.,

$$\frac{\overline{(P^2)}}{(\bar{P})^2} = \frac{\cancel{\left(\frac{2}{\pi}\right)}\int_0^1 \int_0^{\pi/2} P^2(u,\phi) \, du d\phi}{(2/\pi)^{\cancel{2}}} \quad , \tag{1}$$

since $\bar{P} = 2/\pi$, which reduces to

$$\frac{\overline{(P^2)}}{(\bar{P})^2} = \pi/2 \int_0^1 \int_0^{\pi/2} P^2(u,\phi) \, du d\phi = J \quad . \tag{2}$$

Now the neutron physicist defines a "Roughness Factor" for the flux distribution $\phi$ as

$$R = \overline{(\phi^2)}/\overline{(\phi)}^2 \quad . \tag{3}$$

Hence J is the analogue of R.

## Application of the J Parameter to the Study of Preferred Orientation in Uranium Rods Rolled to Various Reductions at 300°C and 600°C

Mueller, Knott, Chernock, and Beck[2] have constructed inverse pole figures for uranium rod rolled at 300°C and 600°C to reductions of 0, 10, 45, and 70% reduction in area. The inverse pole figures are given in Figs. 2 and 4. A study of Figs. 2 and 4 shows (a) for the 300°C rolled rod, increasing PO with increasing cold work, and (b) for the 600°C rolled rods, increasing PO, to a lesser extent, with increasing hot work.

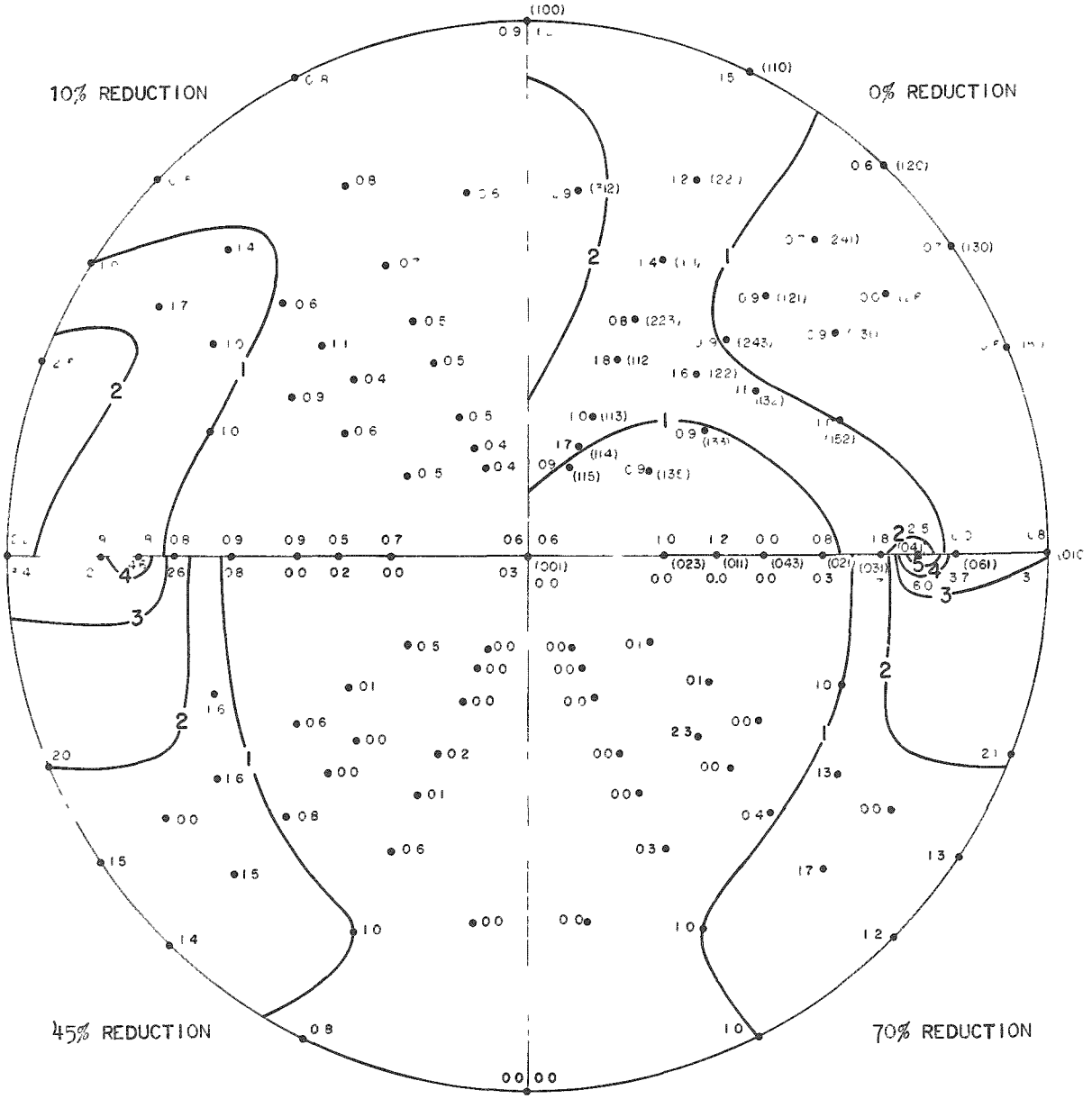


Fig. 2. Inverse Pole Figure of 300°C Rolled Rods with Prior Beta Treatment. After Mueller, Knott, Chernock, and Beck, Reference (2).

$P(u,\phi)$ functions and J values were computed for each reduction given above. A plot of J versus % reduction is given for the 300°C rolled

rod in Fig. 3 and for the 600°C rolled rod in Fig. 5. Note that we can deduce quantitatively from J versus % reduction in Figs. 3 and 5 what we deduce qualitatively from a study of the inverse pole figures 2 and 4.

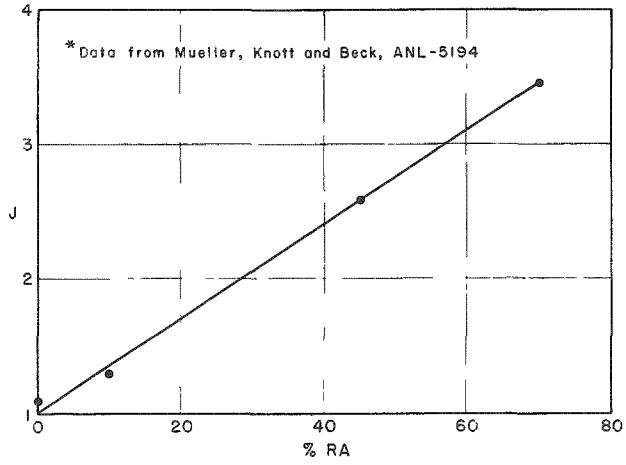


Fig. 3

Quantitative PO Parameter, J, vs % Reduction in Uranium Rod Rolled at 300°C

The J parameter is not a substitute for the inverse pole figure, since it does not specify the kind of orientation. It should, however, provide a handy quantitative method for following the amount of orientation induced by various fabrication schedules. The inverse pole figure is difficult to use for quantitative estimation of PO because, being a stereographic projection, it is not "area true."

## Alternative Expansion Function for $P(u,\phi)$

$P(u,\phi)$ has been expanded(1) as the product of the associated Legendre functions $\Theta_{\ell m}(u)$ and the function $e^{im\phi}$. It was suggested that expansion of $P(u,\phi)$ as a two-dimensional Fourier series might be a more desirable expansion, so such an expansion was carried out. Employing the symmetry properties given in Ref. (1), $P(\gamma,\phi)$* reduces to the form

$$P(\gamma,\phi) = \sum_{\ell=0}^{\infty} \sum_{m=0}^{\infty} A_{\ell m} \cos 2\ell\gamma \cos 2m\phi \qquad (1)$$

or, expanding into an orthonormal set of the first 10 permissible terms,

$$P(\gamma,\phi) = \frac{2}{\pi} A_{00} + \frac{2\sqrt{2}}{\pi} A_{10} \cos 2\gamma + \frac{2\sqrt{2}}{\pi} A_{01} \cos 2\phi + \frac{4}{\pi} A_{11} \cos 2\gamma \cos 2\phi$$
$$+ \frac{2\sqrt{2}}{\pi} A_{20} \cos 4\gamma + \frac{2\sqrt{2}}{\pi} A_{02} \cos 4\phi + \frac{4}{\pi} A_{21} \cos 4\gamma \cos 2\phi$$
$$+ \frac{4}{\pi} A_{12} \cos 2\gamma \cos 4\phi + \frac{4}{\pi} A_{22} \cos 4\gamma \cos 4\phi + \frac{2\sqrt{2}}{\pi} A_{30} \cos 6\gamma \quad . \qquad (2)$$

*Substitution of a second variable, $\cos\gamma = u$ has no advantage in this expansion.

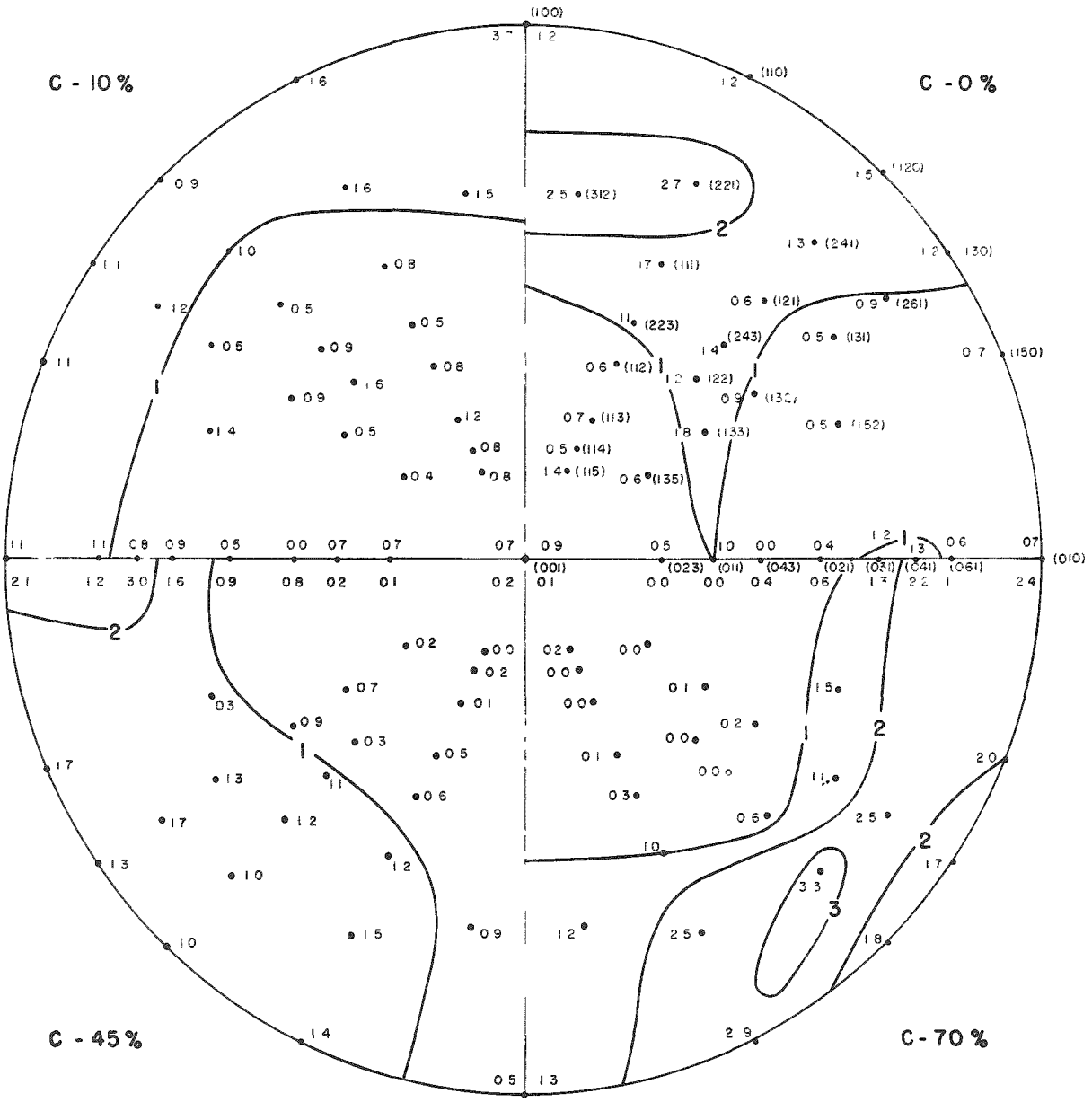


Fig. 4. Inverse Pole Figure of 600°C Rolled Rods with Prior Beta Treatment. After Mueller, Knott, and Beck, Reference (2).

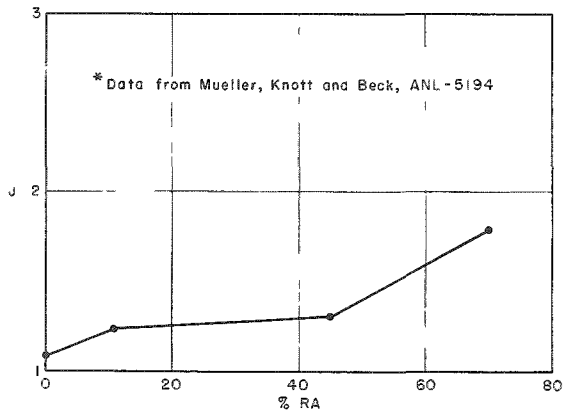


Fig. 5

Quantitative PO Parameter, J, vs % Reduction in Uranium Rod Rolled at 600°C.

The two-dimensional Fourier expansion, Equation (2), has the following undesirable properties:

1. To normalize $R(\gamma,\phi)$ to $P(\gamma,\phi)$ as before[1] requires 4 least-squares coefficients or, in general, all $B_{\ell 0}$ coefficients, rather than simply $B_{00}$, as was the case with the associated Legendre polynomials (ALP).

2. To calculate $G_2$ requires 3 least-squares coefficients or, in general, all $A_{\ell 1}$, rather than simply $A_{22}$, as was the case for the ALP expansion.

3. J will have 44 nonzero terms rather than 10, as was the case for the ten-term ALP expansion. In general, J will be the sum of $A^2_{\ell m}$ plus $A_{\ell m} A_{jk}$, where m = k.

As regards other expansions for $P(u,\phi)$, the only one appearing to have possibilities at this time is the Legendre functions times $e^{im\phi}$ rather than the associated Legendre functions times $e^{im\phi}$.

## Controlled Irradiation Experiment to Correlate Preferred Orientation with Anisotropic Growth

Considerable progress has been made by the committee toward measuring and describing PO ($G_2$, $G_3$ plus employing more precise $I^\circ$ values) in a quantitative fashion.

The correlation of PO with anisotropic growth has been limited.[1,3-5] Predictions at this stage are semiquantitative and leave much to be desired, since many of the factors affecting growth have not been evaluated. As a matter of fact, the irradiation data and experimental conditions, to date, have not been adequate to give a really severe test to our strain-tensor postulate.

A program has been initiated at SRL to correlate PO and anisotropic growth as a function of fuel geometry, grain size, cladding restraint, flux, burnup, and irradiation temperature. The variables will be studied one at a time when feasible (e.g., irradiation temperature and flux normally go hand in hand unless one employs external heating or cooling).

In the first experiment all fabrication variables except PO are to be held constant. PO is varied by machining a series of 2-inch long by $\frac{5}{32}$-inch diameter cylinders at varying angles to the rolling direction from a single section of alpha-rolled plate (fabrication described previously).[4] The diameters of the cylinders were limited by the thickness of the plate, 0.180 inch. Twenty specimens were prepared at 5-degree intervals between 5 and 90 degrees to the rolling direction and in a plane normal to the rolling direction.

PO measurements were performed on the same specimens that were to be irradiated. The small diameter of the specimens presented a special problem, since the area of the X-ray beam was larger than the specimen, thereby forbidding the use of the standard calculated intensities, $I^{\circ}_{hk\ell}$, for normalization.(1) The problem was solved by preparing three "randomly" oriented rod specimens of the same diameter as the test specimens. The rods were machined from three mutually perpendicular directions of a section of hot-pressed powder metal plate. A large section of this plate had given relative intensities in good agreement with the standard calculated intensities, $I^{\circ}_{hk\ell}$.(1) The three rod specimens were each run five times on each of the three diffractometers used for the study. A set of experimental $I^{\circ}_{hk\ell}$ values, composed of a 15-run average, was prepared for each diffractometer. The experimental average $I^{\circ}_{hk\ell}$ for each diffractometer is shown in Table V.

Table V

EXPERIMENTAL RANDOM INTENSITIES FOR SMALL CYLINDERS

| hk$\ell$ | $I^{\circ}_{hk\ell}$ for 15-specimen Average** | | | $I^{\circ}_{hk\ell}$ for 45-specimen Average | |
|---|---|---|---|---|---|
| | A Machine | B Machine | C Machine | ABC Average | $\sigma \sqrt{I^{\circ}} \times 100$ |
| 020 | 0.0760 | 0.0719 | 0.0728 | 0.0736 | 3.0 |
| 110 | 0.9763 | 0.9941 | 0.9971 | 0.9892 | 1.1 |
| 021 | 1.3988 | 1.4304 | 1.3863 | 1.4052 | 1.6 |
| 002 | 0.6929 | 0.7303 | 0.6971 | 0.7068 | 2.9 |
| 111 | 0.9380 | 0.9934 | 0.9660 | 0.9658 | 9.1 |
| 022 | 0.0814 | 0.0798 | 0.0784 | 0.0799 | 2.8 |
| 112 | 1.0446 | 1.1130 | 1.0442 | 1.0673 | 3.7 |
| 130 | 0.0856 | 0.0838 | 0.0783 | 0.0826 | 4.7 |
| 131 | 0.9806 | 1.0054 | 0.9820 | 0.9893 | 1.4 |
| 040 | 0.1691 | 0.1633 | 0.1690 | 0.1671 | 1.9 |
| 023 | 0.4599 | 0.4635 | 0.4608 | 0.4614 | 0.5 |
| 200 | 0.2416 | 0.2259 | 0.2334 | 0.2336 | 3.5 |
| 041 | 0.1417 | 0.1353 | 0.1369 | 0.1380 | 2.8 |
| 113 | 0.3368 | 0.3432 | 0.3305 | 0.3368 | 1.9 |
| 132 | 0.1099 | 0.1083 | 0.1088 | 0.1090 | 2.1 |
| 133 | 0.5343 | 0.5021 | 0.5197 | 0.5187 | 3.1 |
| 114 | 0.3484 | 0.3359 | 0.3430 | 0.3424 | 1.8 |
| 150 | 0.2398 | 0.2230 | 0.2369 | 0.2332 | 3.8 |
| 223 | 0.4335 | 0.3920 | 0.4182 | 0.4146 | 5.0 |
| 152 | 0.4615 | 0.4064 | 0.4558 | 0.4412 | 6.9 |
| 312 | 0.2912 | 0.2374 | 0.2786 | 0.2691 | 10.5 |
| | | | | | Av. 3.5% |

*Three $\frac{5}{32}$-inch rods cut from mutually perpendicular directions of SEP hot-pressed powder metal plate.

**Five runs on each of three rods at depth intervals of approximately 0.010 inch.

The agreement between diffractometers is considered excellent, since one of them employed a Xe-proportional counter detector, whereas the other two employed NaI(Tl) detectors. Because of the close agreement between diffractometers, an average set of $I^{\circ}_{hk\ell}$ values for all 45 runs was prepared and used to compute $G_2$ for all 20 test specimens. A special design, "cup type," specimen holder was used in these experiments to reduce background. The specimen holder along with the specimen polishing mount and spinner is shown in Fig. 6.

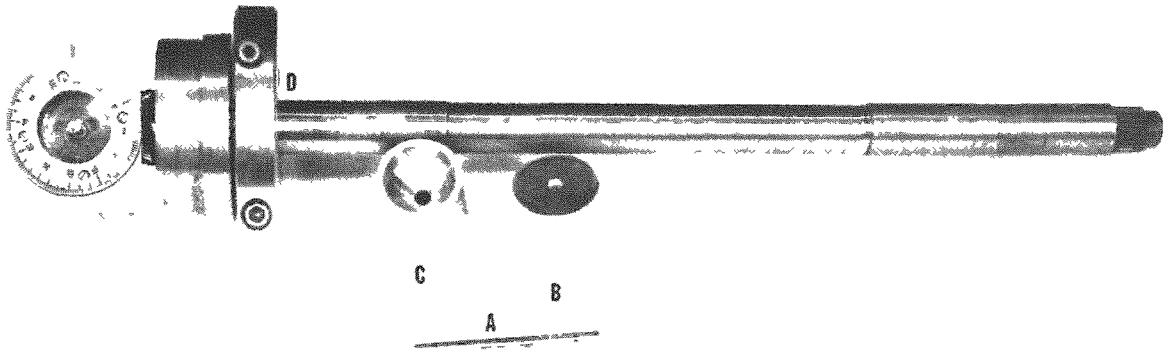


Fig. 6. "Cup" Type Specimens Holder

A, uranium cylinder B, steel polishing mount to avoid polishing at the wrong angle. C, cup type specimen holder to reduce background. D, specimen holder mounted in Norelco spinner.

Five X-ray runs of 21 planes [$G_2$ group + (040)] were made on each end of each test specimen. The initial specimen length was $2\frac{1}{8}$ inches, and the X-ray runs were made in incremental depths of approximately 0.010 inch. The finished length dimension for irradiation was 2 inches. Runs were made on both ends of the specimen to search for texture gradients. Data on $G_2$ for the 20 specimens are given in Table VI. Note that within the precision of the measurements there are no texture gradients.

It is planned to irradiate the specimens "bare" in liquid NaK to provide good heat transfer and to avoid restraint caused by cladding. The specimens will be irradiated in as uniform a flux as possible, and the temperature will be one at which considerable anisotropic growth occurs. Each specimen is provided with a flux monitor. The encapsulation design is given in Figs. 7 and 8. Postirradiation X-ray PO measurements are also planned.

Table VI

$G_2$ VALUES FOR IRRADIATION TEST SPECIMENS

| Angle to RD, degrees | Specimen Number | Marked End | | Unmarked End | |
|---|---|---|---|---|---|
| | | $G_2$ | $t\sigma/\sqrt{N}$ | $G_2$ | $t\sigma/\sqrt{N}$ |
| 0 | 1 | +0 2212 | 0 0346 | +0.2420 | 0 0068 |
| 5 | 2 | +0.2476 | 0 0348 | +0.2524 | 0.0164 |
| 10 | 3 | +0.2037 | 0.0543 | +0.2385 | 0.0192 |
| 15 | 4 | +0.2095 | 0.0387 | +0.2077 | 0.0322 |
| 20 | 5 | +0.2204 | 0.0436 | +0.2169 | 0 0303 |
| 25 | 6 | +0.1882 | 0.0269 | +0.1726 | 0.0299 |
| 30 | 7 | +0.1679 | 0.0068 | +0.1626 | 0.0352 |
| 35 | 8 | +0.1446 | 0.0366 | +0.1029 | 0.0379 |
| 40 | 9 | +0.1042 | 0.0245 | +0.1081 | 0.0150 |
| 45* | 10 | -0.0413 | 0.0146 | -0.0478 | 0.0144 |
| 50 | 11 | +0.0680 | 0.0324 | +0.0713 | 0.0219 |
| 55 | 12 | +0.0291 | 0.0183 | +0 0363 | 0.0094 |
| 60 | 13 | +0.0174 | 0.0216 | +0.0186 | 0.0283 |
| 65 | 14 | -0.0101 | 0.0264 | +0.0089 | 0.0246 |
| 70 | 15 | -0.0224 | 0.0238 | -0.0196 | 0.0427 |
| 75 | 16 | -0.0438 | 0.0283 | -0.0119 | 0.0170 |
| 80 | 17 | -0.0375 | 0.0203 | -0.0438 | 0.0394 |
| 85 | 18 | -0.0520 | 0.0108 | -0.0153 | 0.0565 |
| 90* | 19 | +0.0962 | 0.0252 | +0.1081 | 0.0220 |
| 0 | 20 | +0.2605 | 0.0216 | +0.2512 | 0.0441 |

*These sections were cut near the edge of the plate which apparently had a different texture due possibly to a lower rolling temperature or uneven deformation.

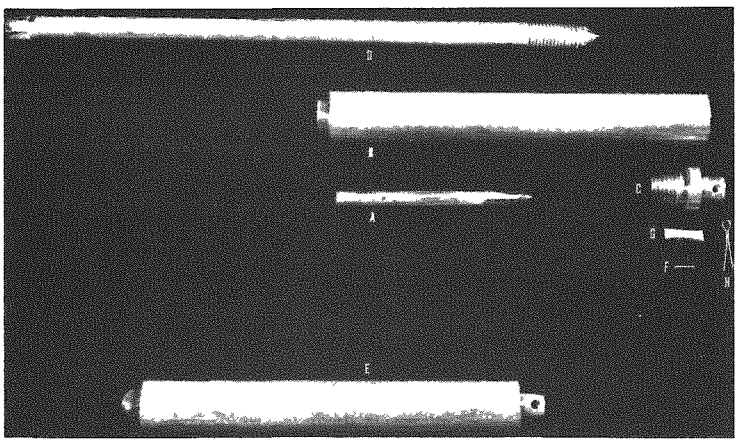

Fig. 7. Capsule before Assembly

The uranium cylinder, A, is loaded into the right of the stainless steel capsule B. Cap C is screwed into B and heliarc welded. Capsule B is filled with NaK under 0.2 micron vacuum then backfilled with high purity helium to 22.5 cm. Rod D is screwed into left end of B while system is still under partial pressure of helium. The capsule is removed, Rod D is sawed off and heliarc welded as shown on the left end of E. An Al-1/2 wt % Mn-1/2 wt % Co flux monitor pin, F, is housed in a 2S Al tube, G, inserted into C and locked with a cotter key, H.

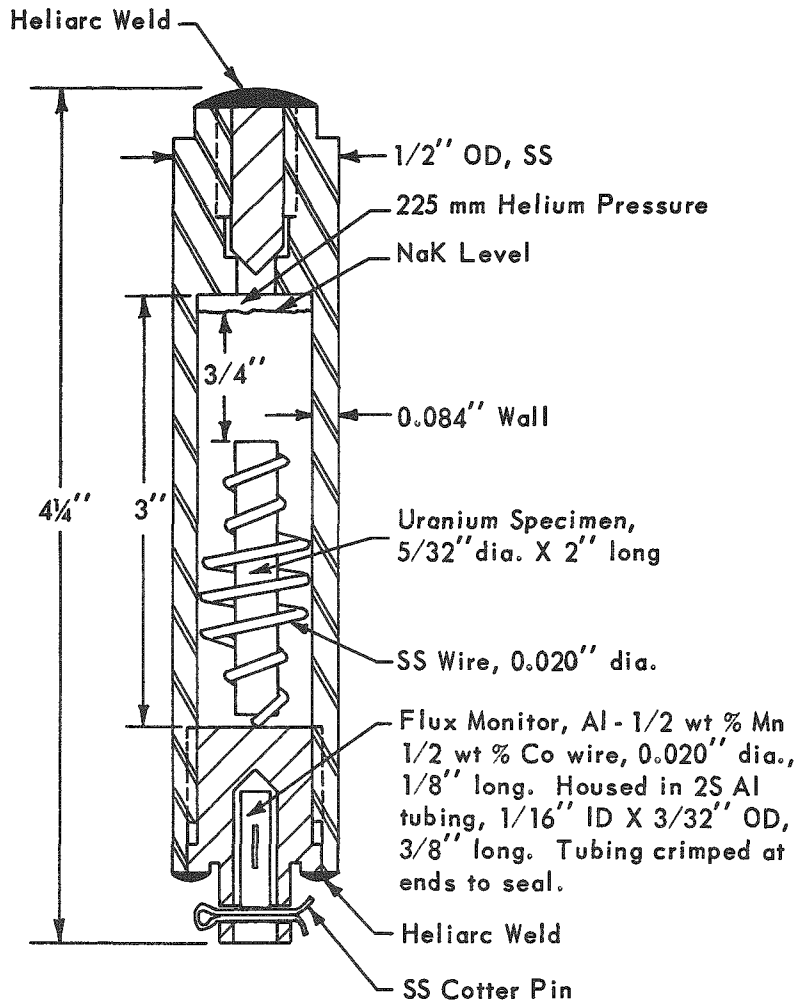


Fig. 8. NaK Irradiation Test Assembly

## ACKNOWLEDGEMENT

This work was done in collaboration with J. W. Croach, Section Director, Pile Engineering and Materials Section, SRL. Thanks are due to B. G. LeFevre of SRL for general assistance, and to J. H. Kittel and L. A. Neimark of ANL for NaK encapsulation of the irradiation specimens.

## REFERENCES


1. Sturcken, E. F., "A Generalized Growth Index Formalism," Papers Presented at the X-ray Preferred Orientation Meeting Held at National Lead Company of Ohio, November 9 and 10, 1959, edited by Morris, P. R., NLCO-804 (July 15, 1960) p. 9.

2. Mueller, M. H., Knott, H. W., Chernock, W. P., and Beck, P. A., Preferred Orientation in Rolled Uranium Rods, Transactions of the Metallurgical Society of AIME, 212 (No. 6) 793-798 (Dec. 1958). For TC data see p. 8 of ANL-5194 (declassified) by the same authors.

3. Barss, W. M., and Ells, C. E., Experimental Support for the Ellipsoid Theory of Growth in Alpha Uranium under Irradiation, NEI-18 (1952).

4. Sturcken, E. F., An X-ray Method for Predicting the Stability of Natural Uranium at Low Burnup, DP-251 (Nov. 1957) (Classified).

5. Sturcken, E. F., "An X-ray Method for Predicting Uranium Stability at Low Burnup, "Proceedings of Fuel Element Conference, Gatlinburg, Tennessee, TID-7559 (Part 2)(May 14-16, 1958) (Secret).

# CORRELATING FABRICATION CONDITIONS AND GROWTH INDEX DATA

Leonard Robins
Bridgeport Brass Company

The problems associated with the production of dimensionally stable fuel elements are well known to the members of this group, especially those engaged in studies to determine the fabrication conditions for forming uranium having a growth index within a desirable range of values One of the problems encountered is the variation in the grain structure and orientation of the slugs due to nonuniform fabrication conditions. The furnace-to-cooling tank transfer time or the cooling medium temperature, e.g., may change during a series of beta-quenching operations. Processing differences of this type can lead to structural inhomogeneities between each sample of a group heat treated in the above manner. The problem is complicated by the presence of the many variables introduced by the thermal and mechanical treatments usually employed in shaping uranium. The list of possible variables might include the impurity content, preliminary working and heat-treating operations, heating or cooling rates, temperatures, time at temperature, type and amount of plastic deformation, secondary working operations, etc.

A logical approach for investigations of growth index is to narrow the long list of possible factors affecting the preferred orientation to the few most influential ones that can be easily handled in commercial fabrication practice. The screening of a large number of possible variables to identify the most important ones is a type of problem that arises in many investigations in one form or another. Table I, taken from part of our uranium-extrusion development program, provides data to illustrate the problem.

In this example different extrusion conditions were employed for the two pushes. Six conditions were varied while two were held constant (other possible variables, e g., billet composition and structure, and lubricant, were not considered). The results indicate that significant differences in tube eccentricity, ovality, hardness, density, grain structure, preferred orientation, irradiation stability, and other properties can arise from the difference in conditions between the two runs. But what do the observed apparent differences in characteristics mean? If, e g., it was desired to extrude slugs with a growth index of $0 \pm 0.050$, we should like to isolate and study the two or three most influential extrusion conditions that can be controlled during fabrication and proceed to optimize them. If the measured differences are real and reproducible, the following question arises: What is the relative contribution of each extrusion variable to this difference in results? The recognition and separation of the most important

Table I

DATA FROM EXTRUSION U-16

A. Extrusion Conditions (for As-cast Billets)

| Tube No. | Billet Location | Billet Furnace Temp, °C | Transfer Time min | Tool Temp, °F | Ram Speed, in./min | Cone and Die Angle, degree | Extrusion Ratio R | Cooling Medium |
|---|---|---|---|---|---|---|---|---|
| 6 | From top half of ingot | 555 | 1.15 | 450 | 45 | 60 | 12:1 | Water |
| 25 | From bottom half of ingot | 625 | 1.15 | 875 | 15 | 130 | 19:1 | Water |

B Test Results

| Tube No. | Extrusion[a] Constant K, tsi | Tool Temp Increase, °F | | Eccentricity,[b] in. | Ovality,[b] in. | Hardness,[b] $R_G$ | Density,[b] gm/cc | Grain Structure |
|---|---|---|---|---|---|---|---|---|
| | | Mandrel | Die | | | | | |
| 6 | 18.2 | 140 | 80 | 0.008 | .013 | 79.0 | 18.992 | All-fine grained |
| 25 | 16.1 | 550 | (110) | 0.019 | .007 | 76.5 | 18.965 | Duplex (Fine & coarse) |

C. X-ray Evaluation Results

| Tube No. | Axial texture coefficients,[c] TC (hkℓ) | | | | | | | | | Axial growth index,[d] $G_3$ | | | |
|---|---|---|---|---|---|---|---|---|---|---|---|---|---|
| | 020 | | | 110 | | | 200 | | | | | | |
| | front | center | rear | front | center | rear | front | center | rear | front | center | rear | ave. |
| 6 | 1.64 | 1.02 | 1.47 | 3.57 | 3.55 | 3.75 | 3.57 | 3.14 | 3.44 | -0.21 | -0.20 | -0.19 | -0.20 |
| 25 | 1.36 | 1 11 | 0.89 | 4 67 | 5 61 | 5.00 | 2.32 | 2.14 | 1.54 | -0.25 | -0.30 | -0.23 | -0.26 |

[a] $K = p/\ln R$, where p is the running extrusion pressure, and R is the billet area reduction ratio (the extrusion ratio).

[b] Average of the measured values for the front, quarter-length, center, three-quarter length, and rear.

[c] $TC_{(hk\ell)} = \dfrac{(I/Io)_{hk\ell}}{\frac{1}{n}\sum (I/Io)_{hk\ell}}$, where n, the number of planes measured, was 10.

[d] $G_3 = \sum (A_w \times TC \times \Delta \cos^2 \alpha)_{hk\ell}$ .

extrusion variables would provide valuable information to enable us to maintain the growth index within the specified limits for irradiation stability.

The Random Balance design experiment, a concept created by F. E. Satterthwaite in 1957, provides a method for attacking the problem of identifying the most significant variables. The technique has been tried on several problems in our research group with some success. The main advantage is that it enables one to weigh the importance of a large number of variables to determine the few outstanding factors. These factors can then be studied in further detail by conventional statistical procedures. The number of tests required for the random balance approach is relatively small in comparison to the sometimes prohibitive number needed for full factorial design experiments.

The following presentation will serve to describe the steps in the random balance method. Only a portion of our experimental data is employed. *

1. Choosing the variables for evaluation - Eight extrusion conditions were selected. They were considered to be the variables most likely to have a major influence on the test results. The evaluation of the extruded material was to consist of metallographic, dimensional, surface condition, X-ray diffraction (texture and growth index), and physical and mechanical property tests and examinations.

2. Choosing the conditions (levels) for the variables - Two levels (a high and a low value) were selected for each of the eight variables. The selections were based on the limiting values of the range over which the extrusion conditions could be varied. Certain practical restrictions involving, e.g., the press capacity, uranium phase changes, and the behavior of the salt employed for billet heating, were taken into consideration. Three or more levels may be employed, although the analysis then becomes more complex.

3. Deciding on the number of test runs - It was decided to extrude 28 billets to give a random sampling of the 28 (256) possible combinations of extrusion conditions. It should be noted that about 30 to 50 tests are required for good, representative sampling of a large number of combinations, e g., 212 (4096) possibilities. This number of tests usually makes for a practical-sized experiment. A $\frac{1}{128}$ replicate of a 212 factorial design, programming twelve variables with two levels each, would reduce the exact balance experiment to 32 test runs. However, the confounding problem becomes complex in this approach.

---

* Our experiment has not yet been completed. Only 20 of the 28 extrusion constants (K values) to be obtained were available for this writing. The X-ray evaluation is still in progress.

4. Assigning the levels and variables to the tests - The two levels were randomly assigned to the eight variables for the 28 test runs. A table of random numbers was employed to assign the 14 high levels for one variable to the 28 extrusion runs. This process was repeated for each of the 8 variables. The results of the random assignment of levels is shown in Table II, where + and - are the designations of the two levels for each variable.

Table II

DESIGN OF EXPERIMENT U-16

| Extrusion Run No. | Levels of each fabrication variable | | | | | | | | Test Results (extrusion constant, grain size, growth index, etc.) |
|---|---|---|---|---|---|---|---|---|---|
| | A | B | C | D | E | F | G | H | |
| 1 | - | + | + | + | - | + | + | + | |
| 2 | + | + | - | - | - | - | - | - | |
| 3 | + | + | + | - | - | + | + | + | |
| 4 | + | + | - | + | - | + | + | - | |
| 5 | - | + | + | + | - | + | - | + | |
| . | . | . | . | . | . | . | . | . | . |
| . | . | . | . | . | . | . | . | . | . |
| . | . | . | . | . | . | . | . | . | . |
| 26 | + | - | + | + | + | - | + | - | |
| 27 | + | - | - | + | + | + | - | - | |
| 28 | - | - | - | + | + | - | + | - | |

The analysis of the test results begins with a scatter diagram for each of the 8 variables. The 8 diagrams are shown in Fig. 1, where the extrusion-constant results have been split into the high and low levels for each variable.

5. Interpreting the data - The test results were plotted to determine the extrusion variable(s) having the largest effect on each class of test measurement. An example of the partial graphical analysis of some extrusion-constant data is shown in Fig. 1.

A simple and rapid method for a first rough analysis is shown in Fig. 1. The median difference (the difference in median location for each level) is shown for each variable. Also shown are the count of the number of test results in the higher level which are higher than the highest test result of the other level, and a similar count for the low test results. For a test of significance, the probability of getting a total of at least R such

counted points with two groups of data of equal size is given by the statistic

$$\frac{C_n^{2n-R} + \sum_{r=1}^{R} \left( C_{n-1-r}^{2n-1-R} \right)}{C_n^{2n} - C_{n-1}^{2n-2}}$$

where R is the sum of points counted at each end, n is the number of points in each group, and $C_w^V = V!/W!(V-W)!$.

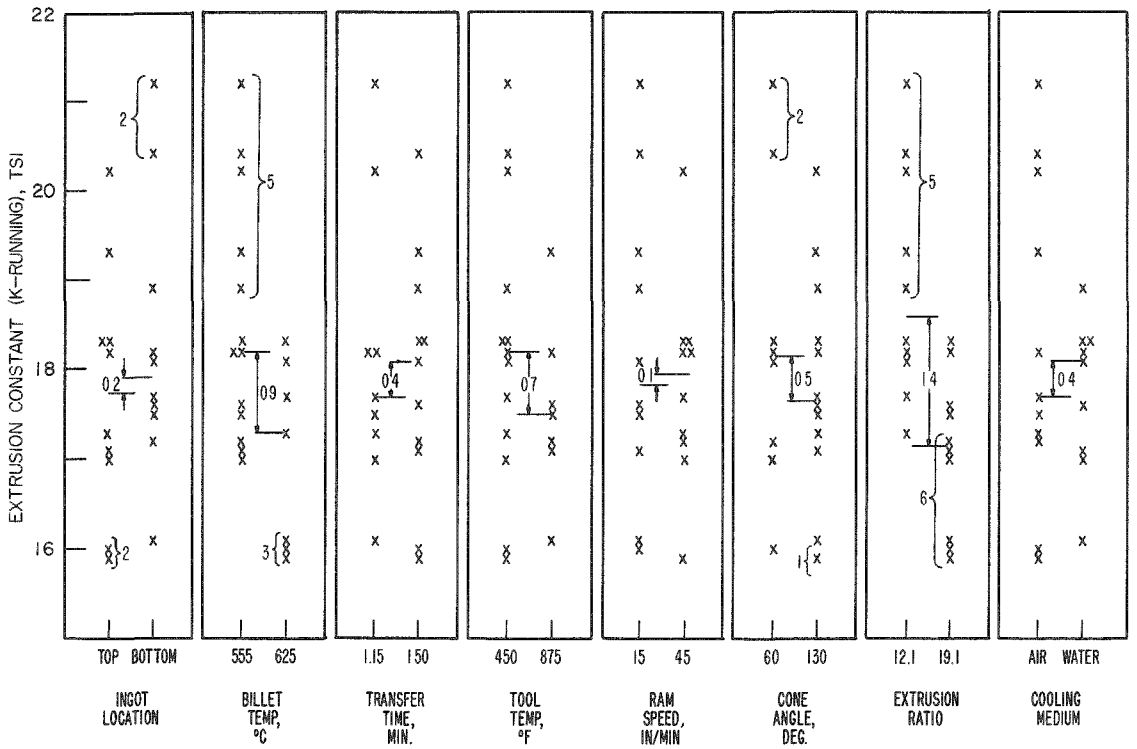


The graphical analysis readily identified (a) the billet temperature and (b) the extrusion ratio as the variables with the greatest effect on the extrusion constant. The large effects produced by these two variables stand out sharply in the figure. They clearly cause real differences. They are the only variables having median differences greater than 0.9 tsi and a total of eight or more points counted at the ends. In comparison, for the other variables, the maximum values are 0.7 tsi and four such points, respectively.

Further analysis can be made to identify other less effective variables and to resolve possible interaction effects covered by the two strongest variables. This will not be done here, since our data are

incomplete. The available data cover only 20 of the 28 extrusion runs to be made. An outline of the steps for removing the effect of the two strongest variables and for handling interaction effects can be found in the reference (by Budne) mentioned below. The first correction involves "subtracting" the effect of the previously determined main variables from the original set of data. The corrected data are replotted and the analysis described above is repeated. All major sources of variations in test results can be determined in this manner. Thus the relative magnitude of the individual effects of each variable can be satisfactorily estimated for all practical purposes within the scope of the screening objective.

Learning of the important role of the extrusion ratio was, in this case, unexpected. The extrusion constant should vary with temperature. However, it should remain constant when the extrusion ratio is changed, since the extrusion constant K is the proportionality constant in the relationship between the extrusion pressure P and the logarithm of the reduction ratio, $\log_e R$. The observed decrease in extrusion constant when the reduction ratio was increased from 12:1 to 19:1 can be explained by assuming that the heavier reduction raises the effective extrusion temperature. The actual extrusion temperature may be increased because of the generation of more heat from the larger work of deformation.

When the problem is one of optimizing fabrication conditions, precise experimental designs, containing the few critical variables previously identified, can be made. The optimum operating conditions may be determined in a limited number of tests by a conventional study of the most significant variables, while the other variables are held constant.

Further information on the random balance method and its limitations, and a detailed description of the advanced stages of the data analysis, can be found in an article entitled Random Balance by T. A. Budne.[1]

## REFERENCE

1. Budne, T. A., Random Balance. Part I - The Missing Statistical Link in Fact Finding Techniques, Industrial Quality Control, 15, (No. 10). 5 - 10 (1959).

   Part II - Techniques of Analysis, Industrial Quality Control, 15, (No. 11), 11 - 16 (1959).

   Part III - Case Histories, Industrial Quality Control, 15, (No. 12), 16 - 19 (1959).

# EMPIRICAL APPROACH TO FUEL ELEMENT IRRADIATION GROWTH PREDICTION*

J. P. LeGeros
Savannah River Plant, E. I. duPont de Nemours and Company

Natural uranium fuel elements normally change dimensions during irradiation These changes in dimensions, termed instability or growth, may cause unequal flow splits in the cooling water, difficulty in unloading irradiated elements, and fuel element failures.

A reliable, inexpensive, out-of-pile test which predicts the dimensional instability to be experienced during irradiation is needed. The in-pile methods presently used are costly, since they require fabrication and finishing of large numbers of test elements, and they may be detrimental to safe reactor operation

Since a theoretical mechanism to explain the change in dimensions of fuel elements during irradiation has not been proven to date, an empirical approach to the problem of certifying test fuel elements to be irradiated in production reactors was evaluated

Texture-limit standards are being established, on a preliminary basis, by measuring the textures of standard production fuel elements taken daily from the production cladding-fabrication process. This work is being done in two phases.

In the first phase, the maximum and minimum axial textures (measured from one diffraction sample from a slug taken from the production line each day for eight months) were set as upper and lower limits between which experimental slugs were certified as probably safe for production reactor irradiation

In the second phase, texture standard limits are being based upon a larger sampling of twenty samples (ten axial and ten in the direction of the circumference) taken from a production slug each day.

In order to help establish which textures and other factors are most important to fuel element growth during irradiation, a study utilizing a multiple regression analysis was made with 956 fuel elements which were irradiated at various flux levels and upon which measurements of dimensional changes were made These fuel elements represented six different heat-treatment groups.

*The information contained in this article was developed during the course of work under Contract AT(07-2)-1 with the U.S. Atomic Energy Commission This information was previously referred to as DPSPU 60-30-14B.

The study was confined to changes in only one dimension: the length of the fuel elements. Changes in diameter were not studied at this time because texture gradients along the radius would have had to be included, thus increasing the scope of the problem (and hence the computer calculation time) beyond the time available for this first study. Therefore, for this preliminary study the term "instability" refers only to changes in slug length (growth or shrinkage). Diameter changes will be considered in subsequent studies.

The factors considered were:

Physical characteristics of fuel elements; and

Reactor geometry and operating characteristics.

The main purposes of this study were:

1. To determine the relative importance of factors causing instability during irradiation and to determine the range of reactor operating and fuel element characteristics contributing to instability during irradiation.

2. To develop criteria for testing theoretical mechanisms of instability.

3. To derive a formula which can be used to predict the type and magnitude of irradiation-induced instability.

The methods of regression analysis were adapted to the problem of correlating the change in length of fuel elements with the properties and exposure conditions of the fuel elements. When the analysis was completed, it was found that the nature of the available data was such that only very limited conclusions could be reached. This initial attempt, which is reported here as a matter of record, will serve as a basis for additional work to develop techniques better suited to the data at hand.

In the analysis, an apparently significant correlation was found between growth and the temperature of the coolant surrounding the fuel elements This indication will be followed up in the additional work that is now planned.

Since only six groups of fuel elements were studied and all fuel elements within a given group were characterized by the same set of X-ray parameters and grain size data, the amount of data available with regard to independent variables describing the material is quite limited. The batch variable inherent in each of the six groups or batches when represented by the mean dimensional change of each batch explains about 43% of the variance in instability observed. The variability explained by the complete regression analysis was 47.6%.

# COMPARISON OF METHODS OF CALCULATING THE GROWTH POTENTIAL OF URANIUM

J. W. Starbuck and H. C. Kloepper, Jr.
Mallinckrodt Chemical Works

## SUMMARY

Three methods of calculating the growth potential of uranium were applied to date from a Jominy-type end-quenched uranium specimen. Scaled growth index (G.I.) yields a somewhat more negative value than does $G_2$ or $G_3$, especially for sections having high C-axis texture.

The effects of changes in certain constants employed in the calculations were evaluated. Reduction of the cosine-squared functions from five decimal places to two decimal places resulted in insignificant changes in scaled G.I. and $G_3$.

A test of the significance of differences in inverse matrices of the $G_2$ formalism as computed at MCW and SRL also indicated inconsequential effects upon the calculated $G_2$ value.

## INTRODUCTION

Several methods of calculating the growth potential of neutron-irradiated uranium fuel cores have been proposed. E. F. Sturcken[1] developed the expression

$$\text{G.I.} = \Sigma \text{ T.C.} \times \cos^2\beta - \Sigma \text{ T.C.} \times \cos^2\alpha \quad ,$$

where

$$\text{T.C.} = \frac{I_{hkl}/I^{\circ}_{hkl}}{\frac{1}{n}\sum_{1}^{n} I_{hkl}/I^{\circ}_{hkl}} \quad ,$$

$\beta$ and $\alpha$ = the angles between (hkl) pole and the a and b axes of alpha uranium, respectively,

$I_{hkl}$ = observed integrated intensity of (hkl) plane

n = number of measured (hkl) planes.

For a randomly oriented specimen, T.C. = 1; then the zero growth potential would be equal to $\Sigma \cos^2\beta - \Sigma \cos^2\alpha$. Due to the asymmetric distribution of measurable planes, this expression is not equal to zero. The limits of the G.I. expression are equal to $\pm n$.

Sturcken later developed a "Generalized Growth Index Formalism,"(2) denoted as $G_2$, wherein the limits of the expression were $\pm 1.0$ for maximum expansion or contraction and dimensional stability was indicated by a value of 0.00.

In addition, P. R. Morris(3) proposed a method called the "Area Weight Method," denoted as $G_3$, having the same limits as $G_2$.

The original G.I. expression has been modified by a "scaling" technique so as to obtain limits of $\pm 1.0$ and a value of 0.0 to correspond to dimensional stability.

The data contained in this report were compiled for the purpose of comparing the values obtained by the three methods of calculation mentioned above.

## CALCULATIONS

The constants used in the calculations were as follows:

The $I^{\circ}_{hkl}$ values reported in private communication, dated April 13, 1960, from Dr. M. H. Mueller were used in a 21-plane set of data. (The 21 planes are listed in Table II.) For the 21-plane set, when all T.C. values equal one, the $\Sigma \cos^2\beta - \Sigma \cos^2\alpha$ is equal to +2.60. (Henceforth $\cos^2\beta - \cos^2\alpha$ will be denoted $\Delta \cos^2$.) Scaled G.I. was calculated on the following basis:

For observed $\Sigma$ T.C. $\Delta \cos^2 > 2.60$ ,

$$\text{Scaled G.I.} = + \frac{\Sigma \text{T.C. } \Delta \cos^2 - 2.60}{21.00 - 2.60}$$

For $\Sigma$ T.C. $\Delta \cos^2 < 2.60$ ,

$$\text{Scaled G.I.} = - \left( \frac{2.60 - \Sigma \text{T.C. } \Delta \cos^2}{21.00 + 2.60} \right)$$

The data from Jominy-type end-quenching experiments(4) were chosen for comparison because of the varying degrees and type of texture represented.

## RESULTS

The data in Table I show the differences in the calculated values. With three exceptions, $G_2$ can be seen to be between scaled G.I. and $G_3$. The differences between scaled G.I. and $G_3$ would be the additive of the last two columns of the table.

Table I

COMPARISON OF SCALED G.I., $G_2$, and $G_3$ VALUES

| Distance from Quenched End, inches | "J" | Scaled G.I. | $G_2$ | $G_3$ | $G_2$ - G.I. | $G_3$ - $G_2$ |
|---|---|---|---|---|---|---|
| 0.010 | 2.35 | -0.433 | -0.423 | -0.405 | 0.010 | 0.018 |
| 0.015 | 1.82 | -0.356 | -0.336 | -0.312 | 0.020 | 0.024 |
| 0.015 Repeat | 1.70 | -0.316 | -0.298 | -0.282 | 0.018 | 0.016 |
| 0.037 | 1.54 | -0.178 | -0.152 | -0.128 | 0.026 | 0.024 |
| 0.041 | 1.57 | -0.188 | -0.166 | -0.136 | 0.022 | 0.030 |
| 0.046 | 1.45 | -0.153 | -0.087 | -0.091 | 0.066 | -0.004 |
| 0.050 | 1.62 | -0.158 | -0.107 | -0.110 | 0.049 | -0.003 |
| 0.062 | 1.55 | -0.113 | -0.078 | -0.065 | 0.035 | 0.013 |
| 0.067 | 1.41 | -0.083 | -0.050 | -0.036 | 0.033 | 0.014 |
| 0.072 | 1.47 | -0.094 | -0.038 | -0.050 | 0.056 | -0.012 |
| 0.077 | 1.51 | -0.092 | -0.045 | -0.041 | 0.047 | 0.004 |
| 0.083 | 1.37 | -0.093 | -0.063 | -0.048 | 0.030 | 0.015 |
| 0.092 | 1.40 | -0.045 | -0.007 | -0.002 | 0.038 | 0.005 |
| 0.108 | 1.23 | -0.076 | -0.040 | -0.028 | 0.036 | 0.012 |
| 0.108 Repeat | 1.27 | -0.076 | -0.048 | -0.032 | 0.028 | 0 016 |
| 0.113 | 1.24 | -0.061 | -0.022 | -0.020 | 0.039 | 0.002 |
| 0.122 | 1.19 | -0.067 | -0.047 | -0.026 | 0.020 | 0.019 |
| 0 162 | 1.06 | -0.094 | -0.073 | -0.060 | 0.021 | 0.013 |
| 0.167 | 1.05 | -0.087 | -0.078 | -0.059 | 0.009 | 0.019 |
| 0.177 | 1.05 | -0.073 | -0.075 | -0.046 | 0.002 | 0.029 |

Area Weight constants have a computation bias of $G_2 = +0.019$ for a random specimen. Removing this bias would yield even more equivalent $G_2$ and $G_3$ values. Regarding scaled G.I., a distortion should theoretically occur due to "scaling" for high C-axis textures. The distortion does, indeed, seem to manifest itself, for in the region from 0.046 to 0.113 inch from the quenched end the differences in G.I. and $G_2$ are larger. It is in this region that [001] texture is prominent, according to observations regarding the effect of cooling rate through the beta-to-alpha transformation. From these data it would appear that scaled G.I. yields a somewhat more negative value for growth potential than $G_2$ or $G_3$ when employing a 21-plane set. The choice of using either $G_2$ or $G_3$ would seem to be arbitrary, with no serious consequence. The accuracy of either of the three units of measure must still be ascertained by pile behavior data.

## THE EFFECT OF CHANGES IN CONSTANTS

Among the areas of uncertainty regarding the determination of preferred orientation in uranium has been the use of certain constants in various steps of the calculation of either G.I., $G_2$, or $G_3$. Considerable effort has been expended towards refining these constants. The question arises as to the significance of the differences.

The data reported herein are differences presented for the purpose of establishing the degree of accuracy required by way of examining the effect of changes in the constants upon the final calculation.

The first area studied dealt with the choice of values of the lattice constants for alpha uranium. The values of the lattice constants determine the angles between crystallographic planes, which, in turn, determine the component of growth potential, $\cos^2\beta - \cos^2\alpha$, used in the G.I. or $G_3$ formalisms. This has the same value as the $V_{22}$ column in the $V_{lm}$ matrix of the $G_2$ formalism. Using the alpha-uranium lattice constants reported by Mueller and Hitterman of ANL, cosine-squared functions had been computed to five decimal places on the LGP 30 computer. These values have been used routinely at MCW for calculating G.I. and $G_3$ for 21-plane sets of data. Three samples were chosen and recalculated using cosine-squared functions of three and two decimal places, respectively. Table II contains the results of these calculations.

These data indicate that there is an insignificant effect on scaled G.I. or $G_3$ introduced by the dropping of as many as three decimal places from the cosine-squared values.

Since there has been concern over differences in elements of the inverse matrix, a similar scheme as above was used for evaluating the differences.

Table II

COSINE-SQUARED EFFECT ON G.I AND $G_3$

| hkl | Texture Coefficients | | |
|---|---|---|---|
| | Sample 4106 | Sample 4107 | Sample 4108 |
| 020 | 1.029 | 1.165 | 0.871 |
| 110 | 10 542 | 4.158 | 1.449 |
| 021 | 0.189 | 0.588 | 1.260 |
| 002 | 0.178 | 0.147 | 0.094 |
| 111 | 0.115 | 1 102 | 1.449 |
| 022 | 0.367 | 0.315 | 0.955 |
| 112 | 0.000 | 0.220 | 0.546 |
| 130 | 1.008 | 1.627 | 1.344 |
| 131 | 0.220 | 1.585 | 0.294 |
| 023 | 0.073 | 0.094 | 1.323 |
| 200 | 4.557 | 1.816 | 2.835 |
| 041 | 0.378 | 1.291 | 0.178 |
| 113 | 0.000 | 0.063 | 0.798 |
| 132 | 0.000 | 0.787 | 0.735 |
| 133 | 0.000 | 0.241 | 0.042 |
| 114 | 0 031 | 0.000 | 0.136 |
| 150 | 0.672 | 1.071 | 0.210 |
| 240 | 0.840 | 1.375 | 0.798 |
| 223 | 0.000 | 0.357 | 1.039 |
| 241 | 0.640 | 1.753 | 3.213 |
| 152 | 0.042 | 1.144 | 1.312 |
| Scaled G.I. | | | |
| $\cos^2$ = X.XXXXX | -0.4725 | -0.0887 | -0 1476 |
| = X.XXX | -0.4722 | -0.0887 | -0.1475 |
| = X.XX | -0.4737 | -0.0896 | -0.1485 |
| $G_3$ | | | |
| $\cos^2$ = X.XXXXX | -0.5177 | -0.1045 | -0.1420 |
| = X.XXX | -0.5174 | -0.1042 | -0.1417 |
| = X.XX | -0.5194 | -0.1055 | -0.1431 |

The fixed point 21-plane inverse matrix (Table III) was calculated to eight decimal places. Intensity data from a single sample were chosen and computation of $G_3$ was carried out by successive dropping of "bits" of the binary code in each element of the matrix. No change in $G_2$ or "J" values occurred until five decimal places remained, indicated by "WWWWOOOO," such that the maximum possible deviation from the true value of any element in the matrix was 0.00003. The data are shown in Table IV.

Table III

FIXED-POINT 21-PLANE INVERSE MATRIX
Computed by MCW

| | | | | |
|---|---|---|---|---|
| 0.07367918 | -0.00424965 | -0.06005776 | -0.01687370 | -0.02100614 |
| 0.04201153 | 0.01523251 | 0.02197417 | 0.03323284 | -0.01685819 |
| -0.00380100 | 0.07135108 | 0.03563704 | 0.00976809 | 0.00220374 |
| -0 02280027 | -0.01901722 | -0.01495175 | -0.01759761 | 0.00230926 |
| -0.03101370 | 0.02057506 | 0.18976951 | 0.01501407 | 0.05063145 |
| -0.08599500 | -0.01985910 | -0 04642227 | -0.07751083 | 0.02153488 |
| -0.01499884 | 0.00970761 | 0.02584410 | 0.06273415 | 0.02270851 |
| -0 02768824 | -0.00962463 | -0.01129459 | -0.03082937 | 0.02135381 |
| -0.01252564 | 0.00146916 | 0.05846416 | 0.01523334 | 0.12488782 |
| -0.06477546 | -0.00738872 | -0.01313748 | -0.07278428 | 0.04059828 |
| 0.01893666 | -0.01149027 | -0.07506264 | -0.01404052 | -0.04896568 |
| 0 17364025 | 0.01327722 | 0 02734066 | 0.09423457 | -0.05815407 |
| 0.01351916 | -0.01887038 | -0.03413136 | -0.00960981 | -0.01099749 |
| 0.02614271 | 0.05294971 | 0.02159892 | 0.02468470 | -0.01514936 |
| 0.01345803 | -0.01023803 | -0.05505681 | -0.00778202 | -0.01349358 |
| 0.03714864 | 0.01490468 | 0.09594201 | 0.02230957 | -0.02305127 |
| 0.01857999 | -0.01099985 | -0.08391818 | -0.01939079 | -0.06824360 |
| 0.11688351 | 0.01554990 | 0.02036575 | 0.17353426 | -0.04867756 |
| -0.00696095 | 0.00106607 | 0.01721931 | 0.00991940 | 0.02811326 |
| -0.05327245 | -0.00704812 | -0.01554116 | -0.03595078 | 0 11180738 |

Table IV

EFFECT OF CHANGES IN 21-PLANE INVERSE MATRIX

Sample: HAPO Size I and E Core 4109 A2 A12
History: 7th Alpha Extrusion Campaign

| Code Notation | "J" | $G_3$ |
|---|---|---|
| WWWWWWWW | 1.09 | -0.0221 |
| WWWWWWWO | 1.09 | -0.0221 |
| WWWWWWOO | 1.09 | -0.0221 |
| WWWWWOOO | 1 09 | -0.0221 |
| WWWWOOOO | 1 09 | -0.0224 |
| WWWJOOOO | 1.09 | -0.0237 |

The next set of trials was carried out for ten samples having various degrees of textures. The dropping sequence was continued through the use of a maximum difference of 0 0078($\frac{1}{128}$). The results are shown in Table V.

Table V

EFFECT OF CHANGES IN 21-PLANE MATRIX

| Sample | "J" | Maximum Matrix Element Deviation | | | | |
|---|---|---|---|---|---|---|
| | | 8-place | 0.00012 | 0.00048 | 0.0039 | 0.0078 |
| | | $G_2$ | | | | |
| 4079 | 2.48 | -0.1701 | -0.1715 | -0.1747 | -0.1645 | -0.1556 |
| 4080 | 2.76 | -0.2093 | -0.2108 | -0.2143 | -0.2024 | -0.1948 |
| 4083 | 1.09 | -0.0221 | -0.0237 | -0.0261 | -0.0429 | -0.0595 |
| 4084 | 1.01 | -0.0131 | -0.0143 | -0.0158 | -0.0194 | -0.0248 |
| 4085 | 1.03 | -0.0014 | -0.0027 | -0.0043 | -0.0102 | -0.0195 |
| 4097 | 1.05 | -0.0037 | -0.0051 | -0.0071 | -0.0189 | -0.0303 |
| 4078 | 2.68 | -0.1966 | -0.1980 | -0.2014 | -0.1893 | -0.1808 |
| 4081 | 2.84 | -0.2363 | -0.2378 | -0.2414 | -0.2300 | -0.2225 |
| 4105 | 5.77 | -0.3331 | -0.3353 | -0.3408 | -0.3347 | -0.3506 |
| 4106 | 6.48 | -0.4988 | -0.5013 | -0.5080 | -0.4978 | -0.5044 |

In comparing MCW and SRP-computer 20-plane inverse matrices, it was noted that six elements differed by 0.01 or more and fourteen differed by 0.005 to 0.01. The differences are shown in Table VI. In addition, the average difference between elements of SRL and MCW-computed matrices was found to be 0.00345, hence, the 0.0039 ($\frac{1}{256}$) step was considered to be a test of these differences. Since some of the elements differed by 0.01, the next step of 0.0078 ($\frac{1}{128}$) was carried out. As can be seen from the data, the largest change in $G_2$ was 0.04, with 0.02 being the average change.

Table VI

DIFFERENCES BETWEEN MCW AND SRL MATRIX VALUES
(20-plane Set)

| | | | | | | | | | |
|---|---|---|---|---|---|---|---|---|---|
| 0.0000 | 0.020 | 0.0004 | 0.0008 | 0.00373 | 0.0012 | 0.005 | 0.001 | 0.003 | 0.005 |
| 0.018 | 0.012 | 0.0017 | 0.012 | 0.0003 | 0.0001 | 0.0031 | 0.0038 | 0.005 | 0.0012 |
| 0.0002 | 0.0009 | 0.006 | 0.0015 | 0.0057 | 0.0026 | 0.0013 | 0.0012 | 0.0019 | 0.0019 |
| 0.0007 | 0.012 | 0.0027 | 0.007 | 0.0002 | 0.0037 | 0.0022 | 0.0012 | 0.0009 | 0.0035 |
| 0.0023 | 0.0002 | 0.0066 | 0.00014 | 0.0014 | 0.0005 | 0.001 | 0.0036 | 0.0029 | 0.003 |
| 0.0006 | 0.0000 | 0.0023 | 0.0019 | 0.00038 | 0.0089 | 0.0034 | 0.0011 | 0.003 | 0.0048 |
| 0.0045 | 0.0029 | 0.0022 | 0.0023 | 0.0015 | 0.0067 | 0.0004 | 0.0090 | 0.012 | 0.0050 |
| 0.0006 | 0.0026 | 0.0015 | 0.0075 | 0.0038 | 0.0014 | 0.0062 | 0.019 | 0.0003 | 0.0037 |
| 0.0016 | 0.0031 | 0.0021 | 0.0006 | 0.0027 | 0.0037 | 0.0078 | 0.0001 | 0.0011 | 0.0013 |
| 0.0020 | 0.0006 | 0.0015 | 0.0016 | 0.0020 | 0.0044 | 0.0023 | 0.0020 | 0.0009 | 0.0079 |

The double underscore indicates the six which deviate by 0.01 or more.

The single underscore indicates fourteen additional which deviate by 0.005 to 0.010.

It is recognized that the above tests do not completely define the possible errors. The problem of matrix statistics is extremely complicated. However, it is felt that these tests shed considerable light on the question of differences. It would appear that the differences in matrices are of insignificant magnitude in relation to the other sources of error in the X-ray determination of growth potential.

## REFERENCES

1. Sturcken, E. F., An X-ray Method for Predicting the Stability of Natural Uranium at Low Burn Up, DP-251 (Nov 1957) (Classified).

2. Sturcken, E. F., A Generalized Growth Index Formalism, NLCO-804 (July 1960), pp. 9-24.

3. Morris, P. R., Comparative Measurements of the Velocity of Propagation of an Ultrasonic Pulse in Uranium Fuel Elements, NLCO-764 (Nov 1958), p. 13.

4. Starbuck, J. W., and Kloepper, H. C., Preferred Orientation of End Quenched Jominy Bars Sampled at Small Increments, MCW-1433, p. 105.

# INTERSITE EVALUATION OF PREFERRED ORIENTATION DATA

J. W. Starbuck and H. C. Kloepper, Jr.
Mallinckrodt Chemical Works

## SUMMARY

X-ray-determined preferred orientation data observed at MCW and HAPO laboratories were in excellent agreement with respect to texture coefficients and $G_3$ observations. It appears that the procedures have been sufficiently standardized for exchange and comparison of data between the two sites.

## INTRODUCTION

To test the quality and control of grain orientation, a testing program was conducted for evaluating I and E cores produced at MCW during the 7th alpha extrusion campaign[1] which consisted of 55 alpha extrusions. The testing program was to serve as a means of comparing X-ray-determined preferred orientation data of alpha-extruded, beta-treated cores with those of other variously processed cores tested at HAPO.

## EXPERIMENTAL

Cores that were nonrecoverable rejects due to failure to meet dimensional and/or surface quality specifications were randomly sampled to furnish test specimens. The number of samples required was determined by sequential statistical evaluation of the observed data. It was found necessary to test 23 cores in order to obtain a representation of various positions over an entire tube length.

A single X-ray scan of a transverse section of a core constituted one sample. A rotating specimen spinner capable of holding a full-diameter core was employed. The X-ray-irradiated area was an annulus having an OD of 1.25 in. and an ID of 0.52 in. This was achieved by 157-rpm rotation of the sample in the plane of the irradiated surface, the center of rotation lying outside the X-ray beam. A Philips Electronics, Inc. X-ray unit was employed, using nickel-filtered copper radiation operated at 40 kv at 18 ma. The detector was a scintillation counter with pulse-height discrimination. Integrated intensities were obtained by a single scan of each peak at 1° $2\theta$/min, the intensities being recorded on the EIT count register of the scaler unit. External timing of the scaler circuit allowed for fixed interval accumulation of intensities. Appropriate background correction was made.

The test specimen was obtained by cutting a wafer approximately $\frac{3}{4}$ in. from the end of the test core. The test surface was faced on a lathe and ground on successive grits of emery paper. Final preparations was by electrolytic polishing in chromic-acetic acid solution. A $\frac{1^{\circ}}{4}$/min scan of the (110), (021), and (002) alpha-uranium peaks was used to monitor surface preparation. Successive electrolytic polishing was carried out until stabilization of the strip-chart-recorded peak heights, as well as $K\alpha_1\alpha_2$ resolution, was achieved so as to insure removal of surface cold work.

The preferred orientation data were computed in accordance with agreed procedure as outlined elsewhere in this document. The same data have been reported elsewhere;[2] however, the calculations in that report were not carried out in accordance with the now standardized methods. Upon completion of the testing program at MCW, the 23 wafers were shipped to HAPO for comparative testing. The results from the two sites are included in this report.

## RESULTS AND DISCUSSION

Table I contains the data determined at the respective sites. The 0.013 difference between the MCW and HAPO averages was found to be significant at greater than 99% confidence. The error limits are the result of processing variables of the seventh alpha-extrusion campaign and the error of the X-ray measurements.

Table II shows the texture coefficient ($P_i$) data observed at the two sites with their respective error limits. Data indicate that nearly random orientation has been achieved. There is, however, a slight excess of (200) and (002) planes parallel to the transverse cross section of the cores. It was also noted that these two planes exhibit the greatest deviation about their mean.

It would appear from the data that techniques have been sufficiently standardized for the attainment of comparable preferred orientation data at the two sites involved. It should be noted that different equipment was employed for this comparison, since MCW uses Philips Electronics, Inc. equipment whereas General Electric X-ray equipment is used at HAPO.

Table I

COMPARATIVE PREFERRED ORIENTATION MEASUREMENTS

| Core No.[a] | Specimen No. | $G_2$ (MCW) | $G_3$ (MCW) | $G_3$ (HAPO) |
|---|---|---|---|---|
| 4135 A1 A3 | 192 | 0.007 | 0.066 | 0.043 |
| 4098 B1 A3 | 109 | 0.010 | 0.014 | 0.034 |
| 4079 B1 A5 | 099 | 0.010 | 0.003 | -0.007 |
| 4108 A2 A6 | 143 | 0.023 | 0.015 | 0.023 |
| 4066 A1 A7 | 065 | 0.010 | 0.007 | 0.044 |
| 4076 A1 A9 | 078 | 0.006 | 0.001 | 0.006 |
| 4098 B1 A11 | 116 | 0.006 | 0.005 | 0.040 |
| 4109 A2 A12 | 166 | 0.003 | 0.006 | -0.032 |
| 4079 B2 A17 | 101 | 0.024 | 0.034 | 0.080 |
| 9101 A2 A18 | 036 | -0.006 | -0.008 | 0.020 |
| 4132 B2 B2 | 209 | 0.022 | 0.020 | 0.034 |
| 4109 A2 B4 | 168 | 0.040 | 0.039 | 0.040 |
| 4108 A1 B6 | 140 | 0.002 | 0.002 | 0.023 |
| 4109 A1 B7 | 158 | 0.025 | 0.021 | 0.000 |
| 4108 A2 B10 | 152 | 0.049 | 0.055 | 0.054 |
| 4132 A1 B11 | 184 | 0.017 | 0.013 | 0.020 |
| 4079 B2 B11 | 105 | -0.015 | -0.026 | 0.010 |
| 4132 A1 B12 | 185 | -0.006 | -0.007 | 0.012 |
| 4066 C1 B12 | 073 | 0.010 | 0.008 | 0.012 |
| 4203 A2 B13 | 216 | 0.022 | 0.016 | 0.012 |
| 4132 B2 B13 | 188 | 0.000 | -0.002 | 0.030 |
| 4203 A2 B14 | 217 | 0.020 | 0.014 | 0.012 |
| 4003 A1 B18 | 023 | 0.000 | 0.007 | 0.041 |
| Average | | +0.012 | +0.011 | +0.024 |
| $t\sigma_x$[b] (95% C.L.) | | ±0.031 | ±0.034 | ±0.048 |
| $t\sigma_{\bar{x}}$[c] (95% C.L.) | | ±0.0064 | ±0.0068 | ±0.0099 |

[a] The first four digits denote the dingot number; the first letter and following digit denote billet number; the second letter denotes alpha-extruded tube, "A" for lead half, "B" for tail half, and the last digits denote core number starting from lead end.

[b] $\sigma_x$ = estimate of error of an individual.

[c] $\sigma_{\bar{x}}$ = estimate of error of the mean.

Table II

TEXTURE COEFFICIENT (T.C.) DATA

| hkl | Average T.C. | | σ | |
|---|---|---|---|---|
| | MCW | HAPO | MCW | HAPO |
| 020 | 1.04 | 1.22 | 0.21 | 0.23 |
| 110 | 1.05 | 0.97 | 0.19 | 0.18 |
| 021 | 1.12 | 1.11 | 0.16 | 0.16 |
| 002 | 1.72 | 1.68 | 0.45 | 0.45 |
| 111 | 0.87 | 0.73 | 0.09 | 0.07 |
| 112 | 0.81 | 0.78 | 0.17 | 0.14 |
| 130 | 0.87 | 0.94 | 0.13 | 0.14 |
| 131 | 0.92 | 0.87 | 0.07 | 0.10 |
| 023 | 1.28 | 1.28 | 0.13 | 0.20 |
| 200 | 1.60 | 1.41 | 0.45 | 0.40 |
| 113 | 1.02 | 1.03 | 0.14 | 0.19 |
| 132 | 0.89 | 0.96 | 0.12 | 0.14 |
| 133 | 0.94 | 0.96 | 0.14 | 0.17 |
| 114 | 1.12 | 1.13 | 0.15 | 0.20 |
| 150 | 0.92 | 0.87 | 0.11 | 0.16 |
| 223 | 0.77 | 0.81 | 0.16 | 0.19 |
| 152 | 0.90 | 0.89 | 0.08 | 0.12 |
| 312 | 0.78 | 0.86 | 0.11 | 0.14 |

## ACKNOWLEDGEMENTS

The authors wish to acknowledge the work and cooperation of Mr. W. G. Jolley, General Electric Company, Hanford Atomic Products Operations, Richland, Washington, who supplied the comparative data herein reported.

## REFERENCES

1. Process Development Quarterly Progress Report, MCW-1459, "Fabrication of I and E Cores by Alpha Extrusion of Gamma-extruded Billet Stock," by Unnerstall, L. A., Padberg, D. J., and Buntz, B. J., p. 61.

2. Process Development Quarterly Progress Report, MCW-1459, "X-ray Evaluation of Cores Processed in the Seventh Alpha-extrusion Campaign," by Starbuck, J. W. and Kloepper, H. C., Jr., p. 81.

# BRIEF DESCRIPTION OF THE "AREA-WEIGHT" TREATMENT FOR THE 18-PLANE SET

R. N. Thudium and P. R. Morris
National Lead Company of Ohio

The Growth Index[1] has been modified by Morris[2] and Sturcken.[3] In the "area-weight" treatment,[2] two assumptions are made: the first, that a finite set of points may be employed to adequately sample an unkown continuous function, and the second, that the pole represents all points within a spherical polygon obtained by making arcs of great circles equidistant between a pole and each of its nearest neighbors. The first assumption is made in other methods.[1,3] As the texture increases, it becomes necessary to increase the number of sampling points. The $G_3$ and $[(A_W \text{ T.C.})/A_W]$ depend upon these assumptions.

The poles of 18 crystallographic planes of uranium were projected on the surface of a sphere. Arcs of great circles were drawn equidistant between a pole and each of its nearest neighbors. Thus, a spherical polygon was formed about each pole. The polygon was divided into spherical triangles and the chords of each triangle were measured with dividers. The surface area of each triangle was determined from the chord lengths. The areas of individual triangles were summed to give the area of each polygon.

In Table I are given (1) the diffraction planes, (2) calculated random intensities, (3) area weight factors, (4) squares of direction cosines, and (5) products of area weight factors and squares of direction cosines.

Table I

| Plane | $I_0$ | $A_W$ | $\cos^2\alpha$ | $\cos^2\beta$ | $\cos^2\gamma$ | $A_W \cos^2\alpha$ | $A_W \cos^2\beta$ | $A_W \cos^2\gamma$ |
|---|---|---|---|---|---|---|---|---|
| 020 | 6.34 | 0.0318 | 0.00000 | 1.00000 | 0.00000 | 0.0000 | 0.0318 | 0.0000 |
| 110 | 72.7 | 0.0634 | 0.80877 | 0.19123 | 0.00000 | 0.0513 | 0.0121 | 0.0000 |
| 021 | 100.0 | 0.0608 | 0.00000 | 0.74035 | 0.25965 | 0.0000 | 0.0450 | 0.0158 |
| 002 | 51.4 | 0.0304 | 0.00000 | 0.00000 | 1.00000 | 0.0000 | 0.0000 | 0.0304 |
| 111 | 58.3 | 0.0738 | 0.63769 | 0.15078 | 0.21153 | 0.0471 | 0.0111 | 0.0156 |
| 112 | 48.3 | 0.0522 | 0.39013 | 0.09224 | 0.51763 | 0.0204 | 0.0048 | 0.0270 |
| 130 | 3.37 | 0.0357 | 0.31969 | 0.68031 | 0.00000 | 0.0114 | 0.0243 | 0.0000 |
| 131 | 40.0 | 0.0684 | 0.28904 | 0.61508 | 0.09588 | 0.0198 | 0.0421 | 0.0066 |
| 023 | 16.8 | 0.0659 | 0.00000 | 0.24059 | 0.75941 | 0.0000 | 0.0159 | 0.0500 |
| 200 | 8.82 | 0.0234 | 1.00000 | 0.00000 | 0.00000 | 0.0234 | 0.0000 | 0.0000 |
| 113 | 11.6 | 0.0477 | 0.23686 | 0.05601 | 0.70713 | 0.0113 | 0.0027 | 0.0337 |
| 132 | 3.65 | 0.0529 | 0.22447 | 0.47769 | 0.29784 | 0.0119 | 0.0253 | 0.0158 |
| 133 | 15.3 | 0.0795 | 0.16558 | 0.34809 | 0.48833 | 0.0130 | 0.0277 | 0.0388 |
| 114 | 10.2 | 0.0749 | 0.15282 | 0.03613 | 0.81105 | 0.0114 | 0.0027 | 0.0607 |
| 150 | 7.43 | 0.0372 | 0.14469 | 0.85531 | 0.00000 | 0.0054 | 0.0318 | 0.0000 |
| 223 | 12.2 | 0.0487 | 0.50434 | 0.11925 | 0.37641 | 0.0246 | 0.0058 | 0.0183 |
| 152 | 12.8 | 0.0689 | 0.12139 | 0.71755 | 0.16106 | 0.0084 | 0.0494 | 0.0111 |
| 312 | 8.85 | 0.0845 | 0.85201 | 0.02238 | 0.12561 | 0.0720 | 0.0019 | 0.0106 |
| $\Sigma$ | | 1.0001 | 5.84548 | 6.34299 | 5.81153 | 0.3314 | 0.3344 | 0.3344 |
| $\frac{1}{18}\Sigma$ | | | 0.3247 | 0.3524 | 0.3229 | | | |

Using the data from Table I, it may be shown that

$$\frac{1}{18}\sum_{i=1}^{18}(\cos^2\beta_i - \cos^2\alpha_i) = +0.028$$

$$\sum_{i=1}^{18} A_{wi}\,(\cos^2\beta_i - \cos^2\alpha_i) = +0.003 \quad ;$$

for a randomly oriented sample

$$\left(\frac{I_i/I_i'}{\sum_{i=1}^{n} A_{wi}\, I_i/I_i'}\right) = 1 \quad .$$

Areas were also determined by laying paper over the spherical polygon, tracing the polygon, and then planimetering the resulting figure on the paper. The maximum difference in an individual $A_w$ between results obtained using the polar planimeter and the spherical triangles was 3.8 per cent. A comparison of the total area with that calculated for the octant indicate a 0.7 per cent difference for the spherical triangles method and a 2.2 per cent difference for the polar planimeter method.

The growth index $G_3$ is given by

$$G_3 = \frac{\sum_{j=1}^{n}(A_{wj}\, I_j/I_j')\,(\cos^2\beta_j - \cos^2\alpha_j)}{\sum_{i=1}^{n}(A_{wi}\, I_i/I_i')} \quad .$$

The primed and unprimed I's correspond to calculated random intensities and measured intensities, respectively.

$G_3$ varies from minus one to positive one, zero corresponding to predicted dimensional stability during irradiation.

# REFERENCES

1. Sturcken, E. F., An X-ray Method for Predicting the Stability of Natural Uranium at Low Burnup, DP-251 (Nov 1957) (Classified).

2. Morris, P. R., Comparative Measurements of the Velocity of Propagation of an Ultrasonic Pulse in Uranium Fuel Elements, NLCO-764, p. 13 (Nov 24, 1958), p. 13.

3. Sturcken, E. F., "A Generalized Growth Index Formalism," Papers Presented at the X-ray Preferred Orientation Meeting Held at National Lead Company of Ohio November 9 and 10, 1959, NLCO-804 (July 15, 1960), p. 9.

# SOME PROBLEMS AND FACTS IN THE DETERMINATION OF GROWTH INDEX IN BETA-TREATED URANIUM

R. B. Russell
Nuclear Metals, Inc.

## I. PROBLEMS

### INTRODUCTION

The determination of texture in beta-treated uranium is somewhat different from the determination of that of alpha-fabricated metal. In the latter case, the grain size is usually much smaller, so that a texture determination is somewhat more reliable, but the difference which gives rise to more problems is that the texture of beta-treated metal is practically random, with the result that the greater number of diffracting peaks tend to interfere with each other, making their quantitative intensity measurements more difficult. Fortunately for the diffractionist, most peaks are separated, including the low angle triplet (110)-(021)-(002). Present growth indices are based on a selection from the group of strong and resolved peaks only, so that growth is predicted on the basis of a determination of only a part of the texture. In attempting to learn whether or not, from the point of view of irradiation growth, this part is a truly representative part of the entire texture, the physical metallurgist must rely primarily on his information of the relative degree of scatter [1] in the relation between measured growth and a particular growth index. Now, aside from the practical problem of choosing enough different $hk\ell$ pole densities to make an adequate representation of the entire texture, he must decide on how to weight these choices. It seems clear that he has only two weighting possibilities: quantized or continuous. The quantized method is exemplified by point weighting (such as $K_{29}$, which has not been pile tested, and G.I. which has) or area weighting (such as $G_3$). The continuous weighting method is used in $G_2$. It would be very helpful to the metallurgist if the weighting method were the only variable, because then he could decide on the basis of experimental evidence alone - always a valuable tool to the scientist - which weighting method is correct. Accordingly, if the components of the terms $\Sigma C$ and $\Sigma A_W C$ were adjusted so that

$$\Sigma C = \Sigma A_W C \text{ (preferably = 0)},$$

he could choose the preferable weighting.

It may turn out that over a part of the curve representing actual vs. predicted growth, the predicted growth index may show a larger degree of scatter or insensitivity to actual growth. In this case it may be that some significant poles have been omitted from the predicted growth index. Certain

diffraction peak intensity data are not collected, not because they are not important, but because they are not well enough resolved to measure. For example:

| (hkℓ) | CuKα$_1$, 2θ | CuKα* rel. int. ($I_0$) | C=(cos$^2\beta$-cos$^2\alpha$) |
|---|---|---|---|
| 221 | 76.57 | 20.4 | -0.5789 |
| 004 | 76.88 | 5.46 | 0 |
| 202 | 77.00 | 10.9 | -0.7500 |
| 310 | 110.09 | 4.06 | -0.9488 |
| 025 | 110.22 | 5.85 | +0.1017 |
| 204 | 110.78 | 6.34 | -0.4287 |

Of these, the (202) and (204) reflections are probably the most important because enhanced reflections from these planes have been observed from surfaces perpendicular to former thermal gradients present near the surfaces of beta-quenched uranium. The progression of pole densities parallel to thermal gradients has been found to be 100, 101, 102, 001, 0kℓ, with 100 associated with the steepest thermal gradients,(2) although Starbuck and Kloepper(3) have reported that the progression is rather 100, 11ℓ, 001, 0kℓ. Figures 1a, 1b, 1c, and 1d show the progression of maximum pole density from 100 to 001 in the metal up to $\frac{1}{4}$ inch from the water-quenched end of a one-inch-diameter Jominy bar.

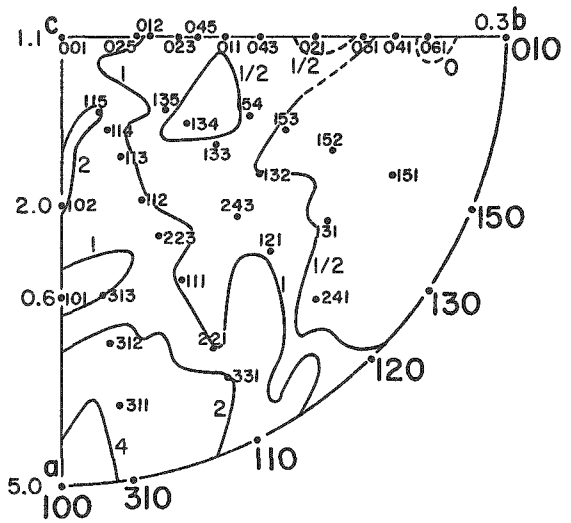


Fig. 1(a)

Crystallographic (inverse) pole figures for the axial direction of Jominy Bar J-3 at increasing distances from the water-quenched end at 0.002 in. from end.
$G_3$ = -0.34, $\overline{K}$ = -173
Drawing No. RA-1556

*E. F. Sturcken, Determination of Theoretical Diffraction Intensities for Alpha Uranium, NLCO-804 (July 15, 1960), p. 57: $I_0$ for (021)=100

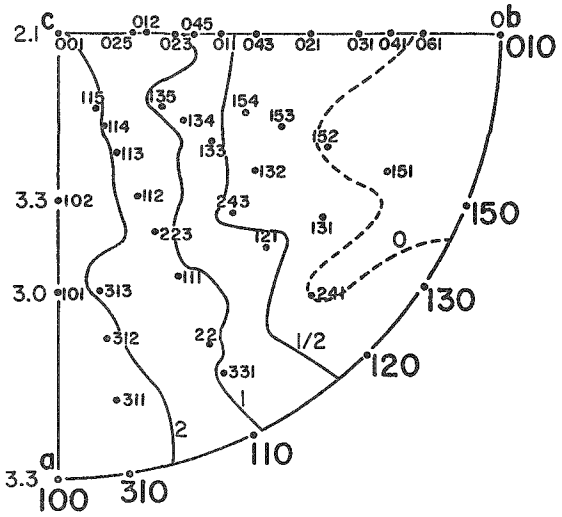


Fig. 1(b)

At 0.010 in. from end,
$G_3$ = -0.33
$\overline{K}$ = -188
Drawing No. RA-1557

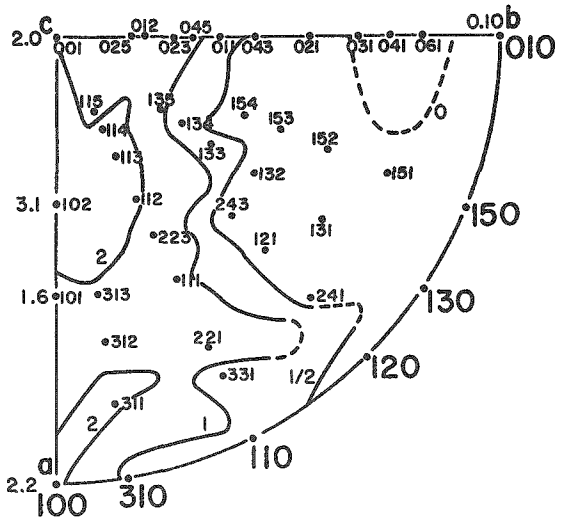


Fig. 1(c) At 0.047 in. from end,
$G_3$ = -0.27
$\overline{K}$ = -166
Drawing No. RA-1597

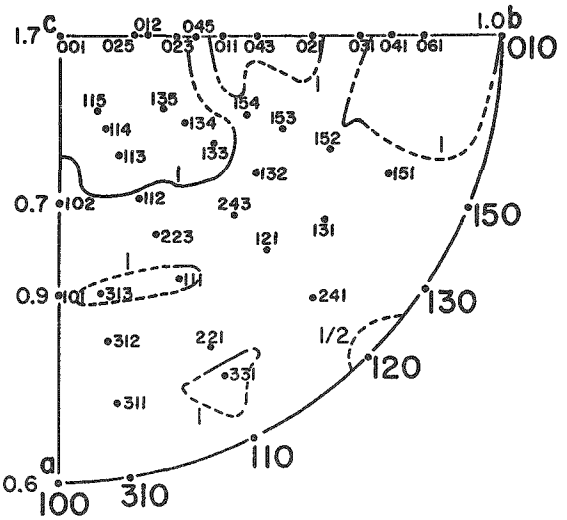


Fig. 1(d) At 0.272 in. from end,
$G_3$ = +0.01
$\overline{K}$ = +6
Drawing No. RA-1558

Since the $G_3$ value is the more important where it is observed or expected to deviate more from zero, it follows that the exclusion of these $10\ell$ poles from a growth index is injurious to a statistical study of the relation between actual and predicted growth of beta treated uranium.

## RESOLUTION OF DIFFRACTION PEAKS

The essential problem of separating close peaks, of course, arises from the fact that several interplanar spacings are nearly identical. Possible methods of resolving diffraction peaks have ordinarily been to increase the collimation and/or to increase the incident wave length. We have used 1° divergence and scatter slits and the narrowest receiving slit on our Philips high angle goniometer, i.e., 0.003 inch. Use of a narrower divergence slit is impractical because of the serious reduction in intensity without any noticeable increase in resolution. Of the targets commonly available: Cu, Ni, Co, Fe, and Cr, only the $K\alpha$, $K\beta$ of Cu, Ni and $CoK\beta$ will cover the spacings required for $G_3$ (assuming a maximum $2\theta$ limit of 164°). There is no appreciable improvement in the resolving power of $NiK\alpha$ or $CoK\beta$ over $CuK\alpha$. Table I shows the $2\theta$ positions of the two triplets containing (202) and (204).

Table I

THE $2\theta$ POSITIONS OF TWO TRIPLETS CONTAINING THE (202) AND (204) DIFFRACTION PEAKS OF ALPHA URANIUM FOR SEVERAL EMISSIONS

(Assuming $\lambda_{CuK\alpha_1}$ = 1.54051 Å, a = 2.85o3 Å, b = 5.8712 Å, and c = 4.9558 Å

| Target | (hkℓ) | | | Δ2θ | | (hkℓ) | | | Δ2θ | |
|---|---|---|---|---|---|---|---|---|---|---|
| | 221 | 004 | 202 | * | ** | 310 | 025 | 204 | * | ** |
| $CrK\alpha_1$ | 134.11 | 135.04 | 135.40 | 0.36 | 0.11 | - | - | - | - | - |
| $K\alpha_2$ | 134.57 | 135.51 | 135.88 | 0.37 | - | - | - | - | - | - |
| $K\beta_1$ | 113.96 | 114.57 | 114.80 | 0.23 | - | - | - | - | - | - |
| $FeK\alpha_1$ | 102.27 | 102.76 | 102.95 | 0.19 | 0.10 | - | - | - | - | - |
| $K\alpha_2$ | 102.56 | 103.05 | 103.24 | 0.19 | - | - | - | - | - | - |
| $K\beta_1$ | 89.90 | 90.29 | 90.44 | 0.15 | - | 138.30 | 138.54 | 139.59 | 1.05 | - |
| $CoK\alpha_1$ | 92.03 | 92.43 | 92.59 | 0.16 | 0.10 | 144.25 | 144.54 | 145.79 | 1.25 | 0.47 |
| $K\alpha_2$ | 92.28 | 92.69 | 92.85 | 0 16 | - | 145.03 | 145.32 | 146.60 | 1.28 | - |
| $K\beta_1$ | 81.3o | 81.70 | 81.83 | 0.13 | - | 119.14 | 119.30 | 119.98 | 0.68 | - |
| $NiK\alpha_1$ | 83.64 | 83.99 | 84.12 | 0 13 | 0.11 | 123.77 | 123.94 | 124.68 | 0.74 | 0.24 |
| $K\alpha_2$ | 83 88 | 84.23 | 84 36 | 0.13 | - | 124.27 | 124.44 | 125.19 | 0.75 | - |
| $K\beta_1$ | 74.22 | 74.51 | 74.63 | 0.12 | - | 105.89 | 106.02 | 106.54 | 0.52 | - |
| $CuK\alpha_1$ | 76 57 | 76.88 | 77.00 | 0.12 | 0.11 | 110.09 | 110.22 | 110.78 | 0.56 | 0.1o |
| $K\alpha_2$ | 76.80 | 77.11 | 77.23 | 0.12 | - | 110.49 | 110.62 | 111.19 | 0.57 | - |
| $K\beta_1$ | 68.10 | 68.37 | 68.47 | 0.10 | - | 95.58 | 95.68 | 96.11 | 0.43 | - |

* $2\theta_{202} - 2\theta_{004}$

** $(2\theta_{004})_{K\alpha_2} - (2\theta_{202})_{K\alpha_1}$

It is clear that (204)K$\alpha_1$ is better separated than is (202)K$\alpha_1$, which occurs only about 0.10° (2$\theta$) from (004)K$\alpha_2$ for all targets. There are several techniques which might be used to determine the intensities of partially resolved peaks:

1) derivation of intensity from associated orders and peak tracing;

2) separation by differential thermal expansion;

3) use of crystal mondchromator; and

4) pole densities of neighboring poles.

## DISCUSSION

### Derivation of Intensity from Associated Orders and Peak Tracing

The nearest interfering (hk$\ell$) reflection to (202) is (004), and since we know that $I_{004}/I_{002}$ = 5.46/51.4 for CuK$\alpha$ and that $I_{002}$ can be measured from a well-resolved reflection, we can compute $I_{004}$. We can usually make some estimate of both the $I_{(221)}K\alpha_1$ and $I_{(202)}K\alpha_2$. Since it is known that the relative intensities[4] $K\alpha_2/K\alpha_1 \cong 0.50$, the total intensity $K\alpha_{1,2}$ can also be estimated. In this way, by trial-and-error peak tracing, a fair estimate of the intensities can be obtained, of course, subject to the rules that the sum of the amplitudes of the separate estimated diffraction curves add up to the actual given amplitude at a particular 2$\theta$ and that the sum of the separate integrated area equals the total area of the triplet envelope.

### Separation by Differential Thermal Expansion

The relative separation of different (hk$\ell$) diffraction peaks is changed by heating:

$$\Delta(2\theta) = -2\alpha_{hk\ell} \tan\theta \, \Delta T.$$

Since alpha uranium is thermally anisotropic, it is possible that the separation of some peaks could be increased by heating. Unfortunately, heating to as high as 300°C (higher might alter the texture) would change 2$\theta$ by only a negligible amount - entirely insufficient for the purpose.

### Use of Crystal Monochromator

Lang[5] has described several variations of the diffracted-beam monochromatization techniques. Figure 2 shows an arrangement where the monochromator is a transmitting bent crystal. This same scheme was conceived independently by Harker.[6] Lang used a LiF crystal, ground parallel to (100) and 0.3 mm thick annealed and plastically bent. He was not able to separate the K$\alpha_1$ component because of the poor quality of his crystal. However, he recommends that the best chance occurs with the

$(13\bar{4}0)$ quartz or the (060) Muscovite mica reflections. It may be seen from Table I that the removal of all wavelengths except $K\alpha_1$ might very well enable one to estimate by graphical separation (7) the intensity of (202) $CrK\alpha_1$ although, because of the large absorption of this wavelength in air (to say nothing of the reduced intensity by monochromatization), a helium path would have to be used. The monochromatization of $K\alpha_1$ rather than $K\beta_1$ for all of these target materials is strongly preferable because of the larger separation of the $K\alpha_1$'s, and especially because of the fact that $K\beta_1$ intensity is only 16 to 20 per cent of the $K\alpha_1$, depending on the target.(4)

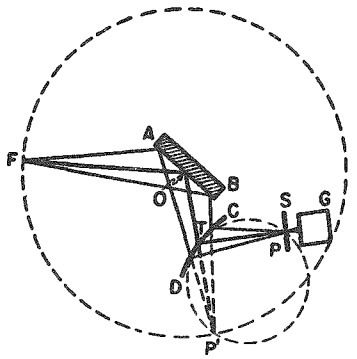


Fig. 2 Combination of a reflection specimen and a transmission monochromator (RT technique).

Pole Densities of Neighboring Poles

Finally, the correctness of the derived (unresolvable peak) may be checked by the $I/I_0$ of a pole located very near to the pole in question. The values of $I/I_0$ for 101 and 102 can be estimated from those of 312, 223, 112 and 113.

Of the possible methods of determination of intensities of poorly resolved peaks, we have used only the methods of peak tracing and intensity of associated orders (1) as checked by a comparison with $I/I_0$ of neighboring poles.

It is earnestly hoped that some laboratory will also try the method of monochromatization by Lang's RT method (3). Some further justifications of constructing an RT monochromator could be summarized:

1. Study of low-atomic-number elements where unmonochromatized X-ray diffraction is complicated by severe Compton scattering. (Lang points out, for example, that a diffracted-beam monochromator which will eliminate $CuK\alpha_2$ will also eliminate Compton-scattered radiation above $\theta = 16°$, where the wavelength change * of Compton radiation is equal to the separation between $CuK\alpha_1$ and $CuK\alpha_2$.)

2. Study of crystals with low symmetry and hence poorly resolved diffraction peaks.

*$\Delta\lambda = 0.04848 \sin^2\theta$ Angstroms.

3. Study of superlattices having elements of neighboring atomic numbers, by selecting a wavelength which will increase the difference in electronic scattering factors in the region of anomalous dispersion.

4. Examination of diffraction peaks at the highest diffraction angles, because of the lack of obstruction between the arm carrying counter and receiving slit by the body of the X-ray tube.

## II. GROWTH INDEX ($G_3$) IN BETA-TREATED URANIUM RODS AND TUBES

When alpha uranium is transformed to beta uranium by heating to a suitable time-temperature and then retransformed to alpha by cooling at rates typical of present practice, it is inevitable that temperature gradients will be present near the cooling surfaces. At these surfaces - both at the ends of the piece, but more importantly, at the longitudinal surfaces - the cooling rates will be higher than at some points below the surfaces. Chiswik and Lloyd[8] have shown that after a uranium rod, cooled uniformly through the beta-alpha transformation by lowering it through a temperature gradient, is completely transformed, it will contain columnar grains whose longer dimensions are parallel to the temperature gradient and to their 001 poles. Starbuck and Kloepper[3] have demonstrated that for larger thermal gradients occurring in end-quenched Jominy bars, the orientation is such that the 100 poles are parallel to the temperature gradient. This has been confirmed by our present work. It was naturally expected that the same texture gradients found in Jominy bars would be observed in both rods and tubes beta treated by total immersion quenching. Figure 3 shows a plot of $G_3$ vs. axial distance from the end in $1\frac{7}{32}$-inch-diameter rod, in $3\frac{1}{8}$-inch-OD by $2\frac{1}{2}$-inch-ID, and $1\frac{1}{2}$-inch-OD by $\frac{3}{8}$-inch-ID tubes beta-treated by total immersion quenching in cold (12°C) water. We can see that the $G_3$ is negative near the water-quenched end and rises to about 0 at a distance of about one-half radius for the rod and about one-half wall thickness for the tubes. Crystallographic pole figures taken at various distances where the $G_3$ is increasing show the textures to be nearly identical to those developed at the water-quenched end of a Jominy bar. Photomacrographs also show, as expected, a columnar grain disposition very similar to those observed by Lewis[9] on end-quenched Jominy bars.

Figure 4 shows a plot of $G_3$ vs. radial distance in these same sizes and heat treatments. It will be noted that $G_3$ increases from a negative value to about zero at about midwall position. In the case of the 3-inch-OD by 2.5-inch-ID tube, the value of $G_3$ is zero only for a small volume of metal at the midwall and is negative near both the ID and OD. One would conclude that a cold water quench of an element of $\frac{1}{4}$-inch wall thickness would be a very bad beta treatment.

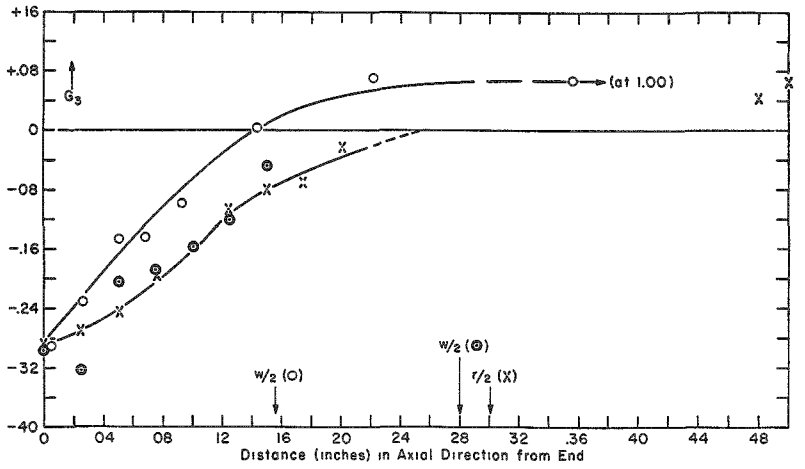


Fig. 3 Change of axial growth index, $G_3$, with distance from end of three 8-in. long cylinders after cold water quenching from molten salt (LH980) at 730°C - 15 min.

⊙ $3\frac{1}{8}$ -in. OD x $2\frac{1}{2}$ -in. ID tube ($M_1$)

◎ $1\frac{1}{2}$ -in. OD x $\frac{3}{8}$ -in ID tube ($H_1$)

X $1\frac{7}{32}$ -in. diameter rod ($K_1$)

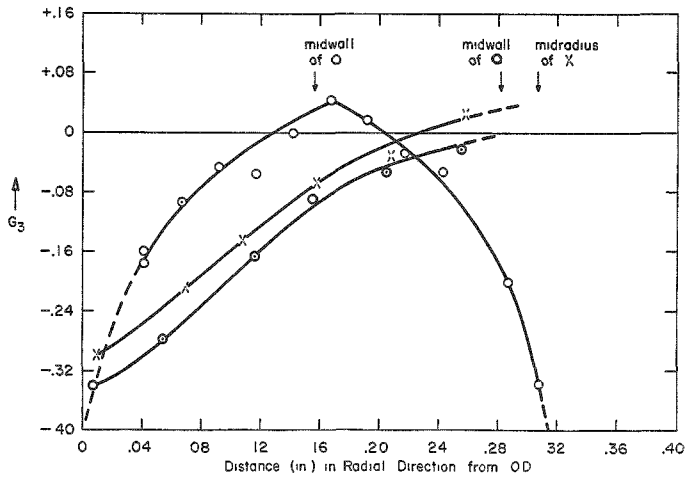


Fig 4 Change of radial growth index, $G_3$, through wall thickness of three 8-in. long cylinders after cold water quenching from molten salt (LH980) at 730°C - 15 min. Drawing No. RA-1750

⊙ $3\frac{1}{8}$ -in OD x $2\frac{1}{2}$ -in. ID tube at 3.5 - 4.5 in. from end ($M_1$)

◎ $1\frac{1}{2}$ -in OD x $\frac{3}{8}$ -in.ID tube at 1 8 - 3.8 in. from end ($H_1$)

X $1\frac{7}{32}$ -in. diameter rod at 1.8 - 3.3 in. from end ($K_1$)

Again, a study of pole figures in the radial direction shows a strong similarity to the axial pole figures near the water-quenched end of Jominy bars.

We are continuing to explore the effect of quenching media (hot water, cold and hot oil, molten metal and salt, etc) on various sizes of uranium in a similar fashion, with the expectation that we shall be able to list the effect of these media on texture gradients in beta-treated ingot and dingot.

## REFERENCES


1. See NMI-RBR-27 (March 21, 1960), p. 5, a memo circulated to the Committee.
2. Russell, R. B., Summary of Progress in the Beta Treatment of Uranium, November 1, 1959-August 31, 1960, NMI-2801, p. 17.
3. Starbuck, J. W., Kloepper, H. C. Preferred Orientation Studies on End-quenched Jominy Bars, MCW-1430, p. 89; Preferred Orientation of End-quenched Jominy Bars Sampled at Small Increments, MCW-1433, p. 105.
4. Compton, A. H. and Allison, S. K., X-rays in Theory and Experiment, Van Nostrand Co., New York (1935) p. 640.
5. Lang, A. R. Diffracted-beam Monochromatization Techniques in X-ray Diffractometry, Rev. Sci. Inst. 27, 17 (1956).
6. Harker, D., U. S. Patent 2,532,810.
7. Peiser, H S. et al., ed., X-ray Diffraction by Polycrystalline Materials, Institute of Physics, London, (1955), p. 406.
8. Chiswik, H. H. and Lloyd, L. T., Some Aspects of the Beta-to-Alpha Transformation in Uranium: Metallographic Structure and Orientation Relationships, ANL-5777 (Nov 1959).
9. Lewis, L., Contribution of the Jominy-type End Quench to Metallographic Phase Identification in Uranium, BRB-44 (Dec 1958).

# RECRYSTALLIZATION IN ROLLED URANIUM SHEET

Lowell T. Lloyd and Melvin H. Mueller
Argonne National Laboratory

## INTRODUCTION

As this group is well aware, the recrystallization of cold-deformed, polycrystalline alpha uranium has been the subject of numerous investigations; unique among these is the work of Cabane and Petit at Saclay in France.[1] In their study of uranium sheet, rolled 80% reduction in thickness at room temperature, the authors reported recrystallization at temperatures between 320 and 420°C without a preferred orientation change, as indicated by dilatometric measurements. At temperatures just above 420°C they found a second recrystallization which was accompanied by a preferred orientation change. Presumably the latter was not the same as the normal "secondary recrystallization" that would occur near the upper temperature limit of stability of the alpha range.

The occurrence of recrystallization without an apparent preferred orientation change is indeed an interesting observation, and we at Argonne have undertaken a program in an attempt to verify this phenomenon. Our work has been with high-purity uranium, for it was felt that the purity of the metal might be a significant factor

The early work on this program has been reported by Yario and Lloyd.[2] In that study, sheet rolled at room temperature was prepared almost identically to that used by Cabane and Petit. Very briefly, the dilatometric results indicated that, indeed, uranium could be recrystallized by long-time anneals at 360°C or lower without indications of preferred orientation change. A texture change accompanied annealing for moderate times at temperatures from 400 to 600°C, and a different preferred orientation accompanied grain coarsening at temperatures above 600°C.

The most significant thermal treatment given to this material, prior to its final fabrication, was an anneal in the beta-phase temperature range followed by slow cooling. Obviously, this caused large alpha grains to be present in the starting material. In turn, there was extreme heterogeneity in the as-rolled and recrystallized grain structures. The as-rolled structure consisted of heavily deformed areas and smaller quantities of lightly deformed material. The annealing of the former was characterized by initial creation of very fine recrystallized grains which were later absorbed by discontinuous growth of larger grains. Lightly deformed areas, upon annealing, first exhibited recovery by polygonization and then underwent normal recrystallization. Another important effect of the large alpha grain size was that it essentially precluded the use of X-ray measurements of preferred orientations, and the indirect method of measuring thermal expansion coefficients had to be used

To overcome the problems associated with the large alpha grain size, Yario undertook a second piece of work wherein, prior to the final room-temperature fabrication of approximately 80% reduction in thickness, the stock was subjected to step-reduction and annealing treatments, similar to those developed by Fisher,[3] to give a relatively small, uniform alpha grain size with a minimum of "banding." Shortly after starting this work, Yario left ANL and is now with the GE ANP project. Mueller and Lloyd have continued this study, and this afternoon I will describe some of the recent work. At various points I will make reference to the earlier work; partially from the viewpoint of comparison and partially because the more recent work is not completely documented with figures, I will spend a good portion of the time on preferred orientation measurements, which obviously are of greater interest to this group; however, some of the thermal expansion and metallographic observations must be included because of their significance.

## EXPERIMENTAL TECHNIQUES

First of all, I should touch upon the experimental aspects of the work very briefly. All rolling was carried out on a mill with 17-in.-diameter rolls. The piece was reversed after each pass so as to give two-fold symmetry about the rolling direction and about the transverse direction.

Thermal expansion measurements were made in directions parallel to the rolling direction (longitudinal samples) and parallel to the transverse direction (transverse samples). The change in mean coefficient of expansion between 200 and 300°C was used as a qualitative measure of preferred orientation change. Metallographic observations, which included quantitative measurements of volume per cent of recrystallization, were made for the most part on sections parallel to the rolling direction and perpendicular to the rolling plane; observations on the other two mutually perpendicular sections indicated no significant differences.

The quantitative measurements of preferred orientation were obtained by the Schulz reflection method with automatic instrumentation developed by Mueller and his co-workers.[4,5] The data for each condition were obtained from 7 sections, treated for corrections, and plotted in the manner previously used by Mueller, Knott, and Beck in their study of deformation and recrystallization textures of rolled uranium sheet.[6] One point of interest may be that the instrumentation is now arranged to record the counts per a given time rather than the time for a given number of counts. In the present work, the time period used was 40 seconds.

## RESULTS AND DISCUSSION

Thermal Expansion: Dilatometric studies were carried out on samples annealed at various times and temperatures. Rather than try to cover the data thoroughly, the results can be summarized with the help of Table I. Recrystallization upon annealing at 360 and 380°C does not result in appreciable change in the mean coefficient of expansion. A greater change is found upon annealing at 400°C, and more significant changes result from annealing at higher temperatures. The individual results are not much different from those of the earlier work. Figure 1 shows a plot for the change in mean coefficient of expansion of transverse samples as a function of volume per cent of recrystallization from that work. The samples annealed at lower temperatures did not show significant changes in expansion coefficient, whereas those annealed at higher temperatures did. I might point out that the material from the first work seemed to recrystallize at a lower temperature than that for the present work. This is probably associated with the greater heterogeneity of deformation in the former.

Table I

SUMMARY OF MEAN THERMAL EXPANSION DATA

| Annealing Temperature, °C | Range of Annealing Time | Change in Mean Expansion Coefficient* for Fully Recrystallized Samples x $10^6$ (per °C) | |
|---|---|---|---|
| | | Longitudinal Samples | Transverse Samples |
| 360 | 140 - 1500 hr | -1 | +1 |
| 380 | 10 - 300 hr | -1 | +1 |
| 400 | 15 min - 51 hr | -2 | +2 |
| 425 | 15 min - 15 hr | -4 | +4 |
| 450 | 5 min - 15 hr | -5 | +4 |
| 600 | 15 hr | -7 | +5 |

* Mean Thermal expansion coefficient between 200 and 300°C for as-rolled samples were:

Longitudinal = approximately $9 \times 10^{-6}$ per °C

Transverse = approximately $20 \times 10^{-6}$ per °C.

Metallography: The microstructures of the as-rolled and annealed samples show some interesting features. Figure 2a is a typical area of the as-rolled structure of the material studied in the earlier work. Some areas show very little deformation, whereas others are very heavily deformed; this, undoubtedly, is related to the anisotropy of the deformation mechanisms of alpha uranium. In contrast, as shown in Fig. 2b, the structure of the as-rolled material for the present work is more homogeneous; obviously, the starting grain size was considerably smaller. Heterogeneous deformation is still evident, but not to the extent found in the earlier work.

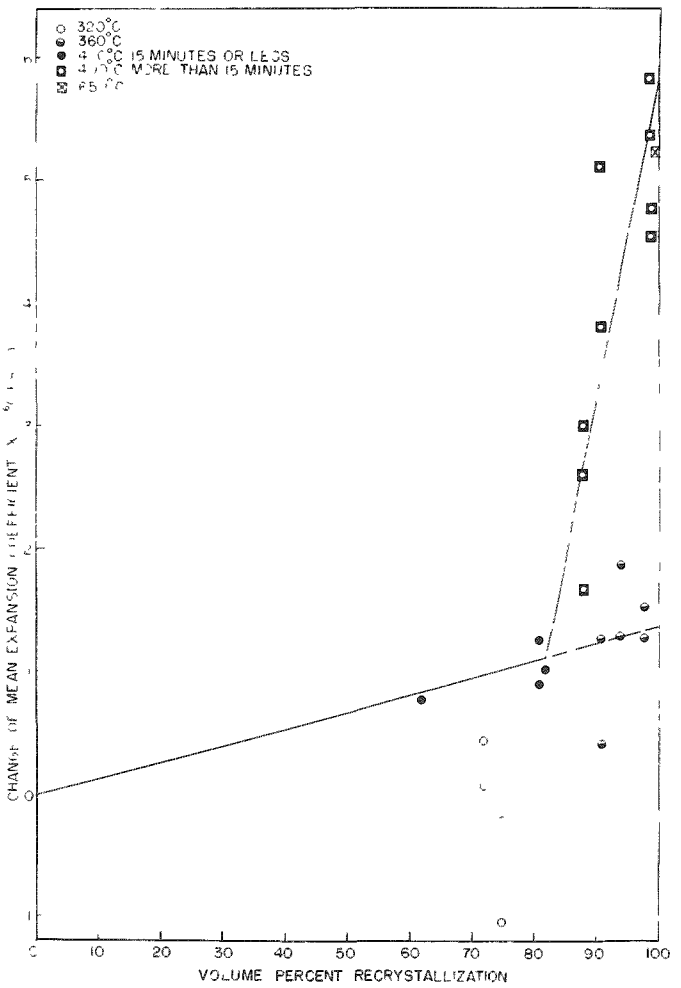


25,098

Fig. 1. Change of Mean Coefficient of Expansion Between 200 and 300°C, over That Obtained from an As-rolled Specimen, as a Function of Volume Per Cent of Recrystallization for Transverse Specimens Annealed for Varying Periods of Time at Different Temperatures.(2)

a. Heterogeneously deformed material studied by Yario and Lloyd.[2]

b. More uniformly deformed material of present study.

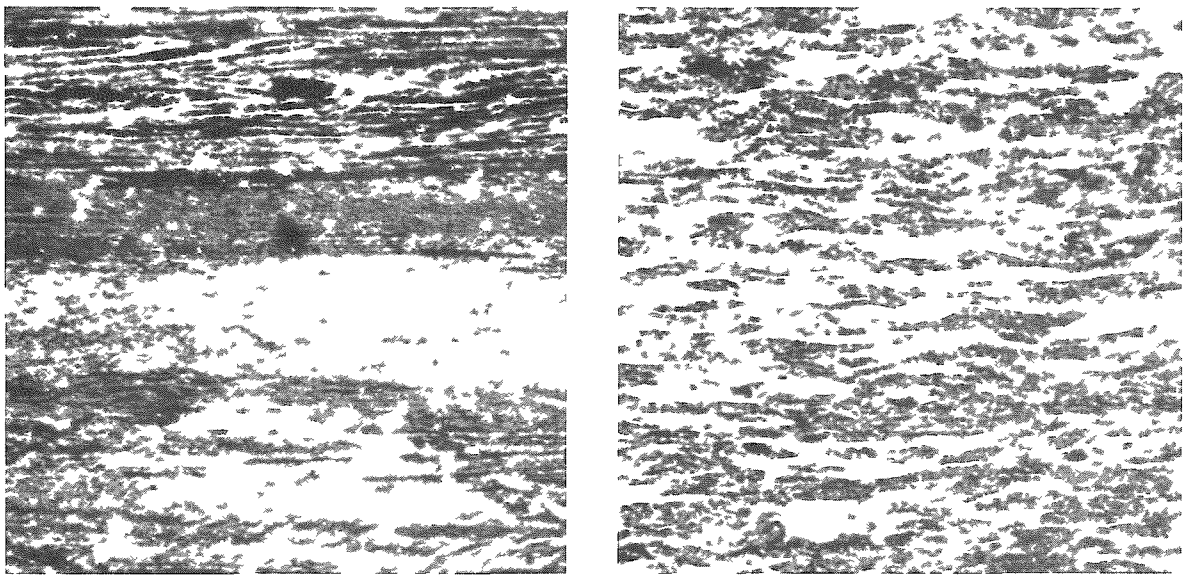

19,783 Pol. Light 400X 23,301 Pol. Light 400X

Fig. 2. Microstructures of Transverse Sections of Uranium Sheet Rolled at Room Temperature.

Figure 3a shows a typical microstructure of a partially recrystallized sample. This photograph was taken of a sample from the earlier work; it was annealed for 15 hr at 360°C. The structure shows unrecrystallized areas, fine-grained areas, and larger grains which appear to be growing by absorption of the fine-grained material. Annealing for 400 hr at 360°C, as shown in Fig. 3b, essentially eliminates the very fine grains. This observation of recrystallization to very fine grains followed by absorption by growth of larger grains was typical of the behavior noted in both the early and present work for samples annealed at low and moderate temperatures.

Preferred Orientation Determinations: X-ray determinations of preferred orientation were made for samples in five different conditions:

1. As rolled
2. Annealed 300 hr at 380°C
3. Annealed 15 hr at 400°C
4. Annealed 15 hr at 450°C
5. Annealed 300 hr at 380°C and 15 hr at 450°C.

a. Annealed 15 hr. b. Annealed 400 hr.

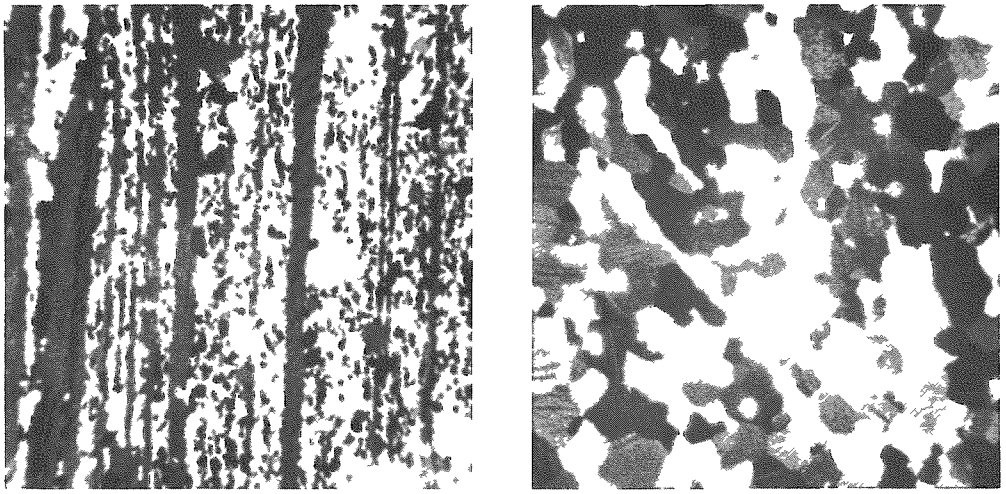

21,346 Pol. Light 1000X 22,249 Pol. Light 1000X

Fig. 3. Microstructures of Uranium Sheet Specimens Annealed Various Times at 360°C.(2)

The fifth set of samples was annealed simultaneously with the second and fourth sets. Because of the interrelationship of sets 1, 2, 4, and 5, I will confine my remarks to these. The preferred orientations of the second and third sets of samples are not significantly different.

First of all, it may be important to take a quick look at typical microstructures for these samples. The as-rolled microstructure is shown in Fig. 2b. Figure 4a shows the microstructure of the sample annealed 300 hr at 380°C. It shows a mixed grain size; although the sample is completely recrystallized, there is evidence of "banding" associated with the as-rolled structure. The structure of the sample annealed for 15 hr at 450°C is shown in Fig. 4b. Here the grain size is much more uniform, but some suggestion of "banding" remains. Figure 4c shows the structure of the duplex annealed samples. It is very similar to that of the 450°C annealed sample, but shows less evidence of banding.

Figure 5 gives the pole figures for the various conditions of the material. Since the sheet was fabricated to give symmetry around the rolling and transverse directions, only one quadrant is needed for each pole figure. Each of the figures plots one pole for each of the four conditions.

a. Annealed 300 hr at 380°C.

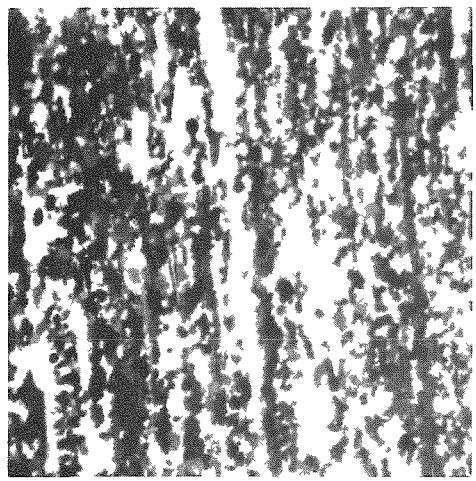

29,445 Pol. Light 400X

b. Annealed 15 hr at 450°C.

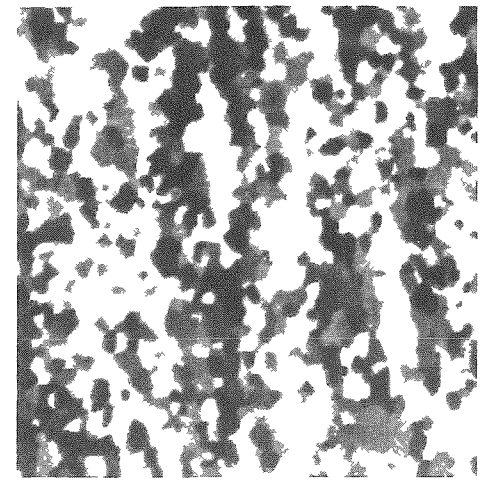

29,448 Pol. Light 400X

c. Annealed 300 hr at 380°C and 15 hr at 450°C.

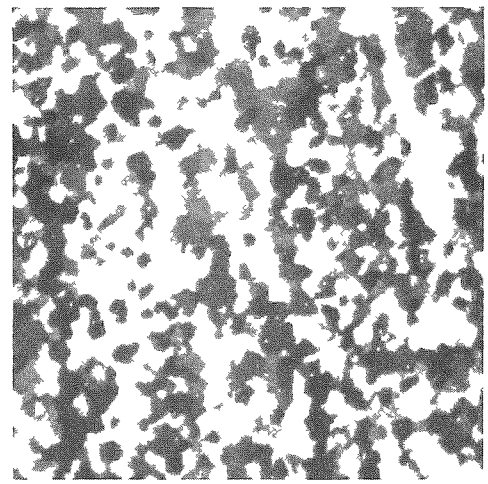

29,447 Pol. Light 400X

Fig. 4. Microstructures of Annealed Uranium Sheet Specimens Used for X-ray Diffraction Studies of Preferred Orientation.

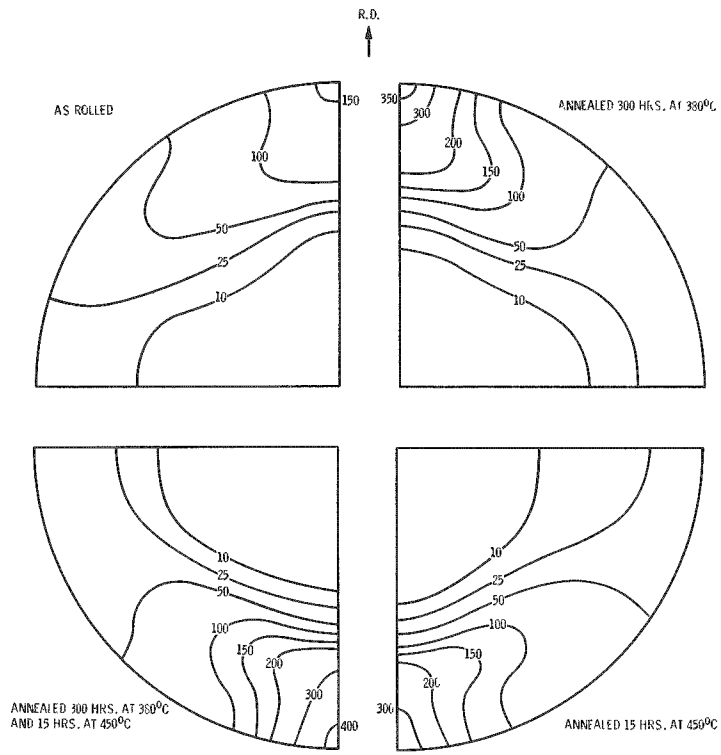
R.D.
AS ROLLED
ANNEALED 300 HRS. AT 380°C
ANNEALED 300 HRS. AT 380°C AND 15 HRS. AT 450°C
ANNEALED 15 HRS. AT 450°C

(020)

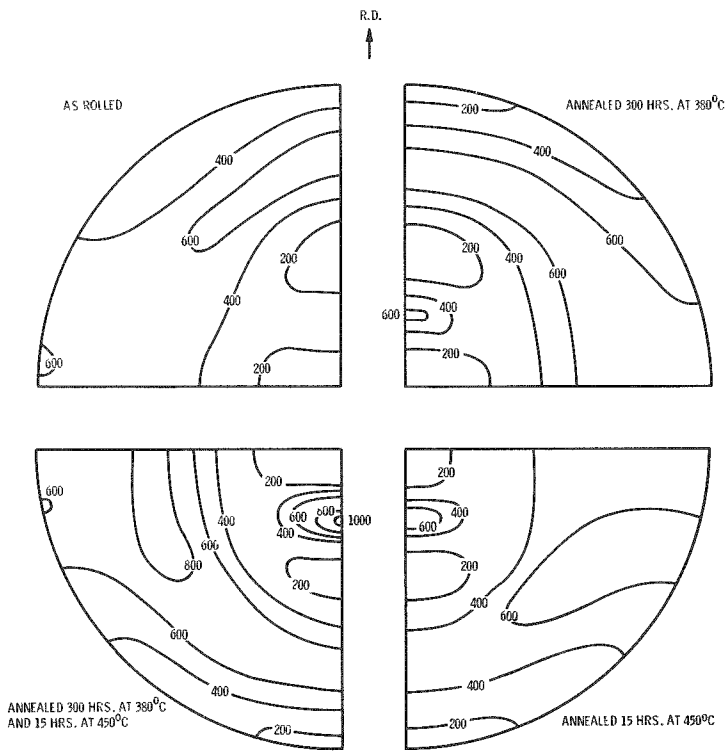
R.D.
AS ROLLED
ANNEALED 300 HRS. AT 380°C
ANNEALED 300 HRS. AT 380°C AND 15 HRS. AT 450°C
ANNEALED 15 HRS. AT 450°C

(110)

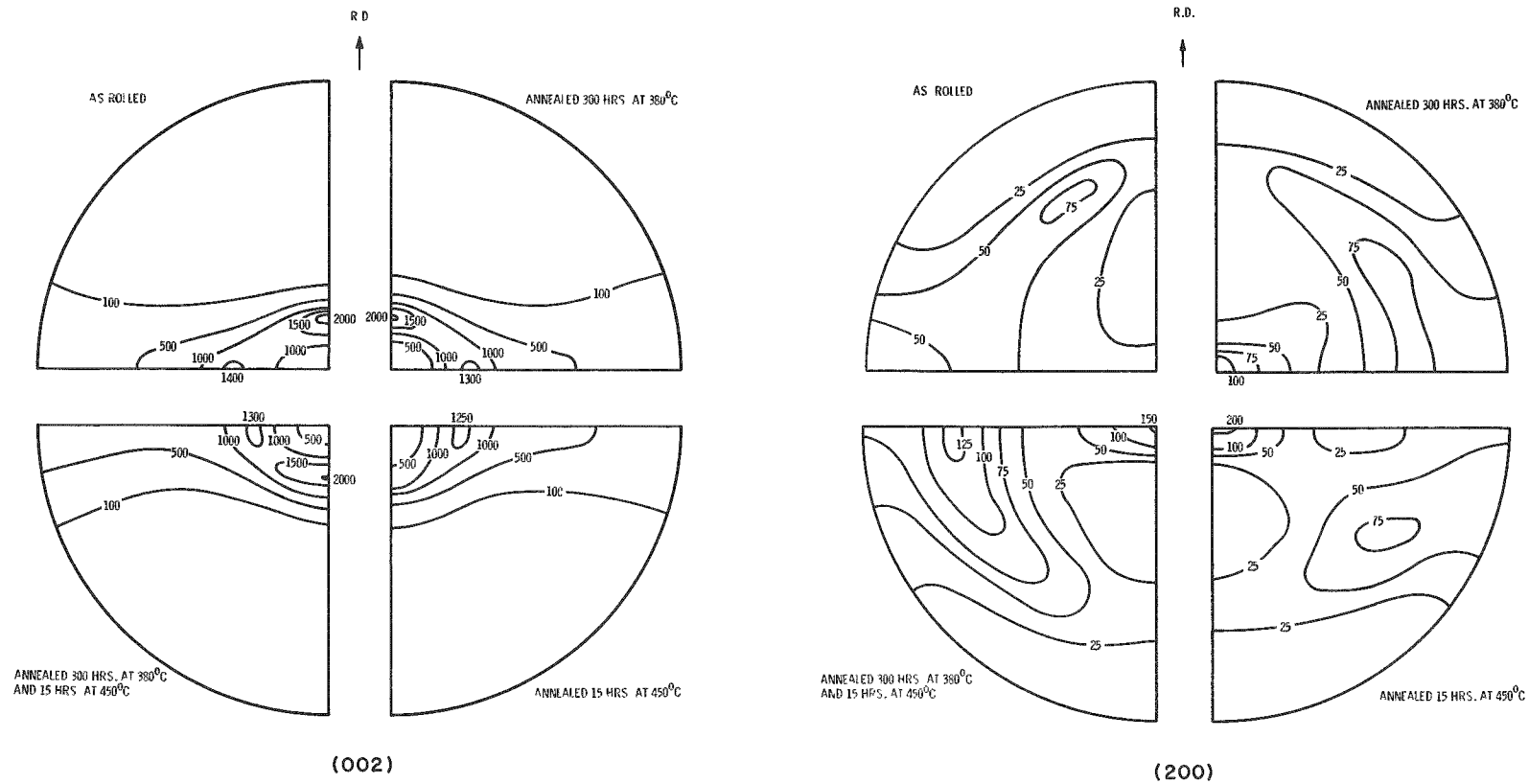


Fig. 5. Composite Pole Figures of As-rolled and Annealed Uranium Sheet

The (020) pole figures for the as-rolled and annealed conditions are very similar, with maxima in the rolling direction. Recrystallization results in a significant increase in intensity of the maximum. These (020) pole figures are very similar to the results obtained by Mueller, Knott, and Beck in their study of 300°C as-rolled and 525°C recrystallized sheet.(6) Subsequent reference to 300°C material will refer to their work.

The (110) pole figures show more striking features. The as-rolled figure has a high-intensity band located approximately 15° from the rolling direction towards the normal direction and spread out towards the transverse direction. In the 300°C work, the maximum of the as-rolled pole figure was in the rolling direction. The pole figures for the recrystallized conditions show spreads of high intensity between the rolling direction and the transverse direction, but the significant feature is the buildup of intensity at a point about 30° from the normal direction towards the rolling direction. This buildup for the material annealed for 300 hr at 380°C gives positive proof of orientation change upon recrystallization at low temperatures. In contrast, the recrystallized material of the 300°C study showed a maximum at approximately 30° from the transverse direction towards the normal direction, with a spread of intensity towards the rolling direction.

The (002) as-rolled pole figure has two regions of high intensity; the highest is approximately 20° from the normal direction towards the rolling direction, and the other is at approximately 30° from the normal direction towards the transverse direction. This is exactly opposite to the relative intensity found for the same locations for the as-rolled material of the 300°C study. The two maxima are retained in approximately the same intensity for the low-temperature annealed and duplex-treated materials; however, the single anneal at 450°C wipes out the maximum between the normal direction and the rolling direction. The latter is the same behavior noted for the recrystallized material of the 300°C study.

Finally, the (200) pole figure of the as-rolled material shows an intensity spread from near the rolling direction towards the transverse direction. The same type of spread was found for the 300°C study of as-rolled material, but the higher values were near the transverse direction. Recrystallization results in the appearance of a maximum in the normal direction with a spread out towards the transverse direction. In contrast, the recrystallized pole figure of the 300°C study showed the highest intensity near the transverse direction, but displaced towards the rolling direction, with a spread up towards that direction, and a secondary maximum in the normal direction. Again, the pole figure for the 300-hr, 380°C annealed material indicates a definite preferred orientation change for the low-temperature annealed material.

## CONCLUSIONS

From metallographic studies, the present work, along with the earlier studies, has shown that recrystallization, at low and moderate temperatures, of high-purity uranium sheet reduced approximately 80% in thickness at room temperature is characterized by the formation of extremely fine recrystallized grains which are later absorbed by growth of larger grains. Dilatometric studies indicate only small changes of the mean coefficient of expansion for samples recrystallized at low temperatures, but significant changes for samples annealed at higher temperatures. If one relies upon thermal expansion data as an indication of preferred orientation change, the dilatometric results indicated no significant change for samples annealed at low temperatures, however, the X-ray diffraction data definitely show a preferred orientation change. Obviously, coefficients of thermal expansion are not reliable indications of preferred orientation. This is not difficult to understand, since a particular mean coefficient of expansion can be produced by a series of directions in the alpha-uranium structure, rather than by a single direction

The question then remains as to why different preferred orientations are obtained for different annealing temperatures. This is probably related to the behavior noted in the metallographic studies. Apparently the crystallographic directions, which grow preferentially to absorb the very fine grains, change with the different annealing temperatures.

## ACKNOWLEDGEMENTS

The authors would like to thank L J. Nowicki, H W Knott, and W H Moses for their assistance in connection with the experimental studies. This work was performed at Argonne National Laboratory under the auspices of the United States Atomic Energy Commission

## REFERENCES

1 Cabane, G and Petit, J , Study of the Annealing of Rolled Uranium, Rev Met. 51 603-613 (1954).

2 Yario, W. R. and Lloyd, L. T., Recrystallization of Heavily Cold-rolled Uranium Sheet, ANL-5966 (May 1959).

3 Fisher, E. S , Preparation of Alpha Uranium Single Crystals by a Grain-coarsening Method, Trans. AIME 209 882-888 (1957).

4 Chernock, W. P , Mueller, M H., Fish, H R. and Beck, P A , An Automatic X-ray Reflection Specimen Holder for the Quantitative Determination of Preferred Orientation, Rev Sci. Inst 24 925-928 (1953)

5 Mueller, M. H. and Knott, H. W., Quantitative Pole Figures for Sheet Material by the Reflection Technique, Rev. Sci. Inst. 25 1115-1118 (1954).

6. Mueller, M. H., Knott, H. W. and Beck, P. A., Deformation and Recrystallization Textures of Rolled Uranium Sheet, Trans. AIME 203 1214-1218 (1955).

# ANALYSIS OF THE AMOUNT OF PREFERRED ORIENTATION BY X-RAY DIFFRACTION LINE INTENSITIES*

D. A Vaughan
Battelle Memorial Institute

## INTRODUCTION

The preferred orientation of crystals in metals during fabrication has been investigated on a qualitative basis for many years. It has been customary to determine the angular distribution of principal crystallographic directions (poles of planes) with respect to the fabrication directions. X-ray diffraction is a convenient method for analyzing the phenomenon. However, there have been few attempts to obtain quantitative results in terms of the per cent concentration of crystallographic poles along a given direction in the fabricated part If the amount of preferred orientation could be expressed quantitatively, the physical behavior of the fabricated part might be predicted from known properties of the crystal lattice. The growth behavior of fabricated uranium during neutron irradiation or thermal cycling has been of considerable interest during the past ten years. It is possible that quantitative analysis of the amount of preferred orientation would aid in understanding this behavior and provide a quality control for the fabricators of this and other materials.

Harris[1] and Mueller et al.,[2] expressed the pole density in uranium by taking a ratio between the observed X-ray diffraction line intensities and the calculated relative intensities for each hkℓ reflection. These ratios were corrected for incident-beam intensity variations by dividing each ratio by the ratio of their sums for all hkℓ reflections examined. This type of analysis is influenced by the number of reflections examined and the choice of hkℓ planes used in the analysis, and does not yield pole density. A more rigorous analysis should evaluate each crystallographic plane independent of the others. In order to obtain such an analysis, a standard specimen of known pole density is required. Such a standard is available for many materials in the extreme conditions of (a) single crystals, and (b) randomly oriented polycrystalline samples. The latter is the most easily obtained and the randomness can be tested by comparison of the observed diffraction-line intensities with the calculated relative intensities. Measurements of single crystals can provide a test of the theory as to the diffraction-line intensity for "perfectly" oriented material. The term "perfect" is used here to indicate one preferred crystallographic direction and is not intended to denote the state of perfection of the individual crystals.

---

*Previously distributed as BMI-X-156 (June 30, 1960).

The work described here presents an analysis of X-ray diffraction theory for the parafocusing diffractometer which involves a correction to the intensity formulas as given by James[3] and by Compton and Allison[4] for the case of reflection from a thick block of randomly oriented powder. Experimental tests of the theory were made with NaCl both in powder form and as a single crystal and then applied to rolled tungsten specimens.

## THEORETICAL CONSIDERATION OF INTENSITY FORMULAS

Specific experimental conditions have been employed[3,4] in deriving the conventional intensity formulas for single crystals and for randomly oriented powder. These conditions differ from those of commercial diffractometers in that the detector is set at the diffraction angle $2\theta$ with wide slits and the diffracting crystal or powder block is rotated through the Bragg angle $\theta$ in a parallel incident beam, whereas under parafocusing conditions a narrow detector slit rotates at twice the angular velocity of the diffracting specimen and a divergent incident beam is employed. In the case of a single crystal, this difference does not modify the intensity formula, because of the necessity for prior alignment of the crystal on the diffractometer and the coupling of the detector and specimen rotation, which maintains alignment. Thus, Equation (1) below, as given by James, applies to a single crystal used in the parafocusing diffractometer,

$$ {}_{hk\ell}I_{sc} = I_0 S Q / 2\mu \quad , \tag{1} $$

where

${}_{hk\ell}I_{sc}$ = the integrated power of the diffracted beam for the particular $hk\ell$ plane of an infinitely thick crystal,

$I_0$ = the intensity per unit area of the incident beam,

$S$ = the area of the incident beam,

$$ Q = \frac{N^2 e^4 \lambda^3}{m^2 c^4} \; \frac{1 + \cos^2 2\theta}{2 \sin 2\theta} \; F^2 \quad , $$

$N$ = number of unit cells per unit volume,

$\mu$ = linear absorption coefficient,

$e,m$ = electronic charge and mass,

$c$ = velocity of light,

$\theta$ = Bragg angle for diffraction, and

$F$ = structure factor.

However, in the development of the equation for the powder-crystal case, as given by James[3] or by Compton and Allison,[4] the experimental procedure is not equivalent to diffractometer use. Furthermore, the angular width of the reflection from a stationary particle cannot be ignored if the incident beam is divergent or the absolute intensities are required. Hence, the following analysis of diffraction-line intensity from a thick block of randomly oriented powder was made for this case.

The probability that a given particle will be in position to diffract a point source of X rays at a given Bragg angle $\theta$ is as stated by James's $\frac{1}{2}\cos\theta\ d\theta$, where $d\theta$ is the angular diffraction width for the particle. However, for a diverging X-ray beam this probability is increased by its divergence angle $\psi$. Thus, the above probability is increased to $\frac{1}{2}\cos\theta(\psi \pm d\theta)$. Since incident-beam divergence is usually considerably larger than $d\theta$, a contribution to the integrated reflection will be produced without rotation of a given particle. Thus, the reflecting power of a particle of volume dV in a divergent beam will be equal to $I_0QdV$, the value for a small crystallite rotated through a parallel beam. Since there will be N particles irradiated and $\frac{1}{2}\cos\theta(\psi \pm d\theta)$ of these will be in position to diffract as the diffractometer rotates through the $2\theta$ values satisfying the Bragg equation ($\lambda = 2d\sin\theta$), the total power diffracted ($P_T$) from a set of $hk\ell$ planes, randomly oriented in the block, will be

$$P_T = N\frac{\cos\theta}{2}(\psi \pm d\theta)\, I_0QdV \quad . \tag{2}$$

However, each set of $hk\ell$ planes with the same spacing will diffract at the given Bragg angle and the above expression must be increased by the multiplicity factor j for the $hk\ell$ plane of interest. Furthermore, by diffractometer methods, only a small segment of the total reflection cone is measured. This segment is fixed by the diffractometer geometry and equals $\ell/2\pi r\sin 2\theta$ of the total reflection produced at the Bragg angle, where $\ell$ is the length of the slits and r is the specimen-to-slit distance. Incorporating these two factors into Equation (2), the measured power $P_r$ becomes

$$P_r = \frac{(\psi \pm d\theta)\ell\, jI_0QV}{8\pi r\sin\theta} \quad . \tag{3}$$

the total volume irradiated, V, is substituted for NdV of Equation (2). The effective V irradiated will vary for different materials because of differences in absorption but can be evaluated by an integration of the reflection from a small volume over the thickness from zero to infinity. This integration is adequately described by James[3] or by Compton and Allison[4] and will not be repeated here, except to give the resulting equation for the

final intensity formula for a thick block of randomly oriented powder:

$$P_r = \frac{(\psi \pm d\theta)\ell j Q I_0 S}{16\pi\mu r \sin\theta} \quad . \tag{4}$$

This differs from previous theory by the factor $(\psi \pm d\theta)$.

The value of $\psi \pm d\theta$ must be evaluated for each material and for the angle of divergence allowed by the incident and diffracted beam slits employed. The $d\theta$ term will vary from 0.01 to 0.5 degree for well-crystallized materials and up to several degrees for plastically deformed metals. The $\psi$ part can be evaluated from a knowledge of the angular divergence allowed by the slits. Since in a random powder there are particles in position to diffract for all angles of the incident beam, the value of $\psi$ is equal to the angle of divergence plus the angle through which the detector can measure a ray diffracted at $2\theta$. For moderate resolution of diffraction lines, 1-degree divergence slits are employed in the incident and diffracted beam, and $\psi$ becomes 2 degrees or 0.035 radian. In the experimental verification of Equation (4), which follows, the value of $d\theta$ was taken as 0.5 degree and, since $d\theta$ modifies both sides of the divergent limiting slits, the $\pm d\theta$ are additive, making $\psi \pm d\theta$ equal to 3.0 degrees or 0.052 radian.

## EXPERIMENTAL INTENSITY MEASUREMENTS

In order to evaluate the merits of the X-ray diffraction intensity theory as presented in the previous section, the intensities for a single crystal and randomly oriented powder of NaCl were measured and the ratios of intensities for the (200), (400), and (600) reflections from the two specimens compared with the calculated ratios obtained by dividing Equation (1) by Equation (4) of the previous section to get

$$hk\ell I_{sc}/hk\ell P_r = \frac{8\pi r \sin\theta}{\ell j(\psi \pm d\theta)} \quad . \tag{5}$$

Relative intensities for the various $hk\ell$ reflections were obtained for both specimens, using the (200) intensity as 1.00. To insure that a random distribution was obtained in the compacted powder and to verify proper alignment of the crystal and diffractometer, the observed relative intensities were compared with the calculated values. The constant factors of Equations (1) and (4) were omitted in this calculation. Results of these experimental tests of the theory are given in Table I.

Table I

COMPARISON OF EXPERIMENTAL AND CALCULATED X-RAY DIFFRACTION LINE INTENSITIES FOR NaCl SPECIMENS CuKα 20 kv 8 ma

| hkℓ | Intensities for Randomly Oriented Powder Compact | | | Intensities for Large Single Crystal | | | Ratio of Intensities Single Crystal/Random | |
|---|---|---|---|---|---|---|---|---|
| | Observed | | Calculated Relative | Observed | | Calculated Relative | Observed | Calculated[a] |
| | Counts | Relative | | Counts | Relative | | | |
| 111 | 416 | 0 093 | 0 089 | | | | | |
| 200 | 4480 | 1.000 | 1 000 | $173 \times 10^6$ | 1 00 | 1 00 | 386 | 375 |
| 220 | 2810 | 0 627 | 0 610 | | | | | |
| 311 | 96 | 0 021 | 0 027 | | | | | |
| 222 | 860 | 0 192 | 0 197 | | | | | |
| 400 | 280 | 0 062 | 0 081 | $365 \times 10^5$ | 0 211 | 0 16 | 1300 | 748 |
| 331 | 64 | 0 014 | 0 021 | | | | | |
| 420 | 880 | 0 196 | 0 209 | | | | | |
| 422 | 556 | 0 124 | 0 123 | | | | | |
| 511-333 | 40 | 0 009 | 0 010 | | | | | |
| 440 | 144 | 0 032 | 0 043 | | | | | |
| 531 | 76 | 0 017 | 0 019 | | | | | |
| 600 | 264 | 0 059 | 0 029 | $1 59 \times 10^5$ | 0 092 | 0 071 | 600 | 1122 |

[a] $I_{hk\ell}/I_{sc/hk\ell}P_r \quad \frac{8\pi r \sin\theta}{\ell J(\psi \pm d\theta)}$

A value of 0 052 radian was taken for $(\psi \pm d\theta)$ as discussed in the previous section

The agreement of experimental results with the present theory, in which the value of $(\psi \pm d\theta)$ is estimated, may be considered reasonable. There are, as yet, some discrepancies which are evident from a comparison of the calculated and observed relative intensities. However, time did not permit further study of these differences. In the case of the single-crystal intensity for the 200 reflection, the correction for the effect of secondary extinction has not been made. Furthermore, the extrapolation to zero absorbers, necessary for determining this very large total count, may be somewhat in error. The 400 and 600 intensities appear to be of the correct relative value, suggesting that the good agreement of the $I_{sc}/P_r$ for the 200 is somewhat fortuitous. However, in the case of the relative intensities for the random specimen, the observed value for the 600 is too large by a factor of 2 and the 400 relative intensity is low by 24 per cent. Superposition of the 622 reflection of CuKβ upon the 600 reflection of CuKα may account for part of the high intensity observed for the 600 reflection. The relative intensities for the general hkℓ reflections were in good agreement with the calculated values, indicating that the compacted specimen had randomly oriented crystallites. Since the general hkℓ intensities for the randomly oriented powder appeared to be correct, it was assumed that the cubic habit of NaCl had a marked effect upon the intensities of the 200, 400, and 600 reflections. If 400 and 600 intensities were corrected to agree with the other hkℓ intensities on a relative basis, then the observed and calculated values in the last two columns would have been in good agreement.

The analysis of diffraction line intensities on an absolute basis as described in the previous section was applied in determining the pole densities for tungsten which had been reduced in thickness by over 90 per cent by rolling. Compacted powder was employed as a standard and the intensities for each hk$\ell$ reflection from specimens with their respective hk$\ell$ poles perfectly oriented normal to the surface was computed by means of Equation (5). The pole density was computed by dividing the observed intensities by the corresponding computed intensities. The results of this study are shown in Table II. Although the tungsten sheet would be expected to be highly oriented as a result of over 90 per cent reduction and this was indicated by the high intensities for the 200 and 400 reflections, only 10 per cent of the 200 poles were aligned normal to the surface of the sheet. The angular spread of the poles about the normal to the surface was probably not very large, but could not be measured because of the limited divergence that could pass through the diffractometer slits. The lack of agreement between the 200 and 400 reflections is not understood.

Table II

QUANTITATIVE ANALYSIS OF THE AMOUNT OF PREFERRED ORIENTATION IN ROLLED TUNGSTEN SHEET USING COPPER RADIATION, 25 kv, 8 ma

| hk$\ell$ | Measurements for Randomly Oriented Powder Compact | | | Calculated Intensity for 100 Per Cent Orientation, Counts x 64 | Measurements for Rolled Sheet, Integrated Intensity Counts x 64 | Pole Density Normal to the Surface of Sheet |
|---|---|---|---|---|---|---|
| | Integrated Intensity, Counts x 64 | Observed | Calculated | | | |
| 110 | 224 | 0.849 | 1.000 | $6.40 \times 10^4$ | 0 | 0 |
| 200 | 43 | 0.163[a] | 0.163 | $3.47 \times 10^4$ | 3540 | 0.102 |
| 211 | 83 | 0.314 | 0.325 | $2.05 \times 10^4$ | 96 | 0.005 |
| 220 | 28 | 0.106 | 0.105 | $1.60 \times 10^4$ | 0 | 0 |
| 310 | 42 | 0.159 | 0.166 | $1.34 \times 10^4$ | 0 | 0 |
| 222 | 14 | 0.053 | 0.055 | $1.47 \times 10^4$ | 125 | 0.008 |
| 321 | 107 | 0.405 | 0.413 | $2.02 \times 10^4$ | 0 | 0 |
| 400 | 25 | 0.094 | 0.094 | $4.05 \times 10^4$ | 2300 | 0.057 |

[a]The 200 reflection was used to compute the relative intensities.

## CONCLUSIONS

The X-ray diffraction intensity formulas published by James[3] and by Compton and Allison[4] were derived for specific experimental conditions which are not employed in the parafocusing diffractometer. Although these equations are satisfactory for relative intensity data, they fail to agree with the experimental data where absolute intensities are required. The formulas presented here have introduced the effect of divergent incident beam geometry which is employed in most diffractometers. Although the evaluation of the effect of this divergence is not precise, the agreement between the observed and calculated is improved considerably over that obtained using previous formulas.

## RECOMMENDATIONS

In the experimental verification of the new intensity formulas, the major difficulty is believed to be the preparation of randomly oriented powders. However, this problem is not insurmountable and would not be as difficult as the preparation of single crystals for all the cases needed in preferred orientation analysis on a quantitative basis.

If refinements in techniques are made, it would appear that one can predict, from intensity measurements with randomly oriented crystals, the diffraction line intensity where 100 per cent of the poles of any $hk\ell$ plane are normal to a surface. From these predicted intensities and the intensity data from specimens of unknown orientation, exposed to the same X-ray source, the fraction of $hk\ell$ poles normal to the surface can be readily computed, and from this an orientation index may be developed. It is possible that some consideration should be given to secondary extinction in extending the theory. This was not included here because other uncertainties were larger in magnitude.

## REFERENCES

1. Harris, G. B., Quantitative Measurement of Preferred Orientation in Rolled Uranium Bars, Phil. Mag., 43, 113 (1952).

2. Mueller, M. H., Knott, H. W., and Beck, P. A., Effects of Varying Reduction on the Preferred Orientation in Rolled Uranium Rods, ANL-5194 (May 1954).

3. James, R. W., The Optical Principles of X-ray Diffraction, G. Bell and Sons, Ltd., London (1950).

4. Compton, A. H., and Allison, S. K., X-rays in Theory and Experiment, D. Van Nostrand Company, Inc., New York, Second Edition (1954).

# THE DETERMINATION OF THE y POSITIONAL PARAMETER IN ALPHA URANIUM AS A FUNCTION OF TEMPERATURE

Melvin H. Mueller, Harold W. Knott and Richard L. Hitterman
Argonne National Laboratory

Jacob and Warren[1] in reporting the structure of alpha uranium indicated that there were four atoms per unit cell located at

$$0,y,\tfrac{1}{4};\ 0,\bar{y},\tfrac{3}{4};\ \tfrac{1}{2},\tfrac{1}{2}+y,\tfrac{1}{4};\ \tfrac{1}{2},\tfrac{1}{2}-y,\tfrac{3}{4}$$

where

$$y = 0.105 \pm 0.005.$$

Konobeevsky[2] has reported values of y = 0.107 at 20°C and 0.115 at 500°C. More recently, Sturcken and Post[3] have reported a value of $0.1025 \pm 0.0003$ for y at room temperature.

At the preferred orientation meeting held at National Lead in 1959, Sturcken and Mueller discussed the possibility of determining the change in the y parameter as a function of temperature; Sturcken agreed to investigate results at the low temperatures and Mueller at the high temperatures.

At the present time, there are some preliminary results. A uranium single crystal, which is approximately $\frac{3}{16}$-inch square, was obtained from Ed Fisher, Argonne, with the major crystal faces corresponding to the cube faces within approximately one degree. This crystal was then mounted on the G. E. Single Crystal orienter by means of a special plate holder and aligned with the "b" face in correct position for diffraction. Since the structure factor F for the (0k0)-type reflection for the alpha-uranium structure is

$$F = 4f \cos 2\pi ky \quad ,$$

it is apparent that the intensities from (0k0) reflections should provide a means of finding the value for the positional parameter y, which is the method used by Sturcken and Post.[3] Intensities were therefore obtained from this crystal for the (0k0) reflections ranging from the (020) to the (0,16,0).

Instead of using the minimization of the R factor as described by Sturcken and Post, it was decided to use the Busing-Levy[4] least-squares program on the IBM-704. In order to compare the results obtained by the minimization technique with the least-squares technique, we obtained the original data as used by Sturcken and Post. A summary of results obtained by various investigators together with those from the presently investigated crystal are shown in Table I.

Table I

SUMMARY OF RESULTS OBTAINED FOR THE y POSITIONAL PARAMETER BY VARIOUS INVESTIGATIONS

| Investigator | Material | Temp | y | B |
|---|---|---|---|---|
| Jacob and Warren[1] | Powder | R.T. | 0.105 ± 0.005 | |
| Konobeevsky[2] | Powder | 10°C | 0.107 ± 0.003 | |
| Konobeevsky[2] | Powder | 500°C | 0.115 ± 0.003 | |
| Sturcken and Post[3] | Single Crystal | 25°C | 0.1025 ± 0.003* | 0.4 |
| | | | 0.1024 ± 0.005** | 0.26 |
| Mueller and Knott | Single Crystal | 25°C | 0.1026 ± 0.003* | 0.3 |
| | | | 0.1023 ± 0.005** | 0.22 |

*Value obtained by minimization of R' plot.
**Value obtained by least-squares computer program.

This crystal was then put into the high-temperature furnace constructed at Argonne for the G. E. X-ray Diffractometer. The b face was then properly aligned, and measurements were obtained for room temperature and several elevated temperatures. Preliminary results indicated a room-temperature value of y = 0.1006 and a value of y = 0.1026 for 500°C. It was noted that the room-temperature value did not match the previously determined value. Therefore sources of error were analyzed, and it was found that the nickel foil, which serves as a heat shield and reflector, was wrinkled severely at the corners, which probably caused a preferential absorption which had an effect on the determined value for y. A more recent value of 0.1012 was obtained with this nickel foil removed, indicating that not all of the sources of error have been removed; therefore further work is necessary.

In addition to determining the value of y in this least-squares procedure it is also possible to obtain B, the temperature factor. The results obtained at room temperature with data from the present crystal and data from Sturcken are shown in Table I. Preliminary B values obtained on the crystal as a function of temperature indicated a rather straight-line increase of B from approximately 0.20 at room temperature to 0.95 at 500°C; however, these values need a further check since the y positional parameter does not check at room temperature for this set of data. If good reliable values for B can be established, it will be of interest to calculate the root-mean-square displacement of the atoms. By obtaining intensities from the (h00) and (00$\ell$) reflections also, it will be possible to determine B values for the other principal directions in the crystal.

Considerable thought has been given to the determination of both y and B as a function of temperature using the present single crystal with neutron diffraction. This technique would offer several advantages over the use of X rays, namely: (1) Since the neutrons have a considerably greater penetration into uranium than X rays, the diffraction would occur from a volume of the single crystal for the neutrons rather than essentially from the surface as with the X rays. This would minimize decreased intensity due to an oxide coating on the surface of the crystal and thus make it possible to compare the intensities at various temperatures. (2) Since the X-ray scattering occurs from the electrons, the scattering factor f is dependent on angle which decreases the intensity of the high-angle lines; however, with neutron diffraction, the scattering occurs from the nucleus and hence is not dependent on angle; therefore the high-angle lines do not suffer from decreased intensity due to the form factor.

## REFERENCES

1. Jacob, C. W., and Warren, B. E., J. Am. Chem. Soc. 59, 2588 (1937).

2. Konobeevsky, S. T., et al., Proceedings of the Second United Nations International Conference on Peaceful Uses of Atomic Energy, Geneva, Switzerland (1958), Vol. 6, p. 194.

3. Sturcken, E. F., and Post, B., Acta Cryst. 13, 852 (1960).

4. Busing, W R., and Levy, H. A., Oak Ridge National Laboratory Report 59-4-37 (1959).